

MODELLING STUDIES OF MAGNESIUM-DEPENDENT  
PHOSPHATE ESTER PROCESSING ENZYMES

by

Joanne W. Yun

B.A., *summa cum laude*  
Chemistry and French  
Amherst College (May, 1992)

Submitted to the Department of Chemistry  
in Partial Fulfillment of  
the Requirements for the Degree of  
Doctor of Philosophy

at the

Massachusetts Institute of Technology

June, 1996

© Massachusetts Institute of Technology  
All rights reserved

Signature of Author.....  
  
Department of Chemistry  
May 20, 1996

Certified by.....  
  
Stephen J. Lippard  
Thesis Supervisor

Accepted by.....  
Dietmar Seyferth  
Chairman, Departmental Committee on Graduate Students

Science

MASSACHUSETTS INSTITUTE  
OF TECHNOLOGY

JUN 12 1996

LIBRARIES



This doctoral thesis has been examined by a Committee of the Department of Chemistry as follows:

.....  
Alan Davison  
Professor of Chemistry  
Committee Chairman

.....  
Stephen J. Lippard  
Arthur Amos Noyes Chair and Professor of Chemistry  
Thesis Supervisor

.....  
Julius Rebek, Jr.  
Camille Dreyfus Professor of Chemistry

MODELLING STUDIES OF MAGNESIUM-DEPENDENT  
PHOSPHATE ESTER PROCESSING ENZYMES

by

Joanne W. Yun

Submitted to the Department of Chemistry on May 20, 1996 in partial fulfillment of the requirements for the Degree of Doctor of Philosophy in Chemistry

ABSTRACT

**Chapter 1.** Magnesium-dependent phosphate ester processing enzymes frequently employ a carboxylate-bridged dimetallic unit in their active sites. Biomimetic modelling chemistry of these magnesium centers has not been investigated previously. A brief introduction of the enzyme systems is presented, along with the focus of the present work.

**Chapter 2.** Several dimagnesium(II) complexes were synthesized and characterized by employing the dinucleating ligand XDK, where  $H_2XDK$  is *m*-xylylenediamine bis(Kemp's triacid imide), to stabilize the  $\{Mg(\mu-O_2CR)\}_2^{2+}$  unit. A  $[Mg_2(XDK)(CH_3OH)_4(H_2O)_2(NO_3)]^+$  complex has been prepared and allowed to react with one or two equivalents of diphenyl phosphate (DPP) to yield  $[Mg_2(XDK)(DPP)(CH_3OH)_3(H_2O)(NO_3)]$  and  $[Mg_2(XDK)(DPP)_2(CH_3OH)_3(H_2O)]$ , respectively. These are the first structurally characterized phosphate ester-bridged dimagnesium complexes which are potential phosphatase models.

**Chapter 3.** The phosphate ester exchange rate of free and bound diphenyl phosphate in  $[Mg_2(XDK)(DPP)_2(CH_3OH)_3(H_2O)]$  in methanol has been measured by variable temperature  $^{31}P\{^1H\}$  NMR spectroscopy and compared to that of structurally analogous dizinc(II) and dicalcium(II) complexes. The synthesis and structural characterization of the dicalcium(II) complex is presented, along with a discussion on the differences between the carboxylate- and phosphate ester-bridged dimagnesium, dizinc, and dicalcium centers.

**Chapter 4.** Modelling studies of magnesium-dependent phosphatase enzymes were extended into aqueous media with the synthesis of a water-soluble XDK analog, WXDK. The synthesis and characterization of the carboxylate-bridged dimagnesium-WXDK complexes are described. The biological relevance of these modelling studies is discussed.

Thesis Supervisor: Stephen J. Lippard

Title: Arthur Amos Noyes Chair and Professor of Chemistry

## Acknowledgments

I would like to begin by thanking Professor Stephen J. Lippard for the opportunity to pursue my graduate studies in his laboratory. He has taught me to think critically in my evaluation of scientific questions and has helped me develop into an independent scientist. I appreciate his guidance throughout my graduate career. I would also like to thank my undergraduate advisor Professor David M. Dooley for introducing me to bio-inorganic chemistry and for his advice and support over the years.

I must also thank the members of the Lippard group, both past and present, for providing me with much entertainment during my graduate career. When I joined the group, Cecilia Bastos, Steve Watton, Kingsley Taft, Dave Goldberg, and Linda Doerrer were there to get me oriented. Tong Ren always gave me helpful advice back then, and he continues to be a very supportive friend and highly respected colleague. Axel Masschelein was a fun teacher and showed how to keep the Raman lab going even after he left. Christy Chow was always willing to engage in discussions about work and basketball. I would like to especially thank Kathy Liu and Brian Bronk for being so helpful during my first couple of years.

In addition, I thank the past and present members of the organometallic subgroup for accepting me and my magnesium chemistry into their subgroup. I have enjoyed working with and learning from everyone in this subgroup. I was very fortunate to work with Dr. Tomoaki Tanase who has been a wonderful teacher, colleague, and friend. I thank Dan LeCloux and Dietrich Steinhuebel for their help and friendship over the past couple of years, and I hope they will continue to take good care of Barney. I wish Chuan He lots of luck with his volleyball games and with his chemistry as I leave my bench to him. Maria Bautista is thanked for keeping me entertained in the lab with discussions about fashion and sports. Susanna Herold has been a terrific friend and labmate who is always there with helpful advice and her famous boomerang cookies.

I am grateful to the entire Manchanda family for making me an honorary cousin. I would like to thank Betsy Redding for her positive attitude and appreciation of golden crowns. C. Chad Davis is acknowledged for fun breaks during Thursdays at 3. I must also thank Launa Johnston for delicious Thai food lunches. I would like to thank Amy Rosenzweig and Ken Comess for their friendship, and especially Amy for her helpful advice and successful shopping trips.

I would like to express special thanks to Tricia Takahara and Mark "Commish" Hasegawa for their friendship and thoughtfulness throughout my years at MIT. They have been wonderful in helping me maintain a positive perspective. I am looking forward to seeing them in southern California. Hopefully the Laser Jocks will beat the TEBFH some day.

I would like to thank some friends outside of MIT who have helped me through my graduate career. Rudy Redmond, Laural Wagner, Desi Wyatt, and Lucy Guerra have always been very supportive and wonderful people. I would also like to acknowledge Henry for some breaks away from the lab and onto Newbury Street.

And finally, I would like to thank my family for their love, support, and encouragement.



## Table of Contents

Abstract.....	4
Acknowledgements.....	5
Table of Contents .....	7
List of Tables.....	9
List of Figures.....	10
Dedication.....	11
Chapter 1. Introduction.....	13
References.....	16
Chapter 2. Structural Models of Magnesium-Dependent Phosphatase Enzymes...19	
Introduction.....	20
Experimental.....	21
Results and Discussion.....	26
Conclusions.....	34
References.....	34
Tables.....	38
Figures.....	47
Chapter 3. Phosphate Ester Exchange Studies of Carboxylate-Bridged	
Dimetallics.....	57
Introduction.....	58
Experimental.....	59
Results.....	61
Discussion.....	65
Conclusions.....	68
Acknowledgement.....	69
References.....	69
Scheme 1. Proposed mechanism for phosphodiester exchange.....	71
Tables.....	72
Figures.....	77
Chapter 4. Studies of Water-Soluble Carboxylate-Bridged Dimagnesium(II)	
Complexes .....	83
Introduction.....	84
Experimental.....	85
Results.....	94
Discussion.....	101

Conclusions.....	104
Acknowledgements.....	105
References.....	105
Scheme 1. Proposed mechanism for the Klenow Fragment.....	108
Scheme 2. Proposed mechanism for a dicobalt(III) complex.....	109
Scheme 3. Synthesis of H <sub>2</sub> WXDK.....	110
Tables.....	111
Figures.....	119
Biographical Note.....	128



## List of Tables

### Chapter 2

Table 1.	Examples of Magnesium-Dependent Phosphatase Enzymes.....	38
Table 2.	Summary of Crystallographic Data.....	39
Table 3.	Selected Bond Distances and Angles for 1(NO <sub>3</sub> ).....	40
Table 4.	Selected Bond Distances and Angles for 2·3CH <sub>3</sub> OH.....	41
Table 5.	Selected Bond Distances and Angles for 3·CH <sub>3</sub> OH.....	42
Table 6.	Selected Bond Distances and Angles for 4.....	43
Table 7.	Structural Parameters of 1(NO <sub>3</sub> ), 2·3CH <sub>3</sub> OH, and 3·CH <sub>3</sub> OH.....	44
Table 8.	Examples of Dimetallic Complexes with Phosphate Esters.....	45

### Chapter 3

Table 1.	Comparison of Magnesium(II), Calcium(II), and Zinc(II).....	72
Table 2.	Crystallographic Data for 3·CH <sub>3</sub> OH.....	73
Table 3.	Selected Bond Distances and Angles for 3·CH <sub>3</sub> OH.....	74
Table 4.	Structural Parameters of 1·CH <sub>3</sub> OH, 2, and 3·CH <sub>3</sub> OH.....	75
Table 5.	Summary of Variable Temperature <sup>31</sup> P{ <sup>1</sup> H} NMR Data.....	76

### Chapter 4

Table 1.	X-ray Crystallographic Data for 5, 6, 8, and 9 .....	111
Table 2.	Intramolecular Bond Distances for 5·H <sub>2</sub> O·CH <sub>3</sub> OH.....	112
Table 3.	Intramolecular Bond Angles for 5·H <sub>2</sub> O·CH <sub>3</sub> OH.....	113
Table 4.	Selected Bond Distances and Angles for 6(OTf) .....	115
Table 5.	Selected Bond Distances and Angles for 8(OTf) .....	116
Table 6.	Selected Bond Distances and Angles for 9(OTf) <sub>0.5</sub> (BNPP) <sub>0.5</sub> .....	117
Table 7.	Structural Parameters of 6, 8, and 9.....	118

## List of Figures

### Chapter 1

Figure 1.	Schematic drawing of $H_2XDK$ .....	15
-----------	-------------------------------------	----

### Chapter 2

Figure 1.	ORTEP view of $XDK$ .....	47
Figure 2a.	ORTEP diagram of <b>1</b> .....	48
Figure 2b.	ORTEP view of dinuclear core of <b>1</b> .....	49
Figure 3.	Packing diagram of $1(NO_3)$ .....	50
Figure 4a.	ORTEP diagram of <b>2</b> .....	51
Figure 4b.	ORTEP view of dimetallic center of <b>2</b> .....	52
Figure 5.	Conductivity data for $3 \cdot CH_3OH$ .....	53
Figure 6a.	ORTEP diagram of <b>3</b> .....	54
Figure 6b.	ORTEP view of dinuclear core of <b>3</b> .....	55
Figure 7.	ORTEP diagram of <b>4</b> .....	56

### Chapter 3

Figure 1.	Conductivity data for $3 \cdot CH_3OH$ .....	77
Figure 2.	ORTEP diagram of <b>3</b> .....	78
Figure 3.	ORTEP view of polymeric structure of <b>3</b> .....	79
Figure 4.	ORTEP view of polymeric dimetallic center of <b>3</b> .....	80
Figure 5.	VT- $^{31}P\{^1H\}$ NMR spectra for $1 \cdot CH_3OH$ and DNMR data.....	81
Figure 6.	VT- $^{31}P\{^1H\}$ NMR spectra for <b>2</b> .....	82

### Chapter 4

Figure 1.	ORTEP view of $5 \cdot H_2O \cdot CH_3OH$ .....	119
Figure 2.	Packing diagram of $5 \cdot H_2O$ .....	120
Figure 3.	Stereoview packing diagram of $5 \cdot H_2O \cdot CH_3OH$ .....	121
Figure 4.	ORTEP view of <b>6</b> .....	122
Figure 5.	ORTEP diagram of <b>8</b> .....	123
Figure 6.	ORTEP view of <b>9</b> .....	124
Figure 7.	$^1H$ NMR spectrum of $9(OTf)_{0.5}(BNPP)_{0.5}$ in $CD_3OD$ .....	125
Figure 8.	pH titration data of $7(NO_3)$ .....	126
Figure 9.	Kinetic data for $7(NO_3)$ .....	127

**To My Parents**



**Chapter 1**

**Introduction**

## INTRODUCTION

Magnesium ion is an indispensable cofactor in biology. It participates in many important biological transformations, including the hydrolysis of phosphate ester bonds. The carboxylate-bridged dinuclear magnesium unit,  $\{\text{Mg}_2(\text{O}_2\text{CR})\}^{3+}$ , is emerging as a ubiquitous structural motif in many phosphate ester processing enzymes. These magnesium-dependent enzymes include the Klenow fragment of DNA polymerase I from *Escherichia coli*,<sup>1</sup> ribonuclease H of HIV-1 reverse transcriptase,<sup>2</sup> inositol monophosphatase,<sup>3</sup> and inositol polyphosphate 1-phosphatase,<sup>4</sup> which have all been structurally characterized to reveal a carboxylate-bridged dimetallic active site center. These metalloenzymes make up a rapidly growing class of systems which are postulated to utilize a two-metal-ion mechanism for phosphate ester hydrolysis. Their dimagnesium centers are believed to serve several important functions, including (i) binding, orienting, and activating the substrate, (ii) modulating the  $\text{p}K_a$  of the incoming nucleophile, (iii) stabilizing the transition state, and (iv) facilitating product release.<sup>1</sup> Furthermore, studies of the catalytic RNA systems have suggested a similar requirement for divalent metal ions,<sup>5</sup> and an analogous two-metal-ion mechanism has been proposed for the ribozymes.<sup>6</sup>

We are particularly interested in studying the manner by which phosphatases employ a carboxylate-bridged dimagnesium center to catalyze the cleavage of phosphate ester bonds. Our approach to investigating the underlying structural and mechanistic principles is to prepare and characterize small molecule inorganic complexes that contain a carboxylate-bridged dimagnesium core to mimic the biological active sites. Despite the biological importance of such dimagnesium centers in the active sites of metalloenzymes, examples of structurally characterized dimagnesium carboxylate complexes are extremely rare. A search of the Cambridge Structural Database revealed only one discrete dinuclear magnesium(II) structure,

dimagnesium(II) *o*-phenylenediaminetetraacetate,  $[\text{Mg}_2(\text{C}_{14}\text{H}_{12}\text{N}_2\text{O}_8)(\text{H}_2\text{O})_6]$ .<sup>7</sup> In the presence of simple carboxylates such as formate, magnesium ions tend to form polymeric structures, with the metals coordinating to the anti lone pairs of the carboxylates.<sup>8</sup>

In order to avoid such polymeric structures in our biomimetic model studies of magnesium-dependent phosphatase systems, we focused our attention on the dinucleating ligand XDK (Figure 1), where  $\text{H}_2\text{XDK}$  is *m*-xylylenediamine bis(Kemp's triacid imide),<sup>9,10</sup> for the synthesis of discrete carboxylate-bridged, dimagnesium complexes. This ligand has been used in the preparation of homo- and heterodimetallic complexes containing Fe(II), Fe(III), Co(II), Mn(II), Mn(III), Ni(II), and Zn(II).<sup>11-19</sup>

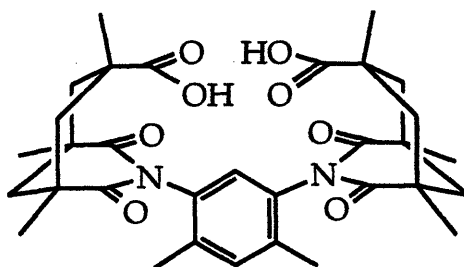


Figure 1.  $\text{H}_2\text{XDK}$

This thesis describes the preparation and characterization of the desired discrete carboxylate-bridged dinuclear magnesium complexes with the XDK ligand. In chapter 2, we report the synthesis and structural characterization of carboxylate- and phosphodiester-bridged dimagnesium complexes as potential models for magnesium-dependent phosphate ester processing enzymes. In chapter 3, we describe phosphate ester exchange processes of a bis(phosphate) dimagnesium-XDK complex together with its dicalcium(II)- and dizinc(II)-XDK analogs. The preparation of a water-soluble analog of the XDK ligand, WXDK, where  $\text{H}_2\text{WXDK} =$

*m*-xylylenediamine bis(trihydroxymethyl-Kemp's triacid imide), is described in chapter 4, along with the synthesis and characterization of several dimagnesium-WXDK complexes containing phosphodiester.

## REFERENCES

- (1) Beese, L. S.; Steitz, T. A. *EMBO J.* **1991**, *10*, 25-33.
- (2) Davies, J. F.; Hostomska, Z.; Hostomsky, Z.; Jordan, S. R.; Matthews, D. A. *Science* **1991**, *252*, 88-95.
- (3) Bone, R.; Frank, L.; Springer, J. P.; Atack, J. R. *Biochemistry* **1994**, *33*, 9468-9476.
- (4) York, J. D.; Ponder, J. W.; Chen, Z.-W.; Mathews, F. S.; Marjerus, P. W. *Biochemistry* **1994**, *33*, 13164-13171.
- (5) Piccirilli, J. A.; Vyle, J. S.; Caruthers, M. H.; Cech, T. R. *Nature* **1993**, *361*, 85-88.
- (6) Steitz, T. A.; Steitz, J. A. *Proc. Natl. Acad. Sci. USA* **1993**, *90*, 6498-6502.
- (7) Nakasuka, N.; Shiro, M. *Acta. Cryst.* **1989**, *C45*, 1487-1490.
- (8) Malard, C.; Pezerat, H.; Herpin, P.; Toledano, P. J. *Solid State Chem.* **1982**, *41*, 67-74.
- (9) Kemp, D. S.; Petrakis, K. S. *J. Org. Chem.* **1981**, *46*, 5140-5143.
- (10) Rebek, J., Jr.; Marshall, L.; Wolak, R.; Parris, K.; Killoran, M.; Askew, B.; Nemeth, D.; Islam, N. *J. Am. Chem. Soc.* **1985**, *107*, 7476-7481.
- (11) Goldberg, D. P.; Watton, S. P.; Masschelein, A.; Wimmer, L.; Lippard, S. J. *J. Am. Chem. Soc.* **1993**, *115*, 5346-5347.
- (12) Watton, S. P.; Masschelein, A.; Rebek, J., Jr.; Lippard, S. J. *J. Am. Chem. Soc.* **1994**, *116*, 5196-5205.
- (13) Watton, S. P.; Davis, M. I.; Pence, L. E.; Rebek, J., Jr.; Lippard, S. J. *Inorg. Chim. Acta* **1995**, *235*, 195-204.
- (14) Tanase, T.; Yun, J. W.; Lippard, S. J. *Inorg. Chem.* **1995**, *34*, 4220-4229.
- (15) Tanase, T.; Lippard, S. J. *Inorg. Chem.* **1995**, *34*, 4682-4690.



- (16) Tanase, T.; Watton, S. P.; Lippard, S. J. *J. Am. Chem. Soc.* **1994**, *116*, 9401-9402.
- (17) Tanase, T.; Yun, J. W.; Lippard, S. J. *Inorg. Chem.* **1996**, in press.
- (18) Hagen, K. S.; Lachicotte, R.; Kitaygorodskiy, A.; Elbouadili, A. *Angew. Chem. Int. Ed. Engl.* **1993**, *32*, 1321-1324.
- (19) Hagen, K. S.; Lachicotte, R.; Kitaygorodskiy, A. *J. Am. Chem. Soc.* **1993**, *115*, 12617-12618.



**Chapter 2**

**Structural Models of Magnesium-Dependent Phosphatase Enzymes**

## INTRODUCTION

Magnesium ion is an important cofactor in many biological systems. It is often encountered as the carboxylate-bridged dimagnesium(II) unit which is found in the active sites of many phosphate ester processing metalloenzymes, including the Klenow fragment of DNA polymerase I from *Escherichia coli*,<sup>1</sup> ribonuclease H of HIV-1 reverse transcriptase,<sup>2</sup> rat DNA polymerase  $\beta$ ,<sup>3</sup> fructose-1,6-bisphosphatase,<sup>4,5</sup> inositol monophosphatase,<sup>6</sup> and inositol polyphosphate 1-phosphatase.<sup>7</sup> These enzymes have been structurally characterized to reveal two magnesium ions bridged by carboxylate side chains of aspartate or glutamate amino acid residues with a metal-metal distance of about 4 Å (Table 1). A two-metal-ion mechanism has been proposed for these enzymes where one metal ion serves to bind, orient, and activate the substrate and the other generates the attacking nucleophile.<sup>1</sup> The dimetallic center is postulated to stabilize the transition state of such a reaction. Furthermore, magnesium ions are also required for activity in ribozymes, and a similar two-metal-ion mechanism has been proposed for the cleavage of phosphate ester bonds in catalytic RNAs.<sup>8</sup>

Despite the essential roles of magnesium in biology, its biomimetic chemistry has received less attention by comparison to the transition metal ions and is generally less well understood.<sup>9,10</sup> We have therefore initiated a program to investigate the chemistry of carboxylate-bridged dimagnesium centers by synthesizing and characterizing such complexes as potential models for phosphatase systems.

Our biomimetic modelling studies for phosphate ester processing enzymes began with the synthesis of carboxylate-bridged, dimetallic complexes by employing the dinucleating ligand XDK (Figure 1), where H<sub>2</sub>XDK is *m*-xylylenediamine bis(Kemp's triacid imide).<sup>11,12</sup> This ligand has two convergent carboxylate groups, positioned about 3 Å apart, and is useful for assembling discrete dimagnesium units.

H<sub>2</sub>XDK has also been employed in the preparation of other carboxylate-bridged homo-<sup>13-18</sup> and heterodimetallic<sup>19-21</sup> complexes. We report here the synthesis and structural characterization of carboxylate-bridged dinuclear magnesium centers and their reactions with phosphate esters. A preliminary account of this work has been communicated.<sup>22</sup>

## EXPERIMENTAL METHODS

### General

All experiments were carried out under aerobic conditions, unless otherwise indicated. Reagents and solvents were used as purchased. The preparation of H<sub>2</sub>XDK was carried out as previously described.<sup>12</sup> <sup>1</sup>H and <sup>31</sup>P{<sup>1</sup>H} NMR spectra were obtained on Varian XL-300 or Varian UNITY300 spectrometers. <sup>31</sup>P{<sup>1</sup>H} NMR spectra were measured at 121.4 MHz with 85% H<sub>3</sub>PO<sub>4</sub> as an external reference. Infrared spectra were recorded on a Bio-Rad FTS7 Fourier transform instrument. Conductivity measurements were carried out at 21 °C in methanol with a Fisher Scientific conductivity bridge model 9-326 with a platinum-black electrode. Molar conductivities (Ω<sup>-1</sup> cm<sup>2</sup> mol<sup>-1</sup>) were derived from the slopes of a conductivity (Ω<sup>-1</sup> cm<sup>-1</sup>) versus concentration (mol cm<sup>-3</sup>) plot. The assignment of the electrolyte type was determined by reference to the molar conductivity of [Bu<sub>4</sub>N][PF<sub>6</sub>] in methanol. Electronic spectra were recorded on a Hewlett Packard 8452A diode array spectrophotometer. Kinetic measurements for the hydrolysis of bis(4-nitrophenyl)-phosphate (BNPP<sup>-</sup>) were carried out in methanol by following the appearance of *p*-nitrophenolate at 404 nm.

### Preparation of [Mg<sub>2</sub>(XDK)(CH<sub>3</sub>OH)<sub>4</sub>(H<sub>2</sub>O)<sub>2</sub>(NO<sub>3</sub>)](NO<sub>3</sub>), 1(NO<sub>3</sub>)

A methanolic solution (5 mL) of Mg(NO<sub>3</sub>)<sub>2</sub>·6H<sub>2</sub>O (176 mg, 0.689 mmol) was added to a solution of H<sub>2</sub>XDK (200 mg, 0.344 mmol) and NaOH (0.689 mmol, 0.5 M

in MeOH) in methanol (5 mL). The mixture was stirred at room temperature for 30 min. The solvent was removed under vacuum, and the residue was further dried under vacuum. The dried white powder was treated with excess pyridine (5 mL) in chloroform (10 mL), and the insoluble salt contaminants were removed by filtration. The py/CHCl<sub>3</sub> filtrate containing the desired complex was placed under vacuum to remove the solvents. The dried sample was then redissolved in methanol, filtered through Celite, and vapor diffusion of ethyl ether afforded colorless crystals in 72% yield (227 mg, 0.248 mmol). The crystals were washed with Et<sub>2</sub>O and dried under vacuum. <sup>1</sup>H NMR, 300 MHz (CD<sub>3</sub>OD): δ 1.19 (s, 6 H), 1.24 (m, 4 H), 1.29 (s, 12 H), 1.61 (d, 2 H, *J* = 13 Hz), 1.93 (s, 6 H), 2.15 (d, 2 H, *J* = 13 Hz), 2.85 (d, 4 H, *J* = 12 Hz), 7.20 (s, 1 H), 7.36 (s, 1 H). IR (Nujol): 3387 (br), 1714 (m), 1680 (s), 1635 (m) (XDK), 1505 (m), 1301 (m), 1191 (m), 1024 (m), 954, 889, 884, 764 cm<sup>-1</sup>. Anal. Calcd. for C<sub>36</sub>H<sub>58</sub>N<sub>4</sub>O<sub>20</sub>Mg<sub>2</sub>: C, 47.23; H, 6.39; N, 6.12. Found: C, 46.96; H, 6.44; N, 6.14.

#### Preparation of [Mg<sub>2</sub>(XDK){μ-η<sup>2</sup>-(PhO)<sub>2</sub>PO<sub>2</sub>}(CH<sub>3</sub>OH)<sub>3</sub>(H<sub>2</sub>O)(NO<sub>3</sub>)]·3CH<sub>3</sub>OH, 2·3CH<sub>3</sub>OH

A methanolic solution (5 mL) of Mg(NO<sub>3</sub>)<sub>2</sub>·6H<sub>2</sub>O (44 mg, 0.172 mmol) was added to a solution of H<sub>2</sub>XDK (50 mg, 0.0861 mmol) and NaOH (0.172 mmol, 0.5 M in MeOH) in methanol (5 mL) and stirred for 20 minutes. A methanolic solution (2 ml) of diphenyl hydrogen phosphate (HDPP) (21.5 mg, 0.0861 mmol) and NaOH (0.0861 mmol, 0.5 M in MeOH) was then added. The combined solution was stirred for 30 minutes, and the solvent was removed under vacuum. The dried compound was redissolved in methanol, filtered, and vapor diffusion of ethyl ether into the solution gave crystalline material. The crystals were collected and treated with excess pyridine (3 mL) in chloroform (5 mL). The salt contaminants were removed by filtration, and the py/CHCl<sub>3</sub> filtrate containing the complex was placed under vacuum to remove the solvents. The dried sample was redissolved in methanol,

and vapor diffusion of ethyl ether afforded single X-ray quality crystals in 36% yield (36 mg, 0.0313 mmol).  $^1\text{H}$  NMR, 300 MHz ( $\text{CD}_3\text{OD}$ ):  $\delta$  1.20 (m, 4 H), 1.23 (s, 6 H), 1.26 (s, 12 H), 1.56 (d, 2 H,  $J = 13$  Hz), 1.90 (s, 6 H), 2.09 (d, 2 H,  $J = 13$  Hz), 2.90 (d, 4 H,  $J = 14$  Hz), 7.02 (m, 2 H), 7.12 (m, 5 H), 7.22 (m, 4 H), 7.45 (s, 1 H).  $^{31}\text{P}\{^1\text{H}\}$  NMR, 121.4 MHz ( $\text{CD}_3\text{OD}$ ):  $\delta$  -15.46 (s). IR (Nujol): 3472 (br), 1720 (m), 1681 (s), 1619 (m) (XDK), 1317, 1263, 1231, 1194, 1128 (m), 1033, 929 (m), 887, 852, 779, 757, 688  $\text{cm}^{-1}$ . Elemental analysis samples were dried under vacuum at 90 ° for 12 h. Anal. Calcd. for  $\text{C}_{47}\text{H}_{62}\text{N}_3\text{O}_{19}\text{Mg}_2\text{P}_1$ : C, 53.63; H, 5.94; N, 3.99. Found: C, 53.22; H, 5.60; N, 4.13.

#### Preparation of $[\text{Mg}_2(\text{XDK})\{\mu\text{-}\eta^2\text{-(PhO)}_2\text{PO}_2\}\{\eta^1\text{-(PhO)}_2\text{PO}_2\}(\text{CH}_3\text{OH})_3(\text{H}_2\text{O})]\cdot\text{CH}_3\text{OH}, 3\cdot\text{CH}_3\text{OH}$

A methanolic solution (2 mL) of HDPP (43 mg, 0.172 mmol) and NaOH (0.172 mmol, 0.5 M in MeOH) was added to a solution of **1** in methanol (5 mL). The mixture was stirred at room temperature for 30 min. The solvent was removed under vacuum. The dried powder was dissolved in methanol and vapor diffusion of ethyl ether gave crystalline compound. The crystals were collected and dried under vacuum, then treated with excess pyridine (3 mL) in chloroform (5 mL), and any salt contaminants were removed by filtration. The py/ $\text{CHCl}_3$  filtrate containing the complex was placed under vacuum to remove the solvents. The dried sample was then redissolved in methanol, filtered through Celite, and vapor diffusion of ethyl ether afforded colorless crystals in 32% yield (35 mg, 0.028 mmol). The crystals were washed with  $\text{Et}_2\text{O}$  and dried under vacuum.  $^1\text{H}$  NMR, 300 MHz ( $\text{CD}_3\text{OD}$ ):  $\delta$  1.18 (d, 4 H,  $J = 14$  Hz), 1.23 (s, 6 H), 1.26 (s, 12 H), 1.56 (d, 2 H,  $J = 13$  Hz), 1.90 (s, 6 H), 2.09 (d, 2 H,  $J = 13$  Hz), 2.91 (d, 4 H,  $J = 13$  Hz), 7.03 (m, 4 H), 7.16 (m, 8 H), 7.24 (m, 9 H), 7.47 (s, 1 H).  $^{31}\text{P}\{^1\text{H}\}$  NMR, 121.4 MHz ( $\text{CD}_3\text{OD}$ ):  $\delta$  -9.14 (s), -15.45 (s). IR (Nujol): 3468 (br), 1717 (m), 1679 (s), 1633 (m), 1597 (m) (XDK), 1288, 1251, 1205 (m), 1135 (m), 1025, 932 (m), 893, 852, 761, 683  $\text{cm}^{-1}$ . Elemental analysis samples were dried under

vacuum at 90 ° for 12 h. Anal. Calcd. for C<sub>59</sub>H<sub>72</sub>N<sub>2</sub>O<sub>20</sub>Mg<sub>2</sub>P<sub>2</sub>: C, 57.16; H, 5.85; N, 2.26. Found: C, 56.76; H, 5.47; N, 2.45.

#### Preparation of [Mg(HXDK)<sub>2</sub>(H<sub>2</sub>O)<sub>2</sub>], 4

Method 1: One equivalent of bis(4-nitrophenyl)phosphoric acid (29.3 mg, 0.086 mmol) was added to a methanolic solution (2 mL) of 1. The solution was stirred for 20-30 minutes and filtered through Celite. Vapor diffusion of ethyl ether into this solution afforded colorless, block crystals in 23% yield (24 mg, 0.020 mmol). Method 2: A methanolic solution (2 mL) of Mg(NO<sub>3</sub>)<sub>2</sub>·6H<sub>2</sub>O (11 mg, 0.043 mmol) was added to a solution of H<sub>2</sub>XDK (50 mg, 0.086 mmol) and NaOH (172 μL, 0.5 M in MeOH) in methanol (3 mL). The off-white product precipitated out of solution. The compound was washed with ether and dried under vacuum. Yield: 50% (26 mg, 0.022 mmol). <sup>1</sup>H NMR 300 MHz (CD<sub>2</sub>Cl<sub>2</sub>): δ 1.08 (br), 1.26 (br), 1.49 (br), 1.93 (s), 2.02 (br), 2.81 (br), 6.86 (s), 7.15 (s), 19.02 (br). IR (Nujol): 3462 (br), 1731 (m), 1680 (s), 1642 (m) (XDK), 1509, 1311, 1246, 1199 (m), 1085, 1026, 954, 854, 757 cm<sup>-1</sup>. Anal. Calcd. for C<sub>64</sub>H<sub>82</sub>O<sub>18</sub>N<sub>4</sub>Mg<sub>1</sub>: C, 63.03; H, 6.78; N, 4.59. Found: C, 62.68; H, 6.86; N, 4.63.

X-ray Diffraction Studies of [Mg<sub>2</sub>(XDK)(CH<sub>3</sub>OH)<sub>4</sub>(H<sub>2</sub>O)<sub>2</sub>(NO<sub>3</sub>)](NO<sub>3</sub>), 1(NO<sub>3</sub>), [Mg<sub>2</sub>(XDK){μ-η<sup>2</sup>-(PhO)<sub>2</sub>PO<sub>2</sub>}(CH<sub>3</sub>OH)<sub>3</sub>(H<sub>2</sub>O)(NO<sub>3</sub>)]·3CH<sub>3</sub>OH, 2·3CH<sub>3</sub>OH, [Mg<sub>2</sub>(XDK){μ-η<sup>2</sup>-(PhO)<sub>2</sub>PO<sub>2</sub>}{η<sup>1</sup>-(PhO)<sub>2</sub>PO<sub>2</sub>}(CH<sub>3</sub>OH)<sub>3</sub>(H<sub>2</sub>O)]·CH<sub>3</sub>OH, 3·CH<sub>3</sub>OH, and [Mg(HXDK)<sub>2</sub>(H<sub>2</sub>O)<sub>2</sub>], 4.

Crystals of 1(NO<sub>3</sub>), 2·3CH<sub>3</sub>OH, 3·CH<sub>3</sub>OH, and 4 suitable for X-ray analyses were grown by ethyl ether diffusion into a methanolic solution of the complex. Single-crystal X-ray diffraction study were carried out on an Enraf-Nonius CAD-4 diffractometer by using graphite monochromated Mo Kα (λ = 0.71069 Å) radiation. General procedures were previously described in detail.<sup>23</sup> The crystals were mounted at room temperature on the end of a quartz fiber in paratone and were



judged to be of acceptable quality on the basis of open-counter omega-scans of several low-angle reflections and axial photographs. Crystallographic data are given in Table 2. All reflection data were corrected for Lorentz-polarization. An absorption correction was only applied to 3·CH<sub>3</sub>OH. The data for the structures described in this chapter, including tables of atomic positional parameters and anisotropic temperature factors, are available on a 4mm DAT tape.

**Structure Solution and Refinement of [Mg<sub>2</sub>(XDK)(CH<sub>3</sub>OH)<sub>4</sub>(H<sub>2</sub>O)<sub>2</sub>(NO<sub>3</sub>)](NO<sub>3</sub>), 1(NO<sub>3</sub>)**

All computations were carried out on a DEC VAXstation II or a DEC VAXstation 3100. Calculations were performed with the TEXSAN crystallographic software package as described by Carnahan et al., 1992.<sup>23</sup> The non-hydrogen atoms were located by direct methods and a series of least squares refinements. Hydrogen atoms were located for the two bound water molecules, O4 and O6 (see Figure 2), and for methyl hydrogens on the methanol ligands. The remaining carbon-bound hydrogen atoms were calculated at the ideal positions with a C-H distance of 0.95 Å. All hydrogen atoms were refined isotropically, and all non-hydrogen atoms were refined with anisotropic temperature factors.

**Structure Solution and Refinement of [Mg<sub>2</sub>(XDK){μ-η<sup>2</sup>-(PhO)<sub>2</sub>PO<sub>2</sub>}(CH<sub>3</sub>OH)<sub>3</sub>(H<sub>2</sub>O)-(NO<sub>3</sub>)]·3CH<sub>3</sub>OH, 2·3CH<sub>3</sub>OH and [Mg<sub>2</sub>(XDK){μ-η<sup>2</sup>-(PhO)<sub>2</sub>PO<sub>2</sub>}{η<sup>1</sup>-(PhO)<sub>2</sub>PO<sub>2</sub>-(CH<sub>3</sub>OH)<sub>3</sub>(H<sub>2</sub>O)]·CH<sub>3</sub>OH, 3·CH<sub>3</sub>OH**

All computations were carried out on a DEC VAXstation 4000 or a DEC VAXstation 3100. Calculations were performed as previously described<sup>23</sup> using an upgraded version of the TEXSAN crystallographic software package (Version 1.6).<sup>24</sup> All non-hydrogen atoms were located using direct methods and a series of least squares refinements. The carbon-bound hydrogen atoms were generated at the ideal

positions with a C-H distance of 0.95 Å, with the exception of solvent molecule hydrogen atoms. All hydrogen atoms were refined isotropically. The non-hydrogen atoms were all refined with anisotropic temperature factors.

#### Structure Solution and Refinement of $[\text{Mg}(\text{HXDK})_2(\text{H}_2\text{O})_2]$ , **4**

The structure of **4** was solved by similar methods to those used for  $2 \cdot 3\text{CH}_3\text{OH}$  and  $3 \cdot \text{CH}_3\text{OH}$ . The hydrogen atoms were calculated at the ideal positions with a C-H distance of 0.95 Å, with the exception of water and carboxylate hydrogens. All carbon atoms were refined isotropically, with the exception of the methyl carbon atoms which were refined anisotropically. Other non-hydrogen atoms were refined with anisotropic temperature factors.

## RESULTS AND DISCUSSION

#### Synthesis and Characterization of $[\text{Mg}_2(\text{XDK})(\text{CH}_3\text{OH})_4(\text{H}_2\text{O})_2(\text{NO}_3)](\text{NO}_3)$ , **1**( $\text{NO}_3$ )

The reaction of  $\text{Mg}(\text{NO}_3)_2 \cdot 6\text{H}_2\text{O}$  (2 equiv) with  $\text{H}_2\text{XDK}$  (1 equiv) and  $\text{NaOH}$  (2 equiv) in methanol and subsequent workup gave colorless crystalline material of  $[\text{Mg}_2(\text{XDK})(\text{CH}_3\text{OH})_4(\text{H}_2\text{O})_2(\text{NO}_3)](\text{NO}_3)$ , **1**( $\text{NO}_3$ ). The IR spectrum indicated the presence of the XDK ligand (1635 - 1714  $\text{cm}^{-1}$ ), nitrate anions (1301  $\text{cm}^{-1}$ ), and hydroxyl groups (~ 3300 - 3400  $\text{cm}^{-1}$ ). The  $^1\text{H}$  NMR spectrum in  $\text{CD}_3\text{OD}$  showed a symmetrical set of XDK resonances, with three singlets for the methyl groups of the ligand integrating at a ratio of 1:2:1 ( $\delta$  1.19, 1.29, and 1.93).

Crystals of **1**( $\text{NO}_3$ ) were obtained from a methanol/ethyl ether solvent system, and an X-ray crystallographic analysis of **1** revealed the structural features of a carboxylate-bridged, dinuclear magnesium complex. The structure of the cation  $[\text{Mg}_2(\text{XDK})(\text{CH}_3\text{OH})_4(\text{H}_2\text{O})_2(\text{NO}_3)]^+$  (**1**) is shown in Figures 2a and 2b. Selected bond distances and angles are given in Table 3. The magnesium ions in **1** are 4.783(2) Å apart, separated by the two bridging carboxylates of the  $\text{XDK}^{2-}$  ligand. There are no

other ligands bridging the two metal ions. The magnesium ions and the carboxylate oxygen atoms are approximately coplanar, as indicated by the values of  $d$ , the distance of the Mg atoms from the dicarboxylate plane, and  $\phi$ , the dihedral angle between [Mg1-Mg2-(OCO<sub>2</sub>)<sub>2</sub>] and the carboxylate planes (Table 7).<sup>14,25</sup> The metal ions appear to be coordinated to the syn lone pairs of the carboxylates, with Mg-OC<sub>carboxylate</sub> bond angles ranging from 151.8(2) to 161.2(2)°. Mg1 adopts a distorted octahedral geometry and is coordinated by one bidentate nitrate group (O11, O12), one methanol (O5), and one water molecule (O6). The geometric distortion is a consequence of the bidentate nitrate group which coordinates unsymmetrically with relatively long Mg1-O11 and Mg1-O12 bond lengths of 2.144(3) and 2.242(3) Å, respectively. The chelate ring of the nitrate anion is approximately perpendicular to the [Mg1-O101-O201] plane (dihedral angle, 94°). Bond distances to the XDK<sup>2-</sup> carboxylates are Mg1-O101 = 1.956(2) Å and Mg1-O201 = 2.003(2) Å, which are shorter than the average Mg-O<sub>carboxylate</sub> bond distance of 2.04 Å.<sup>25</sup> Mg2 is octahedrally coordinated by three methanol ligands (O1, O2, and O3) and one water molecule (O4) in addition to the bridging carboxylates from the XDK<sup>2-</sup> ligand (O102, O202). The Mg2 bond distances to the carboxylate oxygens are Mg2-O102 = 2.013(2) Å and Mg2-O202 = 2.027(2) Å. The water molecules on both metal ions (O4 and O6) are each hydrogen bonded to the imide carbonyl oxygens on the XDK ligand. The oxygen-oxygen hydrogen-bonded distances from O4 to O104 and O203 are 2.83 and 2.78 Å, respectively. The distances from O6 to O103 and O204 are 2.78 and 2.80 Å, respectively. A packing diagram of 1(NO<sub>3</sub>) is shown in Figure 3.

Although the crystal structure of 1 reveals the two magnesium ions to be in different environments, the <sup>1</sup>H NMR spectrum of this compound in CD<sub>3</sub>OD reveals that the metal ions are equivalent in solution, since the ligand appears to be in a symmetrical environment. This result suggests either that the coordinated nitrate

anion is displaced by methanol in solution or that it exchanges rapidly on the NMR timescale.

### Synthesis and Characterization of $[\text{Mg}_2(\text{XDK})\{\mu\text{-}\eta^2\text{-(PhO)}_2\text{PO}_2\}\text{(CH}_3\text{OH)}_3\text{(H}_2\text{O)}\text{(NO}_3\text{)}]\cdot 3\text{CH}_3\text{OH}, 2\cdot 3\text{CH}_3\text{OH}$

The addition of NaDPP (1 equiv) to a methanolic solution of **1** (1 equiv) gave the desired diphenyl phosphate-bridged product  $[\text{Mg}_2(\text{XDK})\{\mu\text{-}\eta^2\text{-(PhO)}_2\text{PO}_2\}\text{(CH}_3\text{OH)}_3\text{(H}_2\text{O)}\text{(NO}_3\text{)}]\cdot 3\text{CH}_3\text{OH}, (2\cdot 3\text{CH}_3\text{OH})$ . The IR spectrum of **2** revealed the presence of XDK, nitrate, diphenyl phosphate ( $1231\text{ cm}^{-1}$ ), and hydroxyl groups. The  $^1\text{H}$  NMR spectrum of **2** in  $\text{CD}_3\text{OD}$  suggested  $C_{2v}$  symmetry for the XDK ligand, as exemplified by the three singlets observed for the methyl groups of the ligand in a 1:2:1 intensity ratio ( $\delta$  1.23, 1.26, and 1.90). The proton NMR spectrum also showed multiplets in the aromatic region ( $\sim 7.0 - 7.2\text{ ppm}$ ) corresponding to the phenyl groups of diphenyl phosphate. The  $^{31}\text{P}\{^1\text{H}\}$  NMR spectrum of **2** in  $\text{CD}_3\text{OD}$  at room temperature suggested the presence of a coordinated diphenyl phosphate ligand with a signal at  $-15.46\text{ ppm}$ , which is  $6.32\text{ ppm}$  upfield from that of free diphenyl phosphate.

Crystals of  $2\cdot 3\text{CH}_3\text{OH}$  were grown by vapor diffusion of ethyl ether into a methanolic solution of **2**. An X-ray diffraction study confirmed the structure to contain a dinuclear magnesium XDK complex with a bidentate bridging diphenyl phosphate ligand. The structure of the complex  $[\text{Mg}_2(\text{XDK})\{\mu\text{-}\eta^2\text{-(PhO)}_2\text{PO}_2\}\text{(CH}_3\text{OH)}_3\text{(H}_2\text{O)}\text{(NO}_3\text{)}]$  (**2**) is shown in Figures 4a and 4b. Selected bond distances and angles are given in Table 4. The magnesium ions in **2** are situated  $4.240(5)\text{ \AA}$  apart. The metal ions are coordinated to the syn lone pairs of the carboxylates and are displaced from the plane of the carboxylate oxygens by  $0.75$  and  $0.55\text{ \AA}$ , for Mg1 and Mg2 respectively (Table 7). The dihedral angle of  $3.0^\circ$  between the planes of the two carboxylate groups indicate that they are approximately coplanar. Mg1 has a

distorted octahedral geometry similar to that of Mg1 in compound 1, with one methanol (O51), one bidentate nitrate group (O41, O42), XDK<sup>2-</sup> carboxylate oxygen atoms (O101, O201), and a phosphate ester oxygen atom (O12). The bidentate nitrate ligand is coordinated unsymmetrically to Mg1, with bond distances of Mg1-O41 = 2.237(8) Å and Mg1-O42 = 2.164(8) Å. The nitrate anion is approximately perpendicular to the magnesium-phosphinyl, [Mg1-O12-P1-O11-Mg2], plane (94°) and roughly parallel to the [Mg1-O101-O201] plane (15°). The Mg1 bond lengths to the XDK<sup>2-</sup> carboxylates are Mg1-O101 = 1.973(7) Å and Mg1-O201 = 1.976(7) Å. Mg2 is octahedrally coordinated by two methanol ligands (O61 and O63), one water molecule (O62), XDK<sup>2-</sup> carboxylate oxygen atoms (O102, O202), and a phosphate ester oxygen atom (O11). The Mg2 bond lengths to the XDK<sup>2-</sup> carboxylate oxygens are Mg2-O102 = 2.040(7) Å and Mg2-O202 = 2.039(7) Å. The Mg-O<sub>phosphate</sub> bond distances are 2.003(7) and 2.003(7) Å for Mg1 and Mg2, respectively. The O11-P1-O12 angle has been deformed from the usual tetrahedral value to 121.2(4)°, whereas two other angles are only slightly larger than tetrahedral (O11-P1-O14 = 110.9(4)° and O12-P1-O13 = 110.6(4)°), and three are smaller (O11-P1-O13 = 104.0(4)°, O12-P1-O14 = 105.3(4)°, and O13-P1-O14 = 103.5(4)°). The distortion around the phosphinyl center may result from the constraint imposed by bidentate coordination to the two magnesium atoms. The O11-P1-O12 bond angle is similar to those found in dimetallic complexes containing  $\mu$ - $\eta^2$  phosphate ester ligands (Table 8). The P1-O11 and P1-O12 bond distances are significantly shorter (1.481(7) and 1.467(6) Å, respectively) than the P1-O13 and P1-O14 distances (1.601(7) and 1.587(7) Å). Such differences in the P-O<sub>metal</sub> versus P-O<sub>C</sub> bond distances have also been observed in other phosphate-metal complexes.<sup>19,21,26-35</sup>

The diphenyl phosphate ligand is coordinated to the magnesium atoms through its syn lone pairs, which is a common coordination mode for phosphate-metal ion interactions.<sup>36</sup> The P1-O12-Mg1 and P1-O11-Mg2 bond angles are 141.1(4)

and  $138.8(4)^\circ$ , respectively, which are comparable to those observed in other phosphorus-oxygen-metal bond angles ( $141^\circ$ , average value).<sup>36</sup> The magnesium ions are approximately coplanar with the phosphinyl group, as indicated by the dihedral angle of  $4^\circ$  between the [P1-O11-O12] and [Mg1-Mg2-O11-O12] planes and the displacement of Mg1 and Mg2 from the [P1-O11-O12] plane (0.04 and 0.20 Å, respectively). This "in-plane" coordination mode for the magnesium atoms to phosphate is less common than the 0.9 Å "out-of-plane" location which has been observed in other phosphate-metal ion compounds.<sup>36</sup> The magnesium-phosphinyl plane is perpendicular to the plane of the xylyl ring (dihedral angle,  $90^\circ$ ).

#### Synthesis and Characterization of $[\text{Mg}_2(\text{XDK})(\mu\text{-}\eta^2\text{-(PhO)}_2\text{PO}_2)(\eta^1\text{-(PhO)}_2\text{PO}_2)\text{-(CH}_3\text{OH)}_3(\text{H}_2\text{O})]\cdot\text{CH}_3\text{OH}, (3\cdot\text{CH}_3\text{OH})$

Addition of 2 equiv of NaDPP to a methanol solution containing **1** gave  $[\text{Mg}_2(\text{XDK})(\mu\text{-}\eta^2\text{-(PhO)}_2\text{PO}_2)(\eta^1\text{-(PhO)}_2\text{PO}_2)(\text{CH}_3\text{OH)}_3(\text{H}_2\text{O})]\cdot\text{CH}_3\text{OH}, (3\cdot\text{CH}_3\text{OH})$ . The IR spectrum of **3** indicated the presence of XDK, diphenyl phosphate, and hydroxyl groups. The  $^1\text{H}$  NMR spectrum of **3** in  $\text{CD}_3\text{OD}$  showed three singlets for the methyl groups of XDK ( $\delta$  1.23, 1.26, and 1.90) integrating at a 1:2:1 ratio, suggesting a symmetrical  $\text{C}_{2v}$  environment for the ligand. The phenyl protons of diphenyl phosphate appeared as multiplet signals in the aromatic region ( $\sim 7.0 - 7.2$  ppm), integration of which revealed a ratio of 2 DPP to 1 XDK. The  $^{31}\text{P}\{^1\text{H}\}$  NMR spectrum of **3** in  $\text{CD}_3\text{OD}$  at room temperature contained 2 signals at -9.14 and -15.45 ppm, corresponding to free and bound diphenyl phosphate, respectively. The assignment was made by using the  $^{31}\text{P}\{^1\text{H}\}$  NMR spectrum of **2** ( $\delta$  -15.46) for the bound phosphate ester. Addition of one equiv of  $[\text{Me}_4\text{N}]\text{DPP}$  to a sample of **3** gave a  $^{31}\text{P}\{^1\text{H}\}$  NMR spectrum which integrated for a 2:1 ratio of free-to-bound phosphodiester groups. These results indicate that the bridging phosphate ester ligand is more stable to dissociation than the terminal one. Although the  $^{31}\text{P}\{^1\text{H}\}$

NMR signal of terminally bound diphenyl phosphate may be the same as that of free DPP<sup>-</sup>, conductivity measurements of **3** in methanol revealed it to be a 1:1 electrolyte (Figure 5), consistent with the observation of a dissociated diphenyl phosphate ligand.

Crystals of **3**·CH<sub>3</sub>OH were grown from a methanol/ethyl ether solvent system, and an X-ray crystallographic analysis of **3** revealed its structure to consist of a dinuclear magnesium center bridged by the carboxylate oxygens of the XDK ligand and one bidentate diphenyl phosphate. The structure of [Mg<sub>2</sub>(XDK){μ-η<sup>2</sup>-(PhO)<sub>2</sub>PO<sub>2</sub>}{η<sup>1</sup>-(PhO)<sub>2</sub>PO<sub>2</sub>}(CH<sub>3</sub>OH)<sub>3</sub>(H<sub>2</sub>O)] (**3**) is shown in Figures 6a and 6b. Selected bond distances and angles are given in Table 5. Mg1 is additionally coordinated by a terminal, monodentate DPP ligand (O21) and a water molecule (O51), which afford trigonal bipyramidal geometry. The Mg1 bond distances to the carboxylate oxygens are Mg1-O101 = 1.986(4) Å and Mg1-O201 = 1.979(4) Å. The Mg1-O12 bond length to the bridging diphenyl phosphate ligand is 2.015(4) Å, which is longer than the distance to the terminal DPP (Mg1-O21 = 1.949(4) Å). Mg2 has three methanol ligands (O61, O62, and O63) to complete its octahedral coordination sphere. The Mg2 bond lengths to the XDK carboxylate oxygens are Mg2-O102 = 2.052(5) Å and Mg2-O202 = 2.065(4) Å. The Mg2 bond length to O11 of the bridging diphenyl phosphate is 2.018(5) Å. The magnesium atoms are displaced from the plane of the carboxylates (*d* = 0.50 and 0.71 Å, for Mg1 and Mg2 respectively), with a Mg···Mg separation of 4.108(3) Å.

The O11-P1-O12 angle in the bidentate, bridging diphenyl phosphate ligand in **3** is 118.9(3)°, whereas the other angles only deviate slightly from tetrahedral values (O11-P1-O13 = 109.1(2)°, O11-P1-O14 = 112.0(2)°, O12-P1-O13 = 111.9(3)°, O12-P1-O14 = 105.4(2)°), with the exception of the O13-P1-O14 angle, which is 97.4(2)°. The P1-O11 and P1-O12 bond lengths are significantly shorter (1.472(4) and 1.470(4) Å, respectively) than the P1-O13 and P1-O14 distances (1.599(4) and 1.586(4) Å), similar

to those observed in **2**. The bridging diphenyl phosphate coordinates to the magnesium atoms in a syn manner, with P1-O12-Mg1 and P1-O11-Mg2 bond angles of 141.9(3) and 138.4(3)°, respectively. The [Mg1-O12-P1-O11-Mg2] plane is approximately perpendicular to plane of the xylyl ring (96°). Mg1 and Mg2 have been displaced from the [P1-O11-O12] plane by 0.74 and 0.70 Å, respectively, which is similar to that observed for other phosphate-metal complexes.<sup>36</sup>

In the monodentate, terminal diphenyl phosphate ligand, the phosphorus atom is roughly tetrahedral, with only one deviating angle (O21-P2-O22 = 115.8(3) Å). The P2-O21 bond length is 1.481(4) Å, which is only slightly longer than the P2-O22 bond length of 1.473(4) Å. The P2-O23 and P2-O24 bond lengths are 1.583(5) and 1.598(5) Å, respectively. There are relatively few dimetallic complexes containing a terminally coordinated phosphate ligand.<sup>19,21,37,38</sup> The structurally characterized examples are listed in Table 8.

#### Synthesis and Characterization of [Mg(HXDK)<sub>2</sub>(H<sub>2</sub>O)<sub>2</sub>], (**4**)

Addition of one equiv of bis(4-nitrophenyl) hydrogen phosphate (HBNPP) to a methanolic solution of **1** gave [Mg(HXDK)<sub>2</sub>(H<sub>2</sub>O)<sub>2</sub>], (**4**), the IR spectrum of which indicated the presence of XDK and hydroxyl groups. The <sup>1</sup>H NMR spectrum of **4** in CD<sub>2</sub>Cl<sub>2</sub> showed some broad features which corresponded to the XDK ligand and a signal at 19.0 ppm consistent with that of a carboxylate proton and characteristic of a short, low-barrier hydrogen bond.<sup>39</sup>

Crystals of **4** were grown by vapor diffusion of ethyl ether into a methanol solution containing **4**. The X-ray crystal structure of **4** revealed a mononuclear magnesium center coordinated by two HXDK ligands. The structure of [Mg(HXDK)<sub>2</sub>(H<sub>2</sub>O)<sub>2</sub>] (**4**) is shown in Figure 7. Selected bond distances and angles are given in Table 6. The magnesium ion sits on an inversion center and is octahedrally coordinated by the HXDK carboxylate ligands and two water molecules.



The Mg1-O102 and Mg1-O202 bond distances are 2.043(5) and 2.084(5) Å, respectively. The magnesium atom is displaced 0.38 Å from the dicarboxylate plane. The two carboxylate groups are approximately coplanar, with a dihedral angle of 4.7 ° between them. The distance between O101 and O201 is 2.423(8) Å.

The magnesium ions in **1** dissociate from XDK under acidic conditions as structurally evidenced by compound **4**. Protonation of one of the XDK carboxylates under acidic conditions is not unexpected since its  $pK_a$  value is unusually high ( $pK_a = 11.1$  in EtOH/H<sub>2</sub>O).<sup>40</sup>

### Relevance to Phosphatase Enzymes

The dinuclear magnesium compounds described here are structurally similar to several phosphate ester processing metalloenzyme active sites.<sup>1,2</sup> The dinuclear magnesium complex **1** is a possible structural model for dimagnesium-dependent metalloenzyme active sites in the absence of bound substrate. Compounds **2** and **3**, the first structurally characterized phosphate ester-bridged dimagnesium complexes, are potential biomimetic models for the binding of phosphodiester to magnesium-dependent phosphatases. The Mg...Mg separations in **2** and **3** are comparable to metal-metal distances in several dimetallic phosphatase enzymes (Table 1). The carboxylate-bridged dimagnesium compounds **1** - **3** have metal-metal distances which range from 4.11 to 4.78 Å. This range indicates that the carboxylates in the XDK ligand can readily accommodate changes in the metal coordination environment. Such intrinsic flexibility of carboxylate donors may help facilitate substrate binding and product release at similar carboxylate-bridged dimagnesium centers in the enzymes.

Whereas the structural models can provide some insightful information about the phosphatase enzymes, a functional model of these systems would be more useful for understanding the mechanism by which a dinuclear metal center can

effect phosphate ester hydrolysis. Reactivity studies of our model compounds towards phosphate ester substrates were carried out to address possible functional activity. Compound **1** hydrolyzes bis(4-nitrophenyl)phosphate (BNPP<sup>-</sup>) under basic conditions in methanol, and interestingly, there is no rate enhancement with **1** in comparison with free Mg(NO<sub>3</sub>)<sub>2</sub>·6H<sub>2</sub>O. The significance of this observation will be discussed in chapter 4 of this thesis.

## CONCLUSIONS

The dinucleating XDK ligand has been successfully employed in the synthesis of several novel carboxylate-bridged dimagnesium complexes. These include the first phosphate ester-bridged dinuclear magnesium compounds which are potential biomimetic models for phosphate ester processing metalloenzymes. Our dinuclear magnesium complexes should also serve as valuable models for fitting electron density in protein X-ray crystal structures, since the current resolution of many dimagnesium-dependent metalloenzymes structures is too low to reveal detailed geometries around the metal center. The dinuclear magnesium-XDK center was found to be unstable in the presence of acid, as evidenced by the protonation of the carboxylate ligand to liberate one magnesium ion.

## REFERENCES

- (1) Beese, L. S.; Steitz, T. A. *EMBO J.* **1991**, *10*, 25-33.
- (2) Davies, J. F.; Hostomska, Z.; Hostomsky, Z.; Jordan, S. R.; Matthews, D. A. *Science* **1991**, *252*, 88-95.
- (3) Pelletier, H.; Sawaya, M. R.; Kumar, A.; Wilson, S. H.; Kraut, J. *Science* **1994**, *264*, 1891-1903.
- (4) Xue, Y.; Huang, S.; Liang, J.-Y.; Zhang, Y.; Lipscomb, W. N. *Proc. Natl. Acad. Sci. USA* **1994**, *91*, 12482-12486.

- (5) Villeret, V.; Huang, S.; Zhang, Y.; Lipscomb, W. N. *Biochemistry* **1995**, *34*, 4307-4315.
- (6) Bone, R.; Frank, L.; Springer, J. P.; Atack, J. R. *Biochemistry* **1994**, *33*, 9468-9476.
- (7) York, J. D.; Ponder, J. W.; Chen, Z.-W.; Mathews, F. S.; Marjerus, P. W. *Biochemistry* **1994**, *33*, 13164-13171.
- (8) Steitz, T. A.; Steitz, J. A. *Proc. Natl. Acad. Sci. USA* **1993**, *90*, 6498-6502.
- (9) Lippard, S. J.; Berg, J. M. *Principles of Bioinorganic Chemistry*; University Science Books: Mill Valley, CA, 1994.
- (10) Black, C. B.; Huang, H.-W.; Cowan, J. A. *Coord. Chem. Rev.* **1994**, *135/136*, 165-202.
- (11) Kemp, D. S.; Petrakis, K. S. *J. Org. Chem.* **1981**, *46*, 5140-5143.
- (12) Rebek, J., Jr.; Marshall, L.; Wolak, R.; Parris, K.; Killoran, M.; Askew, B.; Nemeth, D.; Islam, N. *J. Am. Chem. Soc.* **1985**, *107*, 7476-7481.
- (13) Goldberg, D. P.; Watton, S. P.; Masschelein, A.; Wimmer, L.; Lippard, S. J. *J. Am. Chem. Soc.* **1993**, *115*, 5346-5347.
- (14) Watton, S. P.; Masschelein, A.; Rebek, J., Jr.; Lippard, S. J. *J. Am. Chem. Soc.* **1994**, *116*, 5196-5205.
- (15) Tanase, T.; Yun, J. W.; Lippard, S. J. *Inorg. Chem.* **1995**, *34*, 4220-4229.
- (16) Tanase, T.; Lippard, S. J. *Inorg. Chem.* **1995**, *34*, 4682-4690.
- (17) Hagen, K. S.; Lachicotte, R.; Kitaygorodskiy, A.; Elbouadili, A. *Angew. Chem. Int. Ed. Engl.* **1993**, *32*, 1321-1324.
- (18) Hagen, K. S.; Lachicotte, R.; Kitaygorodskiy, A. *J. Am. Chem. Soc.* **1993**, *115*, 12617-12618.
- (19) Tanase, T.; Watton, S. P.; Lippard, S. J. *J. Am. Chem. Soc.* **1994**, *116*, 9401-9402.
- (20) Watton, S. P.; Davis, M. I.; Pence, L. E.; Rebek, J., Jr.; Lippard, S. J. *Inorg. Chim. Acta* **1995**, *235*, 195-204.
- (21) Tanase, T.; Yun, J. W.; Lippard, S. J. *Inorg. Chem.* **1996**, in press.

- (22) Yun, J. W.; Tanase, T.; Pence, L. E.; Lippard, S. J. *J. Am. Chem. Soc.* **1995**, *117*, 4407-4408.
- (23) Carnahan, E. M.; Rardin, R. L.; Bott, S. G.; Lippard, S. J. *Inorg. Chem.* **1992**, *31*, 5193-5201.
- (24) TEXSAN *Single Crystal Structure Analysis Software*; Molecular Structure Corporation: The Woodlands, TX, 1992.
- (25) Carrell, C. J.; Carrell, H. L.; Erlebacher, J.; Glusker, J. P. *J. Am. Chem. Soc.* **1988**, *110*, 8651-8656.
- (26) Armstrong, W. H.; Lippard, S. J. *J. Am. Chem. Soc.* **1985**, *107*, 3730-3731.
- (27) Turowski, P. N.; Armstrong, W. H.; Roth, M. E.; Lippard, S. J. *J. Am. Chem. Soc.* **1990**, *112*, 681-690.
- (28) Turowski, P. N.; Armstrong, W. H.; Liu, S.; Brown, S. N.; Lippard, S. J. *Inorg. Chem.* **1994**, *33*, 636-645.
- (29) Druke, S.; Wieghardt, K.; Nuber, B.; Weiss, J.; Fleischhauser, H.-P.; Gehring, S.; Haase, W. *J. Am. Chem. Soc.* **1989**, *111*, 8622-8631.
- (30) Krebs, B.; Schepers, K.; Bremer, B.; Henkel, G.; Althaus, E.; Muller-Warmuth, W.; Griesar, K.; Haase, W. *Inorg. Chem.* **1994**, *33*, 1907-1914.
- (31) Norman, R. E.; Yan, S.; Que, L., Jr.; Backes, G.; Ling, J.; Sanders-Loehr, J.; Zhang, J. H.; O'Connor, C. J. *J. Am. Chem. Soc.* **1990**, *112*, 1554-1562.
- (32) Jang, H. G.; Hendrich, M. P.; Que, L., Jr. *Inorg. Chem.* **1993**, *32*, 911-918.
- (33) Mahroof-Tahir, M.; Karlin, K. D.; Chen, Q.; Zubieta, J. *Inorg. Chim. Acta* **1993**, *207*, 135-138.
- (34) Hikichi, S.; Tanaka, M.; Moro-oka, Y.; Kitajima, N. *J. Chem. Soc., Chem. Commun.* **1992**, 814-815.
- (35) Schepers, K.; Bremer, B.; Krebs, B.; Henkel, G.; Althaus, E.; Mosel, B.; Muller-Warmuth, W. *Angew. Chem. Int. Ed. Engl.* **1990**, *29*, 531-533.

- (36) Alexander, R. S.; Kanyo, Z. F.; Chirlian, L. E.; Christianson, D. W. *J. Am. Chem. Soc.* **1990**, *112*, 933-937.
- (37) Bremer, B.; Schepers, K.; Fleischhauer, P.; Haase, W.; Henkel, G.; Krebs, B. *J. Chem. Soc., Chem. Commun.* **1991**, 510-512.
- (38) Glowiak, T.; Podgorska, I.; Baranowski, J. *Inorg. Chim. Acta* **1986**, *115*, 1-10.
- (39) Cleland, W. W.; Kreevoy, M. M. *Science* **1994**, *264*, 1887-1890.
- (40) Rebek, J., Jr.; Duff, R. J.; Gordon, W. E.; Parris, K. *J. Am. Chem. Soc.* **1986**, *108*, 6068-6069.

Table 1. Examples of Magnesium-Dependent Phosphatase Enzymes.

Enzyme	M...M (Å) <sup>a</sup>	Metal-1 Ligands	Metal-2 Ligands	Ref.
Klenow Fragment of DNA Polymerase I	3.9	Asp 355 Asp 357 Asp 501 O-phosphate Water	Asp 355 O-phosphate O-phosphate	1
Ribonuclease H	4	Asp 355 Glu 478	Asp 355 Asp 443 Asp 549	2
Rat DNA Polymerase β	4	Asp 190 Asp 192 O-phosphate O-phosphate Water	Asp 190 Asp 192 Asp 256 O-phosphate O-phosphate Water	3
Fructose-1,6-Bisphosphatase	4.3	Asp 118 Glu 97 Asp 121 Glu 280 O-phosphate	Asp 118 Glu 97 Glu 98 Leu 120	4-5
Inositol Monophosphatase	3.8	Asp 90 Glu 70 Ile 92 O-phosphate Water Water	Asp 90 Asp 93 Asp 220 O-phosphate O-inositol	6
Inositol Polyphosphate 1-Phosphatase	3.9	Glu 79 Asp 153 Asp 156 Asp 317 Water	Glu 79 Asp 54 Ile 155 Water	7

<sup>a</sup>Metal-metal separation.

Table 2. Crystallographic and Experimental Data for 1(NO<sub>3</sub>), 2·3CH<sub>3</sub>OH, 3·CH<sub>3</sub>OH, and 4

compound	1(NO <sub>3</sub> )	2·3CH <sub>3</sub> OH	3·CH <sub>3</sub> OH	4
formula	C <sub>36</sub> H <sub>58</sub> N <sub>4</sub> O <sub>20</sub> Mg <sub>2</sub>	C <sub>50</sub> H <sub>74</sub> N <sub>3</sub> O <sub>22</sub> Mg <sub>2</sub> P <sub>1</sub>	C <sub>60</sub> H <sub>76</sub> N <sub>2</sub> O <sub>21</sub> Mg <sub>2</sub> P <sub>2</sub>	C <sub>64</sub> H <sub>82</sub> N <sub>4</sub> O <sub>18</sub> Mg <sub>1</sub>
fw	915.48	1148.73	1271.82	1219.68
crystal size (mm)	0.3 x 0.3 x 0.4	0.2 x 0.4 x 0.5	0.3 x 0.4 x 0.5	0.2 x 0.2 x 0.2
crystal system	monoclinic	monoclinic	monoclinic	monoclinic
space group	<i>P</i> 2 <sub>1</sub> / <i>c</i>	<i>P</i> 2 <sub>1</sub> / <i>c</i>	<i>P</i> 2 <sub>1</sub> / <i>n</i>	<i>P</i> 2 <sub>1</sub> / <i>n</i>
<i>a</i> , Å	11.240 (3)	16.611 (5)	18.912 (4)	15.210 (5)
<i>b</i> , Å	13.019 (2)	16.059 (6)	16.254 (2)	15.772 (3)
<i>c</i> , Å	30.208 (7)	21.930 (9)	21.646 (5)	13.093 (3)
$\beta$ , deg	99.11 (1)	93.34 (6)	112.26 (2)	96.35 (3)
<i>V</i> , Å <sup>3</sup>	4365 (2)	5840 (4)	6158 (2)	3122 (1)
<i>Z</i>	4	4	4	2
<i>T</i> , °C	-71.4	-82.6	-74.2	-110
<i>D</i> <sub>calcd</sub> , g cm <sup>-3</sup>	1.391	1.31	1.37	1.30
abs coeff, cm <sup>-1</sup>	1.303	1.46	1.69	1.03
trans factor	0.94 - 1.00	0.82 - 1.00	0.91 - 1.00	0.78 - 1.00
2 $\theta$ range, deg	3 < 2 $\theta$ < 50	3 < 2 $\theta$ < 45	3 < 2 $\theta$ < 46	3 < 2 $\theta$ < 45
no. of unique data	8833	8317	8880	4254
no. of obsd data	5203	3682	5184	1840
<i>R</i> <sub>merge</sub> (%)	( <i>I</i> > 3 $\sigma$ ( <i>I</i> )) 0.030	( <i>I</i> > 2 $\sigma$ ( <i>I</i> )) 0.030	( <i>I</i> > 3 $\sigma$ ( <i>I</i> )) 0.026	( <i>I</i> > 2 $\sigma$ ( <i>I</i> )) 0.078
no. of variables	791	673	785	278
<i>R</i> <sup>a</sup>	0.039	0.068	0.060	0.069
<i>R</i> <sub>w</sub> <sup>a</sup>	0.045	0.076	0.072	0.070

<sup>a</sup> $R = \Sigma ||F_o| - |F_c|| / \Sigma |F_o|$ ;  $R_w = [\Sigma w(|F_o| - |F_c|)^2 / \Sigma w |F_o|^2]^{1/2}$ , where  $w = 1/\sigma^2(F_o)$ . More details about the weighting scheme and other experimental protocols may be found in Carnahan, E. M.; Rardin, R. L.; Bott, S. G.; Lippard, S. J., *Inorg. Chem.* 1992, 31, 5193.

Table 3. Selected Bond Distances (Å) and Angles (deg) for 1(NO<sub>3</sub>).<sup>a</sup>

Bond Distances							
Mg1	O5	2.098(3)	Mg2	O1	2.069(3)		
Mg1	O6	2.056(2)	Mg2	O2	2.119(3)		
Mg1	O11	2.144(3)	Mg2	O3	2.113(2)		
Mg1	O12	2.242(3)	Mg2	O4	2.065(2)		
Mg1	O101	2.003(2)	Mg2	O102	2.013(2)		
Mg1	O201	1.956(2)	Mg2	O202	2.027(2)		
Angles							
O5	Mg1	O6	88.24(9)	O3	Mg2	O202	171.5(1)
O5	Mg1	O11	84.15(9)	O4	Mg2	O102	93.8(1)
O5	Mg1	O12	89.0(1)	O4	Mg2	O202	91.8(1)
O5	Mg1	O101	169.3(1)	O102	Mg2	O202	98.7(1)
O5	Mg1	O201	92.7(1)	Mg2	O1	C1	122.9(2)
O6	Mg1	O11	161.2(1)	Mg2	O2	C2	130.7(2)
O6	Mg1	O12	103.96(9)	Mg2	O3	C3	128.8(2)
O6	Mg1	O101	90.74(9)	Mg1	O5	C4	131.6(2)
O6	Mg1	O201	98.7(1)	Mg1	O11	N11	93.6(2)
O11	Mg1	O12	58.84(9)	Mg1	O12	N11	90.3(2)
O11	Mg1	O101	93.56(9)	Mg1	O101	C101	152.1(2)
O11	Mg1	O201	98.84(9)	Mg2	O102	C101	159.8(2)
O12	Mg1	O101	80.89(9)	Mg1	O201	C201	161.2(2)
O12	Mg1	O201	157.3(1)	Mg2	O202	C201	151.8(2)
O101	Mg1	O201	98.0(1)				
O1	Mg2	O2	86.0(1)				
O1	Mg2	O3	91.4(1)				
O1	Mg2	O4	172.6(1)				
O1	Mg2	O102	90.6(1)				
O1	Mg2	O202	93.4(1)				
O2	Mg2	O3	82.4(1)				
O2	Mg2	O4	88.7(1)				
O2	Mg2	O102	170.0(1)				
O2	Mg2	O202	90.9(1)				
O3	Mg2	O4	82.82(9)				
O3	Mg2	O102	88.3(1)				

<sup>a</sup>Estimated standard deviations are given in parentheses. See Figures 1 and 2 for atom labels.



Table 4. Selected Bond Distances (Å) and Angles (deg) for 2·3CH<sub>3</sub>OH.<sup>a</sup>

Bond Distances							
Mg(1)	O(12)	2.003(7)	Mg(1)	O(101)	1.973(7)		
Mg(1)	O(41)	2.237(8)	Mg(1)	O(201)	1.976(7)		
Mg(1)	O(42)	2.164(8)	Mg(2)	O(11)	2.003(7)		
Mg(1)	O(51)	2.118(8)	Mg(2)	O(61)	2.131(7)		
P(1)	O(11)	1.481(7)	Mg(2)	O(62)	2.125(7)		
P(1)	O(12)	1.467(6)	Mg(2)	O(63)	2.121(8)		
P(1)	O(13)	1.601(7)	Mg(2)	O(102)	2.040(7)		
P(1)	O(14)	1.587(7)	Mg(2)	O(202)	2.039(7)		
Angles							
O(11)	P(1)	O(12)	121.2(4)	O(61)	Mg(2)	O(62)	86.4(3)
O(11)	P(1)	O(13)	104.0(4)	O(61)	Mg(2)	O(63)	85.3(3)
O(11)	P(1)	O(14)	110.9(4)	O(61)	Mg(2)	O(102)	85.2(3)
O(12)	P(1)	O(13)	110.6(4)	O(61)	Mg(2)	O(202)	170.1(3)
O(12)	P(1)	O(14)	105.3(4)	O(62)	Mg(2)	O(63)	87.4(3)
O(13)	P(1)	O(14)	103.5(4)	O(62)	Mg(2)	O(102)	88.4(3)
O(12)	Mg(1)	O(41)	89.0(3)	O(62)	Mg(2)	O(202)	86.1(3)
O(12)	Mg(1)	O(42)	91.5(3)	O(63)	Mg(2)	O(102)	169.9(3)
O(12)	Mg(1)	O(51)	176.3(3)	O(63)	Mg(2)	O(202)	87.9(3)
O(12)	Mg(1)	O(101)	94.6(3)	O(102)	Mg(2)	O(202)	101.0(3)
O(12)	Mg(1)	O(201)	98.4(3)	P(1)	O(11)	Mg(2)	138.8(4)
O(41)	Mg(1)	O(42)	58.2(3)	P(1)	O(12)	Mg(1)	149.1(4)
O(41)	Mg(1)	O(51)	87.3(3)	P(1)	O(13)	C(7)	126.9(6)
O(41)	Mg(1)	O(101)	153.9(3)	P(1)	O(14)	C(1)	124.8(6)
O(41)	Mg(1)	O(201)	94.4(3)	Mg(1)	O(41)	N(41)	91.6(7)
O(42)	Mg(1)	O(51)	86.0(3)	Mg(1)	O(42)	N(41)	93.8(7)
O(42)	Mg(1)	O(101)	95.9(3)	Mg(1)	O(51)	C(51)	128.9(7)
O(42)	Mg(1)	O(201)	150.8(3)	Mg(2)	O(61)	C(61)	130.2(7)
O(51)	Mg(1)	O(101)	88.5(3)	Mg(2)	O(63)	C(63)	125.4(7)
O(51)	Mg(1)	O(201)	82.5(3)	Mg(1)	O(101)	C(101)	136.3(7)
O(101)	Mg(1)	O(201)	110.5(3)	Mg(2)	O(102)	C(101)	153.2(6)
O(11)	Mg(2)	O(61)	93.0(3)	Mg(1)	O(201)	C(201)	140.6(6)
O(11)	Mg(2)	O(62)	178.2(3)	Mg(2)	O(202)	C(201)	150.2(7)
O(11)	Mg(2)	O(63)	90.9(3)				
O(11)	Mg(2)	O(102)	93.2(3)				
O(11)	Mg(2)	O(202)	94.3(3)				

<sup>a</sup>Estimated standard deviations are given in parentheses. See Figures 1 and 4 for atom labels.

Table 5 Selected Bond Distances (Å) and Angles (deg) for 3-CH<sub>3</sub>OH.<sup>a</sup>

Bond Distances							
Mg(1)	O(12)	2.015(4)	Mg(2)	O(11)	2.018(5)		
Mg(1)	O(21)	1.949(4)	Mg(2)	O(61)	2.153(6)		
Mg(1)	O(51)	2.145(5)	Mg(2)	O(62)	2.125(5)		
Mg(1)	O(101)	1.986(4)	Mg(2)	O(63)	2.024(6)		
Mg(1)	O(201)	1.979(4)	Mg(2)	O(102)	2.052(5)		
P(1)	O(11)	1.472(4)	Mg(2)	O(202)	2.065(4)		
P(1)	O(12)	1.470(4)	P(2)	O(21)	1.481(4)		
P(1)	O(13)	1.599(4)	P(2)	O(22)	1.473(4)		
P(1)	O(14)	1.586(4)	P(2)	O(23)	1.583(5)		
			P(2)	O(24)	1.598(5)		
Angles							
O(11)	P(1)	O(12)	118.9(3)	O(11)	Mg(2)	O(202)	95.0(2)
O(11)	P(1)	O(13)	109.1(2)	O(61)	Mg(2)	O(62)	81.7(2)
O(11)	P(1)	O(14)	112.0(2)	O(61)	Mg(2)	O(63)	84.2(3)
O(12)	P(1)	O(13)	111.9(3)	O(61)	Mg(2)	O(102)	89.0(2)
O(12)	P(1)	O(14)	105.4(2)	O(61)	Mg(2)	O(202)	169.1(2)
O(13)	P(1)	O(14)	97.4(2)	O(62)	Mg(2)	O(63)	86.8(2)
O(21)	P(2)	O(22)	115.8(3)	O(62)	Mg(2)	O(102)	166.8(2)
O(21)	P(2)	O(23)	109.9(3)	O(62)	Mg(2)	O(202)	88.1(2)
O(21)	P(2)	O(24)	111.3(2)	O(63)	Mg(2)	O(102)	82.8(2)
O(22)	P(2)	O(23)	112.8(3)	O(63)	Mg(2)	O(202)	91.5(3)
O(22)	P(2)	O(24)	110.2(3)	O(102)	Mg(2)	O(202)	100.3(2)
O(23)	P(2)	O(24)	95.1(2)	P(1)	O(11)	Mg(2)	138.4(3)
O(12)	Mg(1)	O(21)	92.6(2)	P(1)	O(12)	Mg(1)	141.9(3)
O(12)	Mg(1)	O(51)	176.5(2)	P(1)	O(13)	C(11)	123.7(4)
O(12)	Mg(1)	O(101)	93.7(2)	P(1)	O(14)	C(21)	127.2(4)
O(12)	Mg(1)	O(201)	95.6(2)	P(2)	O(21)	Mg(1)	151.7(3)
O(21)	Mg(1)	O(51)	84.8(2)	P(2)	O(23)	C(31)	121.2(4)
O(21)	Mg(1)	O(101)	112.5(2)	P(2)	O(24)	C(41)	119.8(4)
O(21)	Mg(1)	O(201)	123.9(2)	Mg(2)	O(61)	C(61)	132.7(6)
O(51)	Mg(1)	O(101)	85.1(2)	Mg(2)	O(62)	C(62)	132.6(4)
O(51)	Mg(1)	O(201)	87.8(2)	Mg(2)	O(63)	C(63)	129.8(8)
O(101)	Mg(1)	O(201)	122.2(2)	Mg(1)	O(101)	C(101)	127.7(4)
O(11)	Mg(2)	O(61)	89.5(2)	Mg(2)	O(102)	C(101)	153.9(4)
O(11)	Mg(2)	O(62)	93.6(2)	Mg(1)	O(201)	C(201)	146.0(4)
O(11)	Mg(2)	O(63)	173.6(3)	Mg(2)	O(202)	C(201)	141.8(4)
O(11)	Mg(2)	O(102)	95.8(2)				

<sup>a</sup>Estimated standard deviations are given in parentheses. See Figures 1 and 6 for atom labels.

**Table 6.** Selected Bond Distances (Å) and Angles (deg) for 4.<sup>a</sup>**Bond Distances**

Mg(1)	O(1)	2.090(6)
Mg(1)	O(102)	2.043(5)
Mg(1)	O(202)	2.084(5)

**Angles**

O(1)	Mg(1)	O(102)	86.6(2)
O(1)	Mg(1)	O(102)*	93.4(2)
O(1)	Mg(1)	O(202)	88.3(2)
O(1)	Mg(1)	O(202)*	91.7(2)
O(102)	Mg(1)	O(202)	94.4(2)
O(102)	Mg(1)	O(202)*	85.6(2)
Mg(1)	O(102)	C(101)	151.2(6)
Mg(1)	O(202)	C(201)	149.3(6)

<sup>a</sup>Estimated standard deviations are given in parentheses. See Figures 1 and 7 for atom labels.

Table 7. Structural Parameters of 1(NO<sub>3</sub>), 2·3CH<sub>3</sub>OH, and 3·CH<sub>3</sub>OH

	1	2	3
Mg1...Mg2, Å	4.783(2)	4.240(5)	4.108(3)
Mg1-O(XDK) <sub>av</sub> , Å <sup>a</sup>	1.980(3)	1.975(10)	1.983(6)
Mg2-O(XDK) <sub>av</sub> , Å <sup>a</sup>	2.020(3)	2.040(10)	2.059(6)
O101-Mg1-O201, deg	98.0(1)	110.5(3)	122.2(2)
O102-Mg2-O202, deg	98.7(1)	101.0(3)	100.3(2)
O11-P1-O12, deg		121.2(4)	118.9(3)
P1-O12-Mg1, deg		149.1(4)	141.9(3)
P1-O11-Mg2, deg		138.8(4)	138.4(3)
$\phi$ , deg <sup>b</sup>	9.8	22.7	19.4
$d(\text{Mg1})$ , Å <sup>c</sup>	0.31	0.75	0.50
$d(\text{Mg2})$ , Å <sup>c</sup>	0.21	0.55	0.71
[O(101)O(102)C(101)C(107)] vs [O(201)O(202)C(201)C(207)], deg <sup>d</sup>	6.5	3.0	8.3

<sup>a</sup> Average value. Estimated deviations in parentheses are derived from  $(\sigma_A^2 + \sigma_B^2)^{1/2}$ . <sup>b</sup> Dihedral angle between the [Mg1Mg2(OCO<sub>2</sub>)<sub>2</sub>] and the dicarboxylate planes (average value). <sup>c</sup> Distance from the metal atom to the dicarboxylate plane. <sup>d</sup> Dihedral angle.

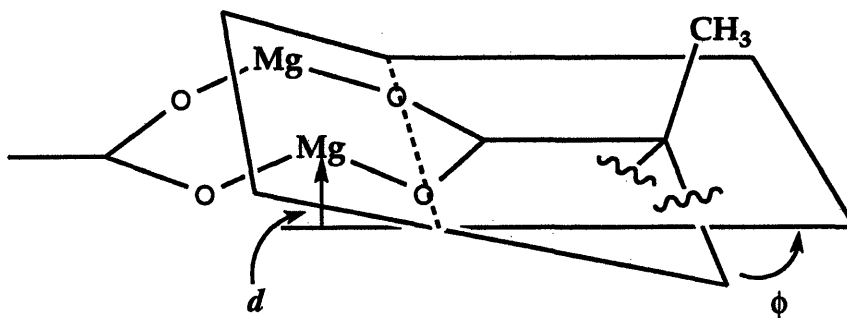


Table 8. Examples of Dinuclear Metal Complexes Containing Phosphate Ester Ligands

Complex	M...M, Å <sup>a</sup>	P binding mode <sup>b</sup>	O <sub>m</sub> -P-O <sub>m</sub> angle (°) <sup>c</sup>	additional bridges <sup>d</sup>
[Fe <sup>III</sup> ] <sub>2</sub> O(DPP) <sub>2</sub> (HBpz <sub>3</sub> ) <sub>2</sub> ] <sup>e</sup>	3.335(1)	(μ-η <sup>2</sup> ) <sub>2</sub>	120.1(3) <sup>f</sup>	μ-oxo
[Fe <sup>III</sup> ] <sub>2</sub> O(Ph <sub>2</sub> PO <sub>2</sub> ) <sub>2</sub> (HBpz <sub>3</sub> ) <sub>2</sub> ] <sup>e</sup>	3.292(2)	(μ-η <sup>2</sup> ) <sub>2</sub>	116.5(2)	μ-oxo
[Fe <sup>III</sup> ] <sub>2</sub> (BHPP)(DPP) <sub>2</sub> (BPh <sub>4</sub> ) <sup>g</sup>	3.549(3)	(μ-η <sup>2</sup> ) <sub>2</sub>	117.3(6) <sup>f</sup>	μ-alkoxo
[Fe <sup>III</sup> ] <sub>2</sub> (BHPMP)(DPP) <sub>2</sub> (ClO <sub>4</sub> ) <sup>g</sup>	3.837(8)	(μ-η <sup>2</sup> ) <sub>2</sub>	119.3(8) <sup>f</sup>	μ-alkoxo
[Fe <sup>III</sup> ] <sub>2</sub> (OH)(DPP) <sub>2</sub> (HBpz <sub>3</sub> ) <sub>2</sub> [(BF <sub>4</sub> ) <sup>h</sup>	3.586(1)	(μ-η <sup>2</sup> ) <sub>2</sub>	116.7(4) <sup>f</sup>	μ-hydroxo
[Fe <sup>III</sup> ] <sub>2</sub> (OH)(Ph <sub>2</sub> PO <sub>2</sub> ) <sub>2</sub> (HBpz <sub>3</sub> ) <sub>2</sub> [(BF <sub>4</sub> ) <sup>h</sup>	3.5599(9)	(μ-η <sup>2</sup> ) <sub>2</sub>	116.7(2)	μ-hydroxo
[Fe <sup>III</sup> ] <sub>2</sub> (DPP) <sub>3</sub> (HBpz <sub>3</sub> ) <sub>2</sub> [(BF <sub>4</sub> ) <sup>h</sup>	4.6771(9)	(μ-η <sup>2</sup> ) <sub>3</sub>	117.7(1) <sup>f</sup>	none
[Fe <sup>II</sup> ] <sub>2</sub> (BPMP)(DPP) <sub>2</sub> ]Cl <sup>i</sup>	3.683(4)	(μ-η <sup>2</sup> ) <sub>2</sub>	121.6(3) <sup>f</sup>	μ-alkoxo
[Cu <sup>II</sup> ] <sub>2</sub> (UNO)(BNPP)](PF <sub>6</sub> ) <sub>2</sub> <sup>j</sup>	3.773(4)	(μ-η <sup>2</sup> )	121.0(6)	μ-alkoxo
[Zn <sup>II</sup> ] <sub>2</sub> {(p-NO <sub>2</sub> PhO)PO <sub>3</sub> }{HB( <i>t</i> Pr <sub>2</sub> pz) <sub>3</sub> ] <sub>2</sub> ] <sup>k</sup>	5.1	(μ-η <sup>2</sup> )	110.8	none

$[\text{Zn}^{\text{II}}\text{Co}^{\text{II}}(\text{XDK})(\text{DPP})_2(\text{MeOH})_2(\text{H}_2\text{O})]^\text{f}$	3.846(1)	$(\mu-\eta^2)(\eta^1)$	118.7(3)	$(\mu\text{-carboxylato})_2$
$[\text{Zn}^{\text{II}}_2(\text{XDK})(\text{DPP})_2(\text{MeOH})_2(\text{H}_2\text{O})]^\text{f}$	3.869(2)	$(\mu-\eta^2)(\eta^1)$	118.8(3)	$(\mu\text{-carboxylato})_2$
$[\text{Mg}^{\text{II}}_2(\text{XDK})(\text{DPP})(\text{NO}_3)(\text{MeOH})_3(\text{H}_2\text{O})] (2)^\text{m}$	4.240(5)	$(\mu-\eta^2)$	121.2(4)	$(\mu\text{-carboxylato})_2$
$[\text{Mg}^{\text{II}}_2(\text{XDK})(\text{DPP})_2(\text{MeOH})_3(\text{H}_2\text{O})] (3)^\text{m}$	4.108(3)	$(\mu-\eta^2)(\eta^1)$	118.9(3)	$(\mu\text{-carboxylato})_2$
$[\text{Fe}^{\text{III}}_2\text{Cl}_2(\text{TBPO})(\text{DPP})(\text{MeOH})](\text{ClO}_4)_2^\text{n}$	3.700(2)	$(\eta^1)$		$\mu\text{-alkoxo}$
$[\text{Cu}^{\text{II}}_2(\beta\text{-ala})_4(\text{DPP})_2](\text{DPP})_2^\text{o}$	2.688(1)	$(\eta^1)_2$		$(\mu\text{-carboxylato})_4$

<sup>a</sup>Metal-metal separation (Å). <sup>b</sup>Binding mode of phosphate esters to dinuclear metal center. <sup>c</sup>Bond angle (°) at O<sub>metal</sub>-P-O<sub>metal</sub> center. <sup>d</sup>Additional bridging ligands other than phosphate esters. <sup>e</sup>Ref. 26 and 27. HBPz<sub>3</sub> = hydrotris(1-pyrazolyl)borate. HDPP = diphenyl hydrogen phosphate. <sup>f</sup>Average O<sub>metal</sub>-P-O<sub>metal</sub> angle. Estimated deviations in parentheses are derived from  $(\sigma_{\text{A}}^2 + \sigma_{\text{B}}^2)^{1/2}$ . <sup>g</sup>Ref. 30. H<sub>3</sub>BHPP = 1,3-bis[(2-hydroxybenzyl)(2-pyridylmethyl)amino]-2-propanol. H<sub>3</sub>BHPMP = 2,6-bis[(2-hydroxybenzyl)(2-pyridylmethyl)amino)methyl]-4-methylphenol. <sup>h</sup>Ref. 28. <sup>i</sup>Ref. 32. HBPMP = 2,6-bis[(bis(2-pyridylmethyl)amino)methyl]-4-methylphenol. <sup>j</sup>Ref. 33. HUNO = 2-[bis(2-pyridylethyl)aminomethyl]-6-[bis(2-pyridylethyl)amino]-phenol. HBNPP = bis(4-nitrophenyl) hydrogen phosphate. <sup>k</sup>Ref. 34. HB (*i*Pr<sub>2</sub>pz)<sub>3</sub> = hydrotris(3,5-diisopropyl-1-pyrazolyl)borate. <sup>l</sup>Ref. 21. <sup>m</sup>This work. <sup>n</sup>Ref. 37. HTBPO = N,N,N',N'-tetrakis(2-benzimidazolylmethyl)-2-hydroxy-1,3-diaminopropane. <sup>o</sup>Ref 38.  $\beta\text{-ala} = \text{-OOC}(\text{CH}_2)_2\text{NH}_3^+$ .

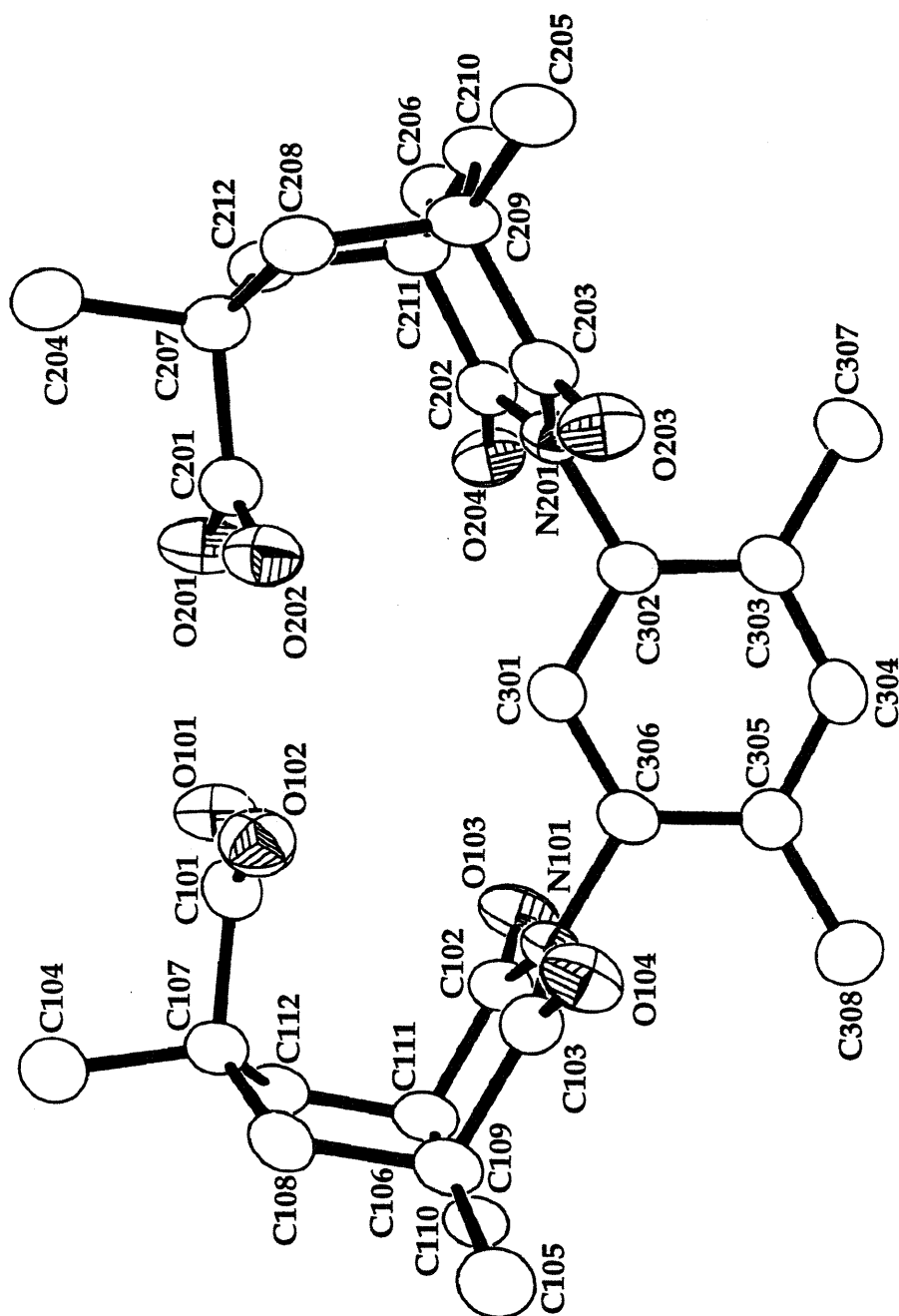
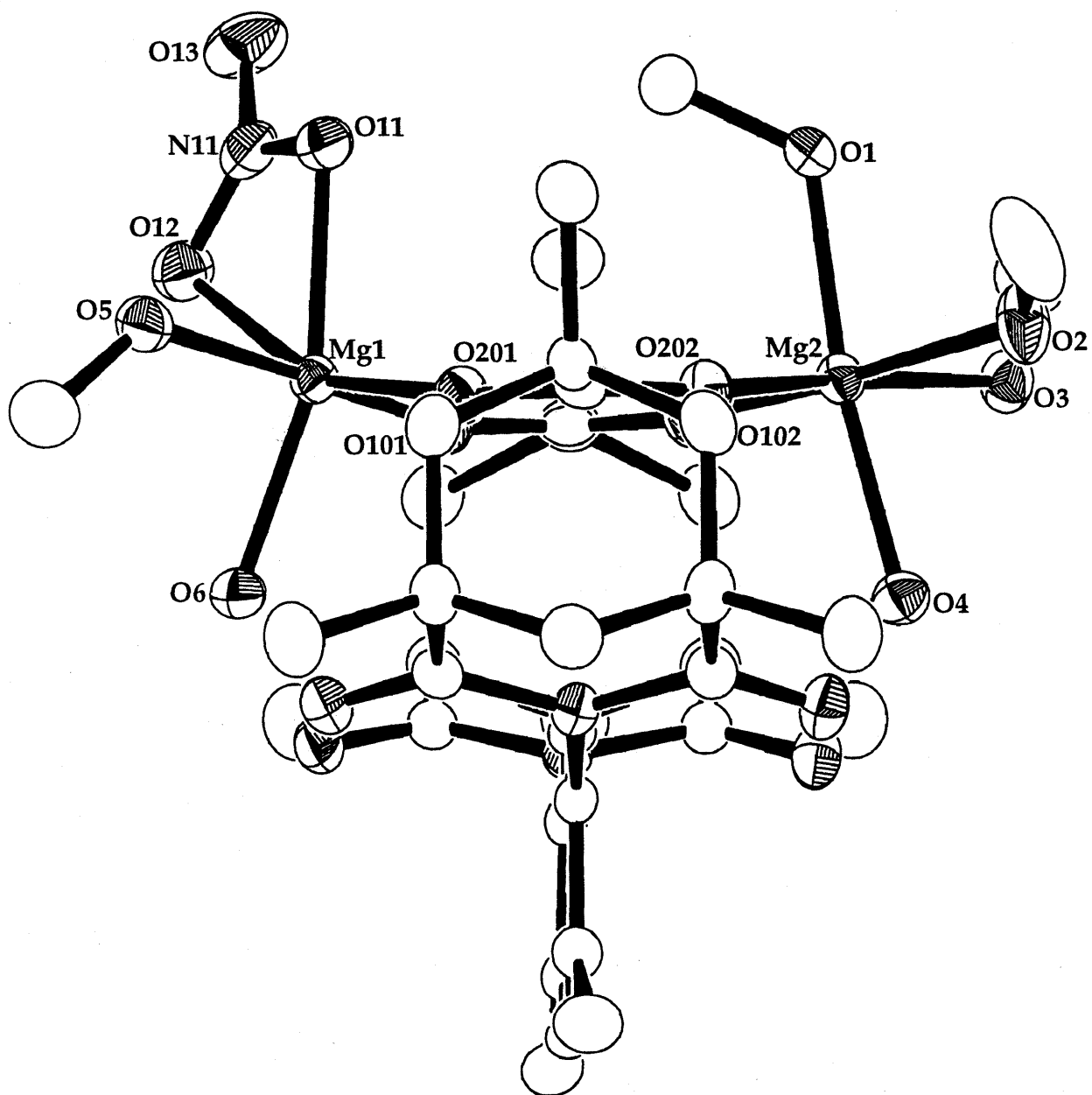
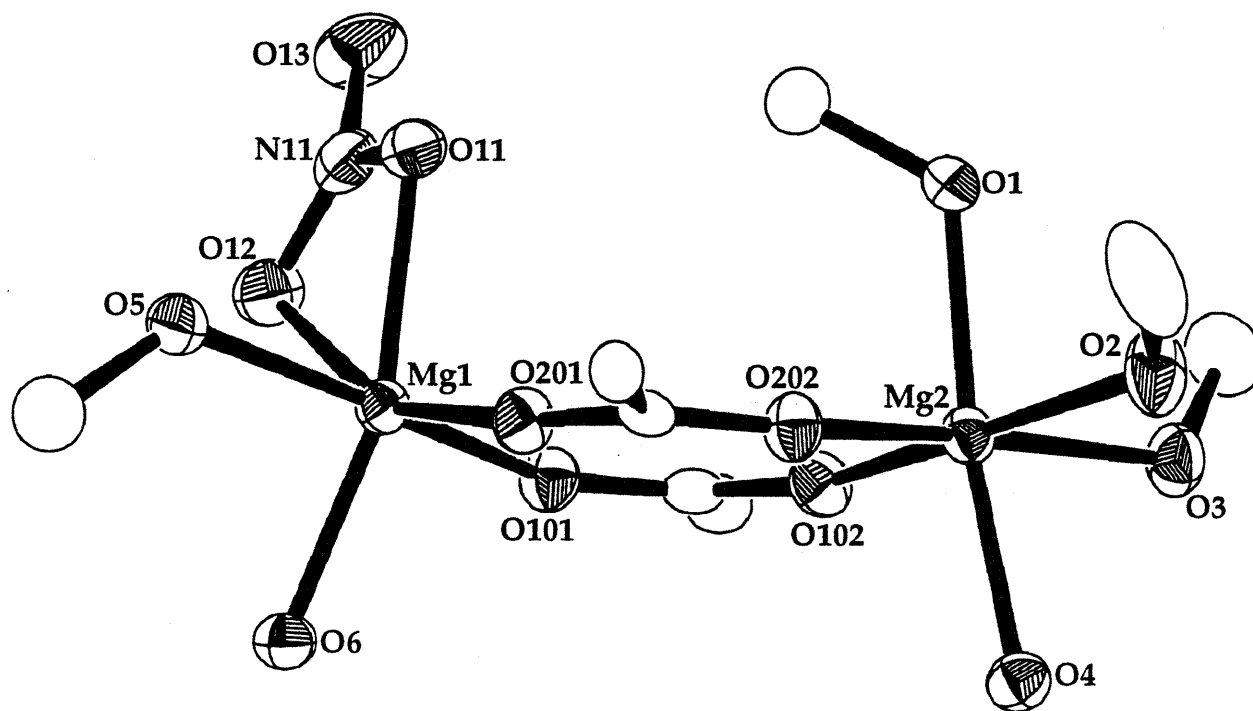


Figure 1. A view of the XDK ligand, along with the atomic numbering scheme.



**Figure 2a.** An ORTEP view of  $[\text{Mg}_2(\text{XDK})(\text{CH}_3\text{OH})_4(\text{H}_2\text{O})_2(\text{NO}_3)]^+$  (**1**). Thermal ellipsoids are drawn at the 50% probability level, and hydrogen atoms are omitted for clarity.





**Figure 2b.** ORTEP view of the dinuclear core of **1**. Hydrogen atoms and all atoms of the XDK ligand, except for the carboxylate groups, have been omitted for clarity.

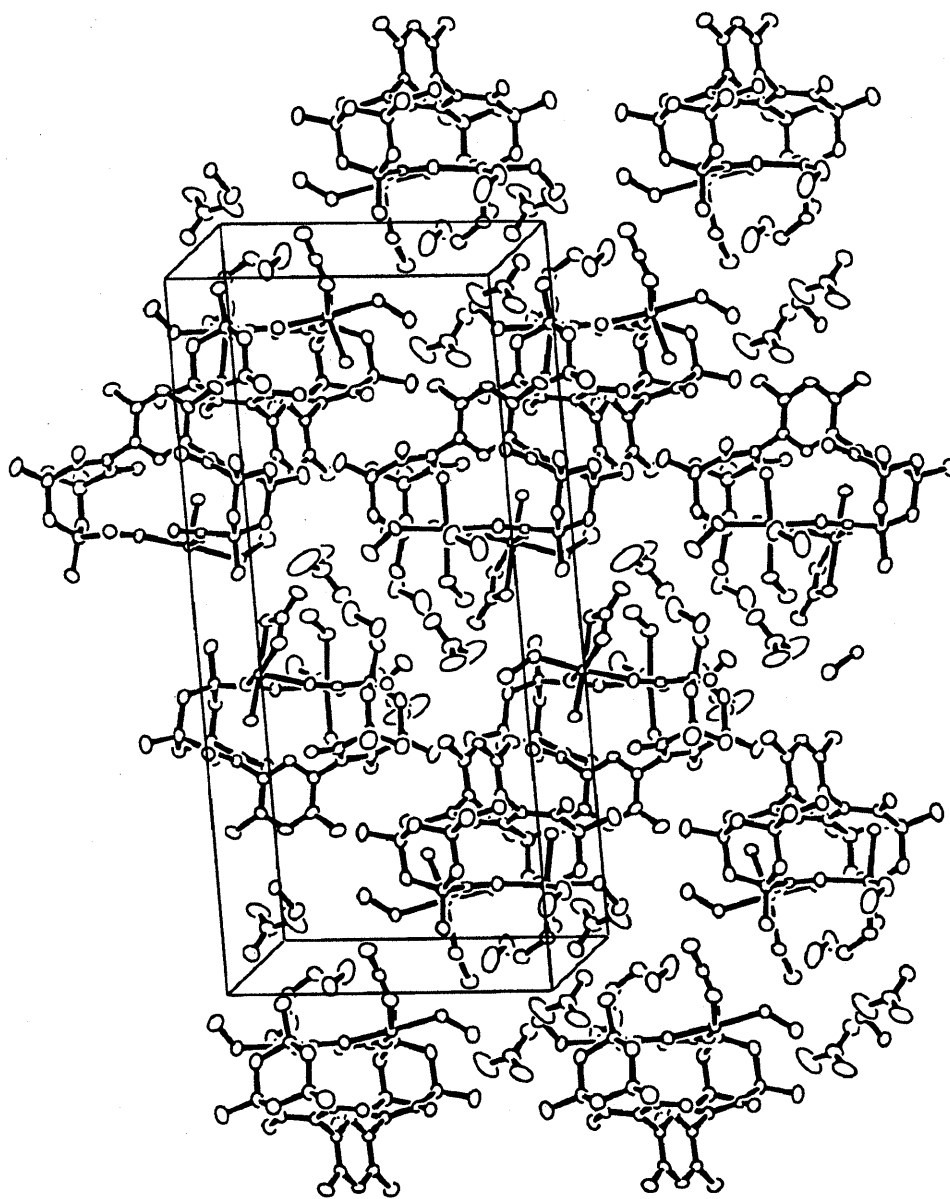
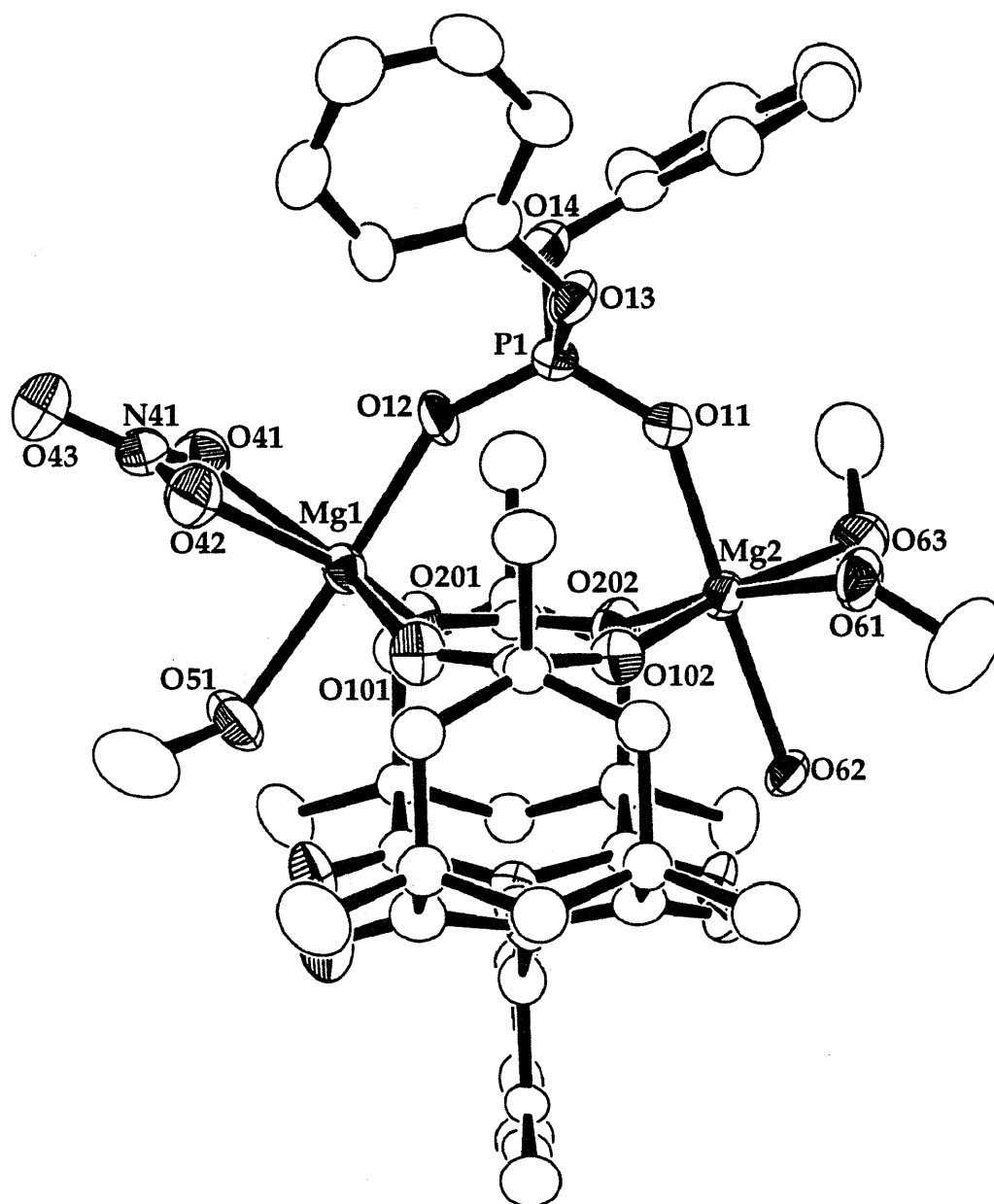
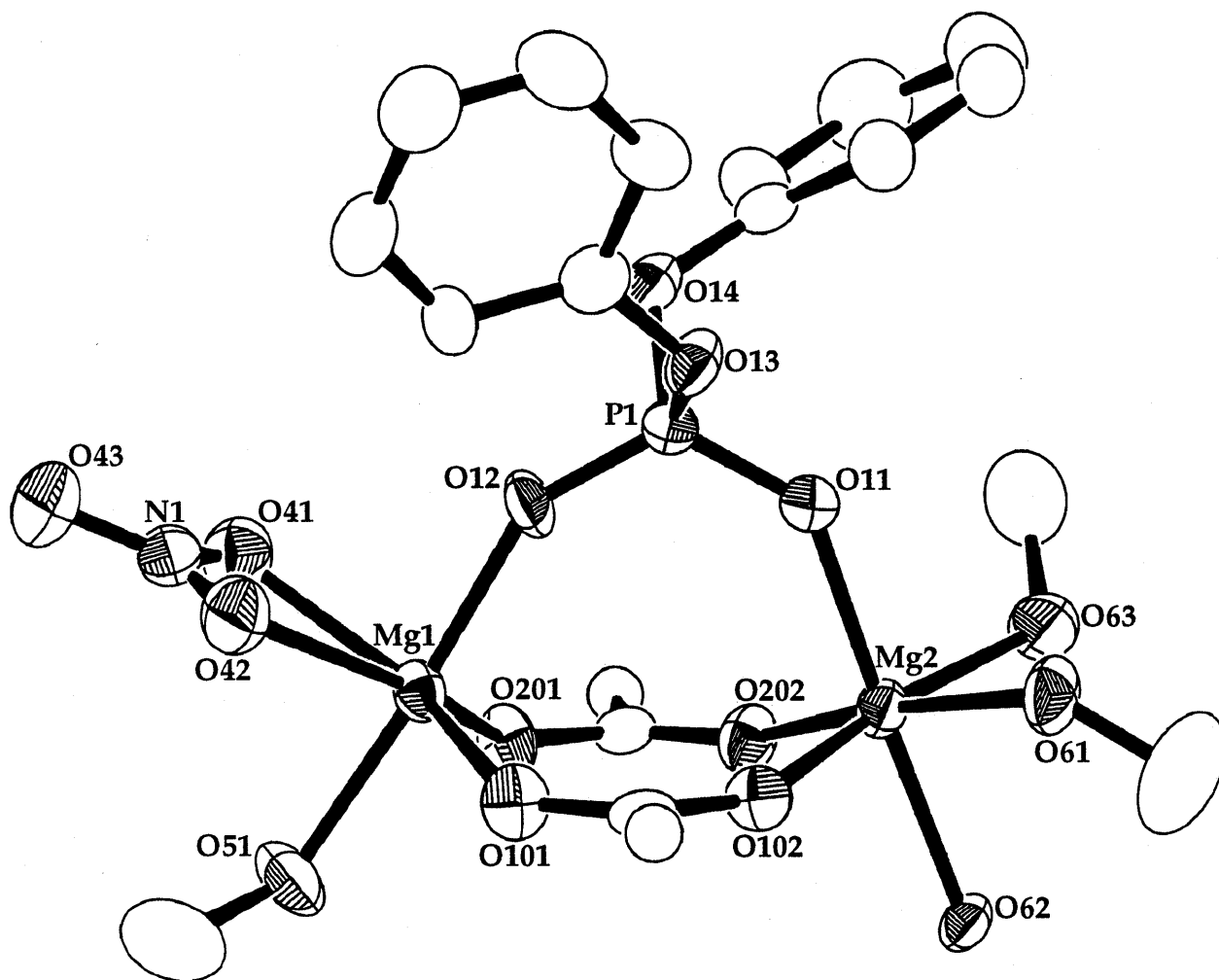


Figure 3. A packing diagram of  $1(\text{NO}_3)$ .



**Figure 4a.** ORTEP diagram of [Mg<sub>2</sub>(XDK)(DPP)(CH<sub>3</sub>OH)<sub>3</sub>(H<sub>2</sub>O)(NO<sub>3</sub>)] (2). Thermal ellipsoids are drawn at the 50% probability level. Hydrogen atoms are omitted for clarity.



**Figure 4b.** An ORTEP plot of the dinuclear center of **2**. Hydrogen atoms and all atoms of the XDK ligand, except the carboxylate groups, are omitted for clarity.

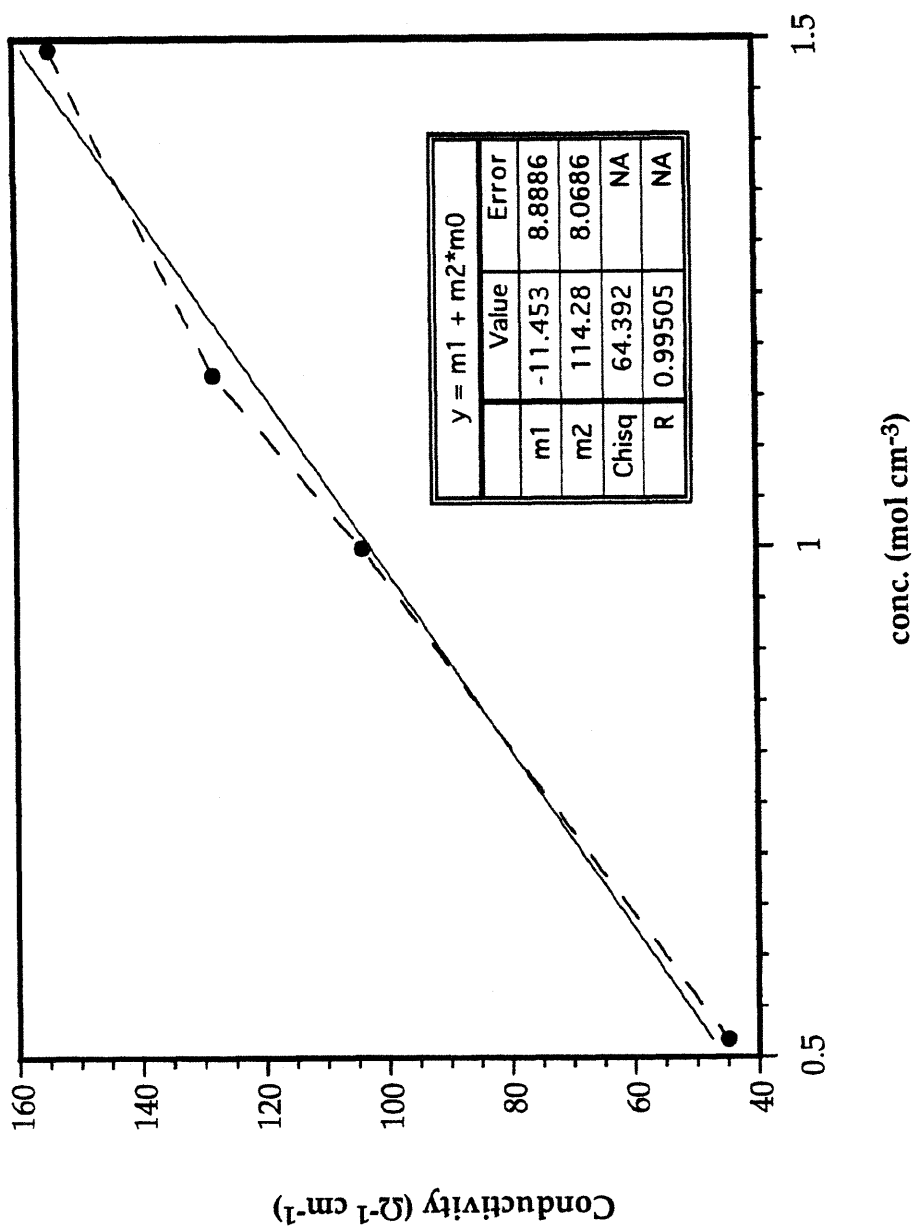


**Figure 5.** A plot of conductivity vs. concentration for 3·CH<sub>3</sub>OH. The molar conductivity of 114 Ω<sup>-1</sup>cm<sup>2</sup>mol<sup>-1</sup> corresponded to 1:1 electrolyte behavior by comparison to [Bu<sub>4</sub>N][PF<sub>6</sub>] (108 Ω<sup>-1</sup>cm<sup>2</sup>mol<sup>-1</sup>).

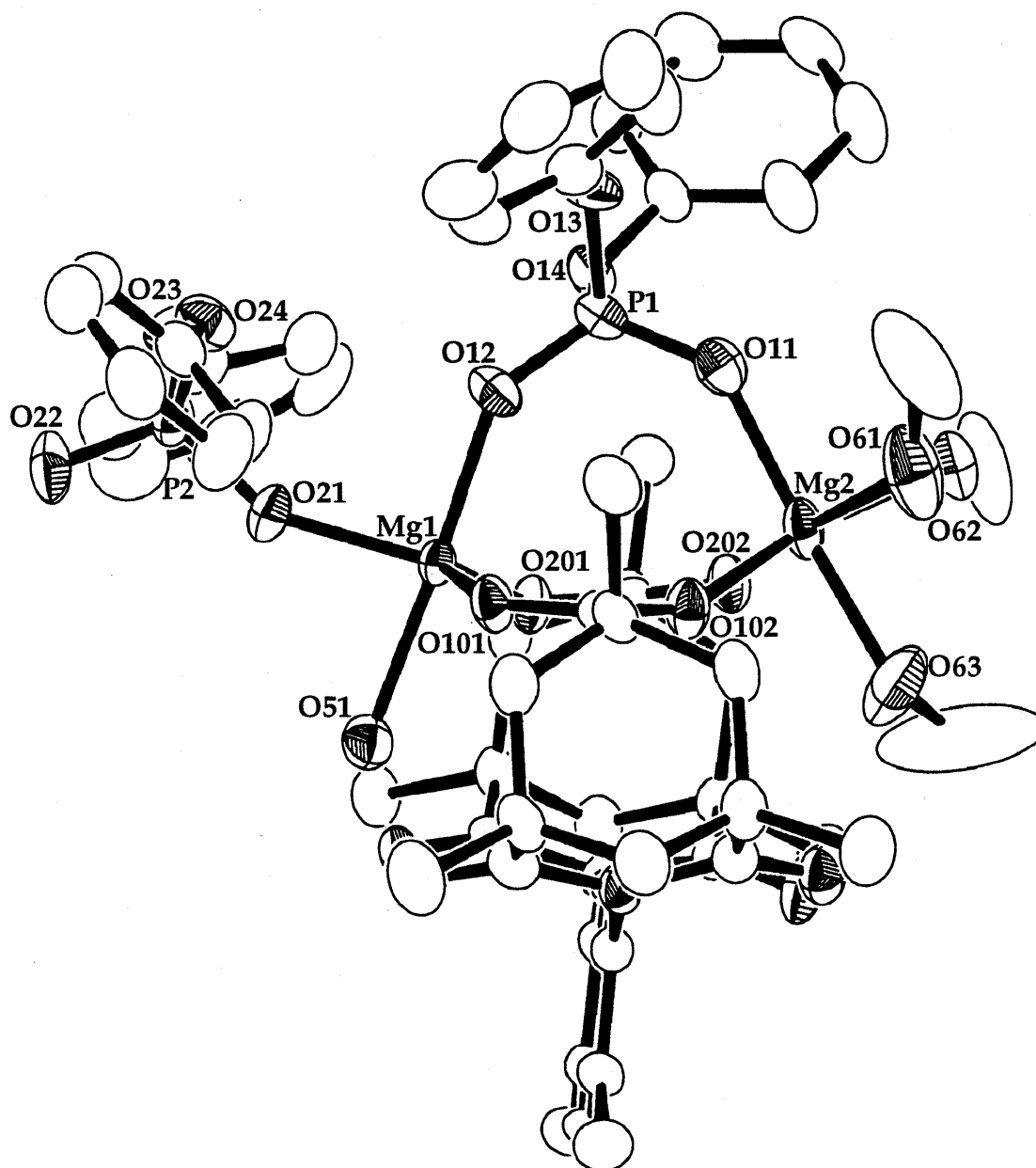
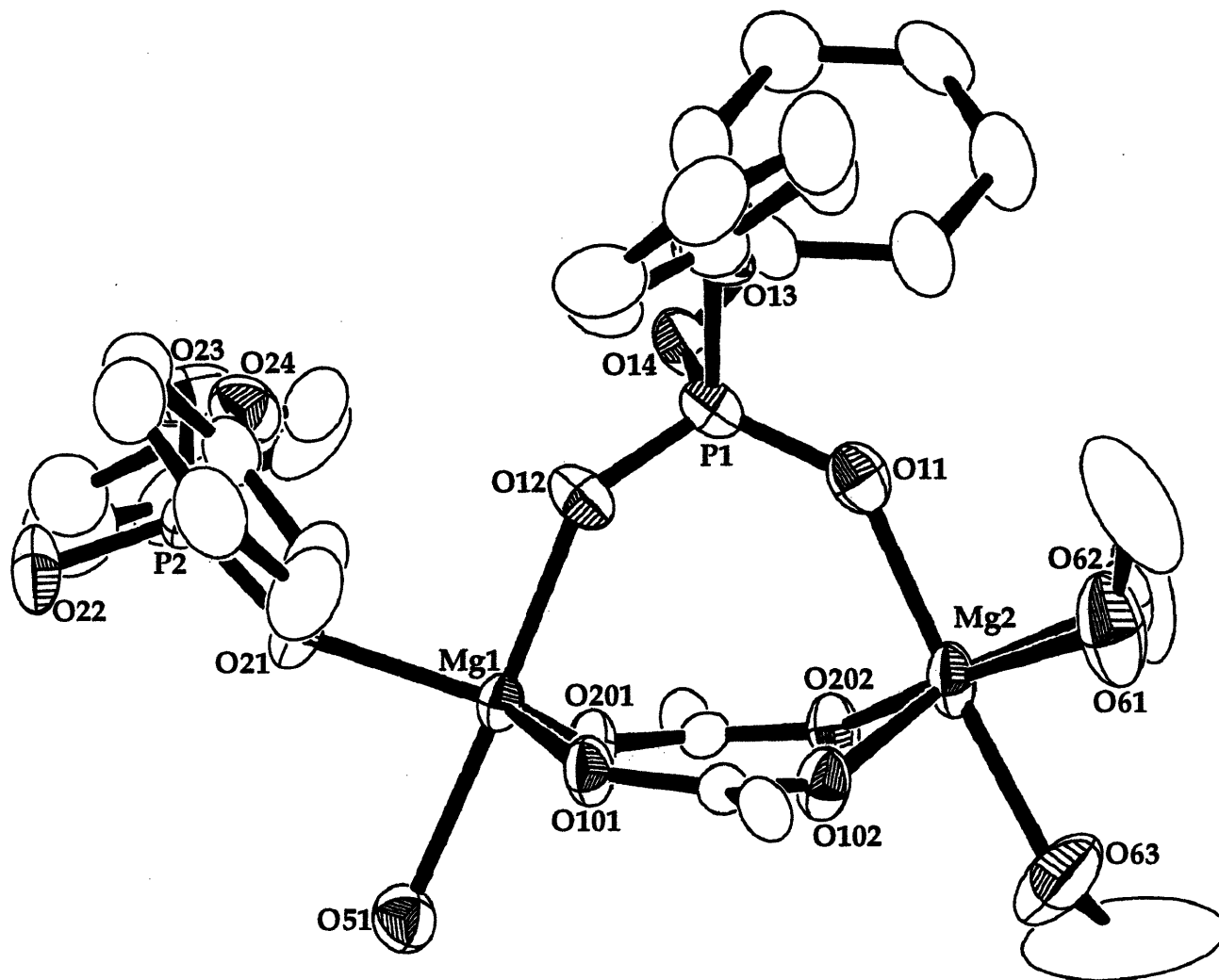


Figure 6a. An ORTEP diagram of  $[\text{Mg}_2(\text{XDK})(\text{DPP})_2(\text{CH}_3\text{OH})_3(\text{H}_2\text{O})]$  (3). Thermal ellipsoids are drawn at the 50% probability level. Hydrogen atoms are omitted for clarity.



**Figure 6b.** An ORTEP diagram of the dinuclear core of **3**. Hydrogen atoms and all atoms of the XDK ligand, except for the carboxylate groups, are omitted for clarity.

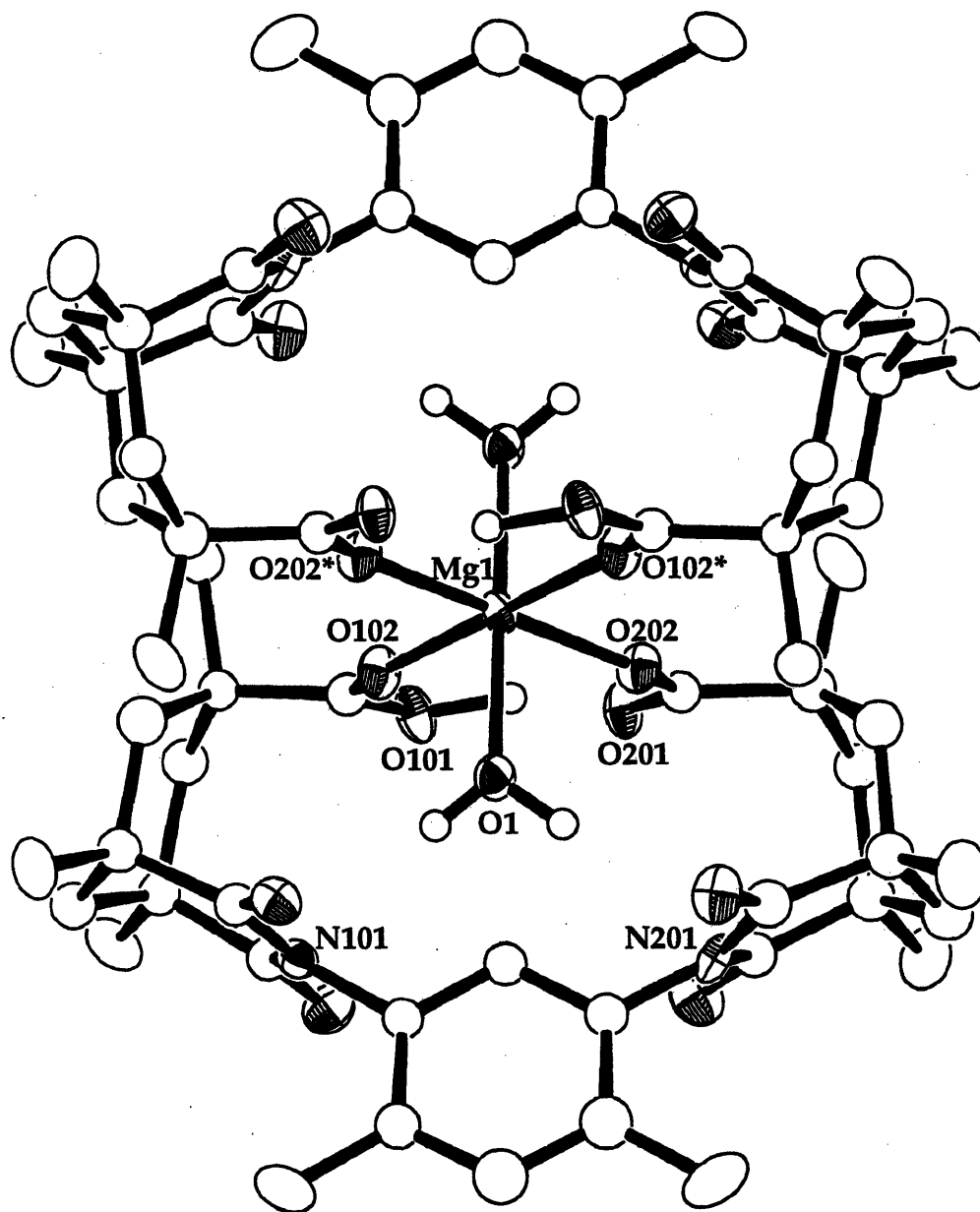


Figure 7. An ORTEP view of  $[\text{Mg}(\text{HXDK})_2(\text{H}_2\text{O})_2]$  (4). Thermal ellipsoids are drawn at the 50% probability level, and hydrogen atoms are omitted for clarity.



**Chapter 3****Phosphate Ester Exchange Studies of Carboxylate-Bridged Dimetallics**

## INTRODUCTION

The interaction of metal ions with phosphate esters is of considerable importance in biology. These metal ions serve numerous functions, including the stabilization of the phosphate ester backbone in nucleic acid structures and the activation of many phosphatase enzymes.<sup>1</sup> Phosphate ester processing enzymes, which include the Klenow fragment of DNA polymerase I from *Escherichia coli*<sup>2</sup> and Staphylococcal nuclease (SNase),<sup>3</sup> require divalent metal ions such as magnesium, calcium, and zinc coordinated by carboxylate amino acid side chains in their active site cavities. These metal ions are postulated to bind and activate the phosphate esters, generate the attacking nucleophile, and stabilize the transition state of the reaction.<sup>2,4</sup> Although  $Mg^{2+}$ ,  $Ca^{2+}$ , and  $Zn^{2+}$  are believed to have similar roles these enzymes, the properties of these metal ions are quite different (Table 1).

Despite the importance of divalent metal ions in phosphate ester processing enzymes, the biomimetic chemistry of such metal complexes, particularly of  $Mg^{2+}$  and  $Ca^{2+}$ , as phosphatase models has been slow to develop.<sup>1</sup> We became interested in understanding the chemistry of  $Mg^{2+}$ ,  $Ca^{2+}$ , and  $Zn^{2+}$  coordinated by both carboxylates and phosphate esters. Toward this end, we initiated a program to synthesize and characterize structurally such complexes and to investigate the reactions of these metal complexes in biologically relevant environments. We report here a comparative study of three such compounds,  $[Mg_2(XDK)\{\mu-\eta^2-(PhO)_2PO_2\}\{\eta^1-(PhO)_2PO_2\}(CH_3OH)_3(H_2O)\} \cdot CH_3OH$  (1·CH<sub>3</sub>OH),  $[Zn_2(XDK)\{\mu-\eta^2-(PhO)_2PO_2\}\{\eta^1-(PhO)_2PO_2\}(CH_3OH)_2(H_2O)\}]$  (2), and  $[Ca_2(XDK)\{\mu-\eta^2-(PhO)_2PO_2\}\{\eta^1-(PhO)_2PO_2\}(MeOH)_3(H_2O)\}]$  (3·CH<sub>3</sub>OH), where H<sub>2</sub>XDK is *m*-xylylenediamine bis(Kemp's triacid imide).<sup>5,6</sup> The monodentate diphenyl phosphate ligand in each of these complexes is dissociated in solution and exchanges with the bridging bidentate phosphodiester group at elevated temperatures, as revealed by phosphorus-31 NMR spectroscopy. From variable-temperature <sup>31</sup>P{<sup>1</sup>H} NMR

experiments, the phosphate ester exchange rates for these complexes were determined.

## EXPERIMENTAL METHODS

**Synthesis of  $[M_2(XDK)\{\mu-\eta^2-(PhO)_2PO_2\}\{\eta^1-(PhO)_2PO_2\}(CH_3OH)_n(H_2O)]$  Complexes,  $M = Mg$  ( $n = 3$ ),  $Zn$  ( $n = 2$ ),  $Ca$  ( $n = 3$ ).**

The syntheses of  $[Mg_2(XDK)\{\mu-\eta^2-(PhO)_2PO_2\}\{\eta^1-(PhO)_2PO_2\}(CH_3OH)_3(H_2O)] \cdot CH_3OH$  ( $1 \cdot CH_3OH$ ) and  $[Zn_2(XDK)\{\mu-\eta^2-(PhO)_2PO_2\}\{\eta^1-(PhO)_2PO_2\}(CH_3OH)_2(H_2O)]$  (2) were previously reported.<sup>7,8</sup> In order to prepare  $[Ca_2(XDK)\{\mu-\eta^2-(PhO)_2PO_2\}\{\eta^1-(PhO)_2PO_2\}(MeOH)_3(H_2O)] \cdot CH_3OH$ , ( $3 \cdot CH_3OH$ ), a methanolic solution (1 mL) of  $Ca(NO_3)_2 \cdot 4H_2O$  (41 mg, 0.172 mmol) was added to a solution of  $H_2XDK$  (50 mg, 0.0861 mmol) and NaOH (350  $\mu$ l, 0.5 M in MeOH) in methanol (3 ml). The solution was stirred at room temperature for 10 min and a methanolic solution of NaDPP (HDPP = diphenyl hydrogen phosphate, 47 mg, 0.172 mmol) was added. This mixture was stirred for another 10 min and the solvent was removed in vacuo. The white residue was redissolved in methanol, and vapor diffusion of ethyl ether into the resulting solution afforded colorless needles. The crystals were collected and treated with excess pyridine (3 mL) in chloroform (5 mL). The inorganic salt contaminants were removed by filtration, and the py/ $CHCl_3$  filtrate containing the complex was placed under vacuum to remove the solvents. The dried sample was redissolved in methanol. Vapor diffusion of ethyl ether into the solution gave long colorless block crystals in 32% yield (35 mg, 0.0272 mmol).  $^1H$  NMR, 300 MHz ( $CD_3OD$ ):  $\delta$  1.18 (s, 6 H), 1.18 (d, 4 H,  $J = 13.5$  Hz), 1.25 (s, 12 H), 1.55 (d, 2 H,  $J = 13.2$  Hz), 1.90 (s, 6 H), 2.09 (d, 2 H,  $J = 13.3$  Hz), 2.83 (d, 4 H,  $J = 13.1$  Hz), 7.03 (m, 4 H), 7.13-7.26 (m, 17 H), 7.47 (s, 1 H).  $^{31}P\{^1H\}$  NMR, 121.4 MHz ( $CD_3OD$ ):  $\delta$  -11.66 (s). IR (KBr): 3485 (br), 3053 (m), 2960 (s), 2918 (s), 2882 (s), 2429 (m), 1784, 1722 (s), 1682 (s), 1603 (s), 1489, 1452, 1414, 1366, 1203 (m, P-O), 1097 (s), 1025 (m), 916 (s), 834, 772, 689, 644, 518, 448

cm<sup>-1</sup>. Anal. Calcd. for C<sub>60</sub>H<sub>78</sub>N<sub>2</sub>O<sub>22</sub>Ca<sub>2</sub>P<sub>2</sub> (3·CH<sub>3</sub>OH·H<sub>2</sub>O): C, 54.54; H, 5.95; N, 2.12. Found: C, 54.26; H, 5.55; N, 2.23.

**X-ray Diffraction Study of [Ca<sub>2</sub>(XDK){μ-η<sup>2</sup>-(PhO)<sub>2</sub>PO<sub>2</sub>}{η<sup>1</sup>-(PhO)<sub>2</sub>PO<sub>2</sub>}(MeOH)<sub>3</sub>(H<sub>2</sub>O)]·CH<sub>3</sub>OH, 3·CH<sub>3</sub>OH**

Crystals of 3·CH<sub>3</sub>OH were grown by diffusion of ethyl ether into a methanolic solution of the complex. Single-crystal X-ray diffraction studies of 3 were carried out on a Siemens CCD X-ray diffraction system controlled by a pentium-based PC running the SMART version 4.0 software package,<sup>9</sup> as previously described in detail.<sup>10</sup> A colorless block crystal of 3 measuring approximately 0.3 x 0.3 x 0.5 mm was mounted at room temperature on the end of a glass fiber in paratone and data collection was carried out at -80 °C. The crystals were judged to be of acceptable quality on the basis of initial unit cell matrices and reflection profiles. Crystallographic data are given in Table 2. The data for this structure, including tables of atomic positional parameters and anisotropic temperature factors, are available on a 4mm DAT tape.

**Structure Solution and Refinement of [Ca<sub>2</sub>(XDK){μ-η<sup>2</sup>-(PhO)<sub>2</sub>PO<sub>2</sub>}{η<sup>1</sup>-(PhO)<sub>2</sub>PO<sub>2</sub>}(MeOH)<sub>3</sub>(H<sub>2</sub>O)]·CH<sub>3</sub>OH, 3·CH<sub>3</sub>OH**

Computations were carried out on Silicon Graphics Indy workstations. The raw data frames were processed by the SAINT version 4.0 software package<sup>11</sup>. All aspects of the structure solution and refinement were handled by the SHELXTL version 5.0 software package.<sup>12</sup> Non-hydrogen atoms were located by direct methods and a series of least squares refinements and difference Fourier maps and were refined with anisotropic temperature factors. The structure of [Ca<sub>2</sub>(XDK){μ-η<sup>2</sup>-(PhO)<sub>2</sub>PO<sub>2</sub>}{η<sup>1</sup>-(PhO)<sub>2</sub>PO<sub>2</sub>}(MeOH)<sub>3</sub>(H<sub>2</sub>O)] is shown in Figure 2, and selected bond distances and angles are given in Table 3.

## Physical Measurements

$^1\text{H}$  and  $^{31}\text{P}\{^1\text{H}\}$  NMR spectra were recorded on Varian XL-300 and UNITY300 spectrometers.  $^{31}\text{P}\{^1\text{H}\}$  NMR spectra were measured at 121.4 MHz using 85%  $\text{H}_3\text{PO}_4$  as an external reference. The temperature was calibrated with a methanol standard. The VT-NMR data for **1** and **2** were fit with the DNMR program.<sup>13</sup> Infrared spectra were recorded on a Bio-Rad FTS7 Fourier transform instrument. Conductivity measurements were carried out at 23 °C in methanol with a Fisher Scientific conductivity bridge model 9-326 with a platinum-black electrode. Molar conductivities ( $\Omega^{-1} \text{cm}^2 \text{mol}^{-1}$ ) were derived from the slopes of a conductivity ( $\Omega^{-1} \text{cm}^{-1}$ ) versus concentration ( $\text{mol cm}^{-3}$ ) plot. The electrolyte type assignment was determined by reference to the molar conductivity of  $[\text{Bu}_4\text{N}][\text{PF}_6]$  in methanol.

## RESULTS

The structure of  $[\text{Mg}_2(\text{XDK})\{\mu\text{-}\eta^2\text{-(PhO)}_2\text{PO}_2\}\{\eta^1\text{-(PhO)}_2\text{PO}_2\}(\text{CH}_3\text{OH})_3\text{(H}_2\text{O)}]\cdot\text{CH}_3\text{OH}$  was described in the preceding chapter.<sup>7</sup> The structure of  $[\text{Zn}_2(\text{XDK})\{\mu\text{-}\eta^2\text{-(PhO)}_2\text{PO}_2\}\{\eta^1\text{-(PhO)}_2\text{PO}_2\}(\text{CH}_3\text{OH})_2(\text{H}_2\text{O})]$  was reported previously.<sup>8</sup> It contains a dinuclear zinc center bridged by the carboxylates of the XDK ligand and a bidentate diphenyl phosphate ligand. One zinc is also coordinated by a monodentate, terminal DPP ligand. This complex is structurally similar to the dimagnesium analog **1**, except that one of the magnesium atoms in **1** adopts a trigonal bipyramidal geometry whereas tetrahedral geometry is observed for one of the zinc atoms in **2**. The metal-metal distance in **2** is 3.869(2) Å, which is shorter than the  $\text{Mg}\cdots\text{Mg}$  distance of 4.108(3) Å in **1**. Structural parameters for **1** and **2** are compared in Table 4.

Reaction of  $\text{Ca}(\text{NO}_3)_2\cdot 4\text{H}_2\text{O}$  (2 equiv) with  $\text{H}_2\text{XDK}$  (1 equiv) and  $\text{NaOH}$  (2 equiv) in methanol, followed by the addition of  $\text{NaDPP}$  (2 equiv), gave the desired

calcium analog  $[\text{Ca}_2(\text{XDK})\{\mu\text{-}\eta^2\text{-(PhO)}_2\text{PO}_2\}\{\eta^1\text{-(PhO)}_2\text{PO}_2\}(\text{MeOH})_3(\text{H}_2\text{O})]\cdot\text{CH}_3\text{OH}$ , ( $3\cdot\text{CH}_3\text{OH}$ ). The IR spectrum indicated the presence of XDK, diphenyl phosphate, and hydroxyl groups. The  $^1\text{H}$  NMR spectrum in  $\text{CD}_3\text{OD}$  showed singlets for the methyl groups of XDK ( $\delta$  1.18, 1.25, and 1.90) and doublets for the methylene groups ( $\delta$  1.18, 1.55, 2.09, and 2.83), consistent with  $C_{2v}$  symmetry for XDK. The phenyl protons of diphenyl phosphate gave multiplet signals in the aromatic region, and integrations showed a DPP:XDK ratio of 2:1. The  $^{31}\text{P}$  NMR spectrum of **3** in  $\text{CD}_3\text{OD}$  at room temperature exhibited one sharp singlet at -11.66 ppm. Conductivity measurements of **3** in methanol revealed it to be a 1:1 electrolyte (Figure 1), suggesting the dissociation of a diphenyl phosphate in solution.

X-ray quality crystals of **3** were grown from a methanol/ethyl ether solvent system, and a crystallographic analysis revealed its polymeric solid state structure. The repeating unit comprises a dinuclear calcium center bridged by the carboxylates of XDK and by a bidentate diphenyl phosphate ligand (Figure 2). We hereafter refer to this unit as the intramolecularly-bridged dicalcium moiety. The structure of **3** differs slightly from that of the dimagnesium **1** and the dizinc **2** analogs since both calcium ions are octahedrally coordinated. The other diphenyl phosphate ligand coordinates to one calcium atom (Ca1) and forms a bridge to the calcium (Ca2\*) of a neighboring unit, resulting in a polymeric structure (Figure 3). The carboxylate groups in **3** are roughly coplanar, with a dihedral angle of  $6.1^\circ$ . Ca1 and Ca2 are displaced 0.87 and 0.71 Å, respectively, from the dicarboxylate plane. Ca1 is octahedrally coordinated by the bridging phosphates (O12) and (O21), the carboxylates of XDK (O101 and O201), and two methanol ligands (O51 and O52). The Ca1-O12 bond distance is 2.295(3) Å, which is similar to that of Ca1-O21, 2.306(2) Å. The Ca1-O101 and Ca1-O201 bond distances of 2.351(2) Å and 2.318(2) Å, respectively, are slightly longer. The reported average  $\text{Ca-O}_{\text{carboxylate}}$  bond distance is 2.3 Å for a coordination number of 6.<sup>14</sup> Ca2 is also octahedrally coordinated by the bridging

phosphate (O11), the other phosphate of a neighboring molecule (O22A), the carboxylate oxygens of XDK (O102 and O202), a methanol (O62), and a water molecule (O61). The Ca2 bond distances to O11 and O22A are 2.282(2) and 2.289(2) Å, respectively. The Ca2 bond distances to O102 and O202 are 2.298(2) and 2.240(2) Å, respectively, which are shorter than those of Ca1. The calcium atoms are coordinated to the syn lone pairs of the carboxylates, as suggested by the average Ca1- and Ca2-OC<sub>carboxylate</sub> bond angles of 132.6(3) and 153.4(3)°, respectively. This mode of calcium binding to carboxylate groups is often observed.<sup>14</sup> The Ca...Ca distance is 4.4628(9) Å, which is longer than the M...M distance in 1 and 2 (Table 4). The longer metal-metal separation in 3 may be due to the greater ionic radius of calcium<sup>15</sup> (Table 1) and to the effect of the terminal diphenyl phosphate bridging the calcium ions in two asymmetric units.

The O11-P1-O12 angle in the bridging diphenyl phosphate in 3 is 118.5(2)°, which is smaller than that for O21-P2-O22 of the other phosphate (119.67(14)°). The other angles around P1 and P2 are roughly tetrahedral, except the O13-P1-O14 angle of 97.52(13)°. The phosphorus-oxygen bond distances are shorter to the metal coordinated oxygens in both P1 and P2 (Table 3), which is similar to that observed in other metal-phosphate complexes.<sup>7</sup> The calcium ions are coordinated to the syn lone pairs of the bridging phosphate with Ca1- and Ca2-O-P1 bond angles of 151.1(2) and 139.1(2)°, respectively. The Ca1 and Ca2 atoms lie roughly in the plane defined by the phosphinyl group [O11-P1-O12], as indicated by displacements of 0.27 and 0.37 Å for Ca1 and Ca2, respectively, and the 8° dihedral angle between the phosphinyl plane and [Ca1-O12-P1-O11-Ca2]. The [Ca1-Ca2-O11-O12] plane is approximately perpendicular to that of the xylyl spacer (89 °). Ca2 and Ca1A are displaced by -1.1 and 1.0 Å from the [O21A-P2A-O22A] plane (Figure 4). Ca2 and Ca1A are coordinated to the syn lone pairs of the phosphate. The Ca1-O21-P2 and Ca2-O22A-

P2A bond angles are 151.3(2) and 139.27(14) °. The P2A phosphinyl plane is 87 ° from the P1 phosphinyl plane.

### Variable Temperature Phosphorus-31 NMR Studies

Samples of 1 - 3 (30 mM) in CD<sub>3</sub>OD were used for VT <sup>31</sup>P{<sup>1</sup>H} NMR studies. Each compound exhibited two sharp singlets in its low temperature limiting spectrum. Compound 1 displayed resonances at δ -9.07 and -15.69, corresponding to free and bound diphenyl phosphate, respectively. This assignment was made by addition of (Me<sub>4</sub>N)DPP to confirm the identity of the free diphenyl phosphate resonance and by comparison to the <sup>31</sup>P chemical shift of [Mg<sub>2</sub>(XDK){μ-η<sup>2</sup>-(PhO)<sub>2</sub>PO<sub>2</sub>}(CH<sub>3</sub>OH)<sub>3</sub>(H<sub>2</sub>O)(NO<sub>3</sub>)] at δ -15.46.<sup>7</sup> Complexation of magnesium, zinc, and calcium to phosphate esters shifts the <sup>31</sup>P NMR signals to lower fields.<sup>16</sup> Figure 4 shows the spectra of 1 over the temperature range -24 < T < 60 °C, indicating diphenyl phosphate exchange at elevated temperatures. A line shape analysis of the <sup>31</sup>P{<sup>1</sup>H} NMR spectral changes for 1 was carried out, and the free energy of activation for phosphate ester exchange was calculated from the coalescence temperature (54 °C) to be 60 kJ mol<sup>-1</sup>.<sup>13</sup> The spectra of 2 are shown in Figure 5, and a value of 45 kJ mol<sup>-1</sup> for the free energy of activation for exchange was calculated from the coalescence temperature (-30 °C). The free energy of activation for phosphodiester exchange for 3 was determined to be 39 kJ mol<sup>-1</sup> from its coalescence temperature of -58 °C. These results are summarized in Table 5.

The phosphorus signals for 1 at the low temperature limit integrate to give a 1:1 ratio of free-to-bound phosphate. In the spectra of both 2 and 3, however, the intensity ratio for the free phosphate is slightly greater than that for the bound one (55:45) (Figure 5). The ΔG<sup>‡</sup> values for 2 and 3 were calculated from the rate constants determined at the coalescence temperatures based on a 1:1 two-site exchange model using the equation  $k = (\pi/\sqrt{2})\Delta\nu$ , where  $k$  is the rate constant for exchange at the



coalescence temperature and  $\Delta\nu$  is the difference in the chemical shifts (in Hz) of the two species.<sup>13</sup> This procedure is often used for unequally populated two-site cases as well, since such results have been shown to be in good agreement with those for a complete line shape analysis.<sup>17</sup> Furthermore, the values of  $\Delta G^\ddagger$  are not highly sensitive to errors in the rate constant.<sup>13,17</sup> The difference in the intensity ratios for 2 and 3 suggests that some fraction of the bridging diphenyl phosphate ligand is further dissociated from the dinuclear center. This observation indicates that the diphenyl phosphate ligands are more labile in the carboxylate-bridged dizinc and the dicalcium complexes than in the dimagnesium analog (*vide infra*).

## DISCUSSION

The carboxylate-bridged dimagnesium, dicalcium, and dizinc phosphate ester complexes afford a comparison of these metal ions in biologically relevant environments. To our knowledge, this work provides the first direct comparison of  $Mg^{2+}$ ,  $Ca^{2+}$ , and  $Zn^{2+}$  from a biomimetic perspective.

The solid state structures of 1 - 3 reveal some of the unique characteristics of the different metal ions. In all three, there is a dinuclear metal center bridged by the carboxylate oxygen atoms of XDK and a bidentate diphenyl phosphate ligand. In the dimagnesium complex 1, Mg1 has trigonal bipyramidal and Mg2 octahedral stereochemistry, with the monodentate phosphate ester bound to Mg1. For the dizinc analog 2, Zn1 is tetrahedral and Zn2 is octahedral, the terminal diphenyl phosphate ligand being coordinated to Zn1. In the dicalcium analog 3, Ca1 and Ca2 are both octahedral, with a phosphate group bridging Ca1 and Ca2\* from a neighboring molecule, leading to a polymeric structure. The results reflect the preferred coordination numbers for these metals, with calcium adopting the highest coordination number, followed by magnesium, then zinc.<sup>15</sup>

The metal-metal separations in **1** and **2**, 4.108(3) Å and 3.869(2) Å, respectively, are comparable to the distances found in phosphate ester processing enzymes containing similar dimetallic centers in their active sites. Included among these enzymes is the Klenow fragment of DNA polymerase I which can accommodate a 2 Mg<sup>2+</sup>, 2 Zn<sup>2+</sup>, or a Mg<sup>2+</sup>/Zn<sup>2+</sup> in its carboxylate-bridged center at a M····M distance of 3.9 Å.<sup>2</sup> Interestingly, this enzyme is not activated by calcium.<sup>18</sup> The Ca····Ca distance of 4.4628(9) Å in **3** suggests that the inability of calcium to activate this enzyme may be due in part to the larger metal-metal separation required for this carboxylate-bridged center.

Currently, there are no examples of carboxylate-bridged dicalcium metalloenzymes which have been structurally characterized. In SNase, two calcium ions are required for catalysis of phosphate ester hydrolysis,<sup>19</sup> but in the available crystal structures, only one calcium ion coordinated by two monodentate aspartate residues has been observed.<sup>3,4</sup> One of the monodentate aspartate residues in the active site could potentially coordinate to the other required calcium ion in this enzyme. The dicalcium complex **3** may be a useful model structural model for biochemists studying SNase and other calcium-dependent enzymes.

Since **1** - **3** have structural similarities to phosphate ester processing metalloenzymes, their phosphodiester ligand exchange properties in solution were investigated. Solution studies of **1** - **3** in methanol are consistent with the dissociation of the monodentate diphenyl phosphate in solution. The two metal ions are in equivalent environments, as evidenced by their <sup>1</sup>H NMR spectra which clearly indicate the XDK ligand to be in a symmetrical (C<sub>2v</sub>) environment. The <sup>31</sup>P{<sup>1</sup>H} NMR spectrum of **1** in CD<sub>3</sub>OD at room temperature showed 2 signals corresponding to free and bound diphenyl phosphate. Conductivity measurements revealed 1:1 electrolyte behavior for **1** - **3**, supporting the observation of a dissociated

diphenyl phosphate ligand. These results indicate that the bridging phosphate ester ligand is more stable to exchange than the terminal one.

A variable temperature  $^{31}\text{P}\{^1\text{H}\}$  NMR study of **1** in  $\text{CD}_3\text{OD}$  revealed that the bound and free phosphodiester ligands exchange at elevated temperatures (Scheme 1). Although the details of the exchange mechanism are not known, one reasonable possibility is shown in Scheme 1. Here, the free diphenyl phosphate associates and undergoes terminal/bridged ligand exchange. The free energy of activation for this process was determined to be  $60 \text{ kJ mol}^{-1}$  for **1**. This value can be compared with those estimated for **2** ( $45 \text{ kJ mol}^{-1}$ ) and **3** ( $39 \text{ kJ mol}^{-1}$ ). The phosphate ester exchange rates at  $25 \text{ }^\circ\text{C}$  were  $1.9 \times 10^2 \text{ s}^{-1}$ ,  $7.5 \times 10^4 \text{ s}^{-1}$ , and  $9.1 \times 10^5 \text{ s}^{-1}$ , respectively, for **1**, **2**, and **3**. Thus, the phosphate ester exchange rate of the dimagnesium(II) compound (**1**) is  $\sim 10^2$  times slower than that of the dizinc(II) analog (**2**) and  $\sim 10^3$  times slower than that of the dicalcium(II) complex (**3**). These relative values reflect the differences in  $\text{H}_2\text{O}$  exchange rates of hydrated magnesium, zinc, and calcium ions,  $10^5$ ,  $3 \times 10^7$ , and  $\sim 10^8 \text{ s}^{-1}$ , respectively,<sup>20</sup> and is consistent with a mechanism in which reassociation of the free  $\text{DPP}^-$  is involved in the rate-determining step. The fact that the dimagnesium center in **1** is kinetically less labile with respect to diphenyl phosphate ligand exchange than the dizinc center in **2** and the dicalcium center in **3** may be useful for understanding the metal ion preferences of phosphate ester processing enzymes.

In the Klenow fragment of DNA polymerase I, the carboxylate-bridged dimetallic active site can employ a  $2 \text{ Mg}^{2+}$ ,  $2 \text{ Zn}^{2+}$ , or a  $\text{Mg}^{2+}/\text{Zn}^{2+}$  pair. Although the identity of the metal ions in vivo has not yet been determined, the X-ray structure of the Klenow fragment complexed with a deoxynucleoside monophosphate product in the presence of both zinc and magnesium revealed a pentacoordinate  $\text{Zn}^{2+}$  ion in one site (site A) and an octahedral  $\text{Mg}^{2+}$  ion in the other (site B).<sup>2</sup> In the two-metal-ion phosphoryl transfer mechanism proposed for

this enzyme, the metal ion in site A is postulated to generate the attacking hydroxyl ion nucleophile, and the metal ion in site B to stabilize the pentacovalent phosphorus transition state. Our observation that carboxylate-bridged dimagnesium(II) centers provide a kinetically more stable binding site for phosphate esters than the corresponding dizinc(II) center is consistent with this site preference. Furthermore, our results offer some insight into the inability of calcium ions to activate the Klenow fragment. The relatively large metal-metal separation in a dicalcium carboxylate-bridged environment may be incompatible with the enzyme active site structure, and the more rapid phosphate ester exchange rate may be too fast to bind and orient the substrate properly.

The faster rate of phosphate ester exchange for the dicalcium complex (3) may be useful in explaining the metal ion preferences of SNase. This highly proficient calcium-dependent enzyme accelerates the hydrolysis of phosphodiester bonds by a factor of  $10^{16}$ .<sup>21</sup> Other metal ions such as  $\text{Co}^{2+}$  and  $\text{Mn}^{2+}$  bind competitively at the  $\text{Ca}^{2+}$  binding site, but are at least  $10^5$ -fold less effective at activating the enzyme.<sup>22</sup> Magnesium ions have been reported to be ineffective at activating this enzyme,<sup>23</sup> and zinc is a potent inhibitor.<sup>24</sup> The rate determining step for SNase is believed to be product release.<sup>25</sup> Our results that carboxylate-bridged dicalcium(II) centers exchange phosphate esters more rapidly than dimagnesium(II) and dizinc(II) analogs are consistent with the preference of SNase for calcium.

## CONCLUSIONS

The carboxylate- and phosphodiester-bridged magnesium, zinc, and calcium complexes presented here are useful structural models for studying the behavior of these metal ions in relevant biomimetic environments. The metal-metal separation in the dimagnesium (1) and the dizinc (2) complexes are comparable to those found in similar carboxylate-bridged phosphatase active sites. The structural

features of **1 - 3** may also be useful as models for fitting the electron density of protein crystal structures to provide more detailed geometries around the metal centers. The observed differences in phosphate ester exchange rates for **1 - 3** were found to be comparable to the differences in water exchange rates for the hydrated metal ions. The phosphodiester exchange rates of **1 - 3** may be useful to biochemists studying phosphate ester processing metalloenzymes.

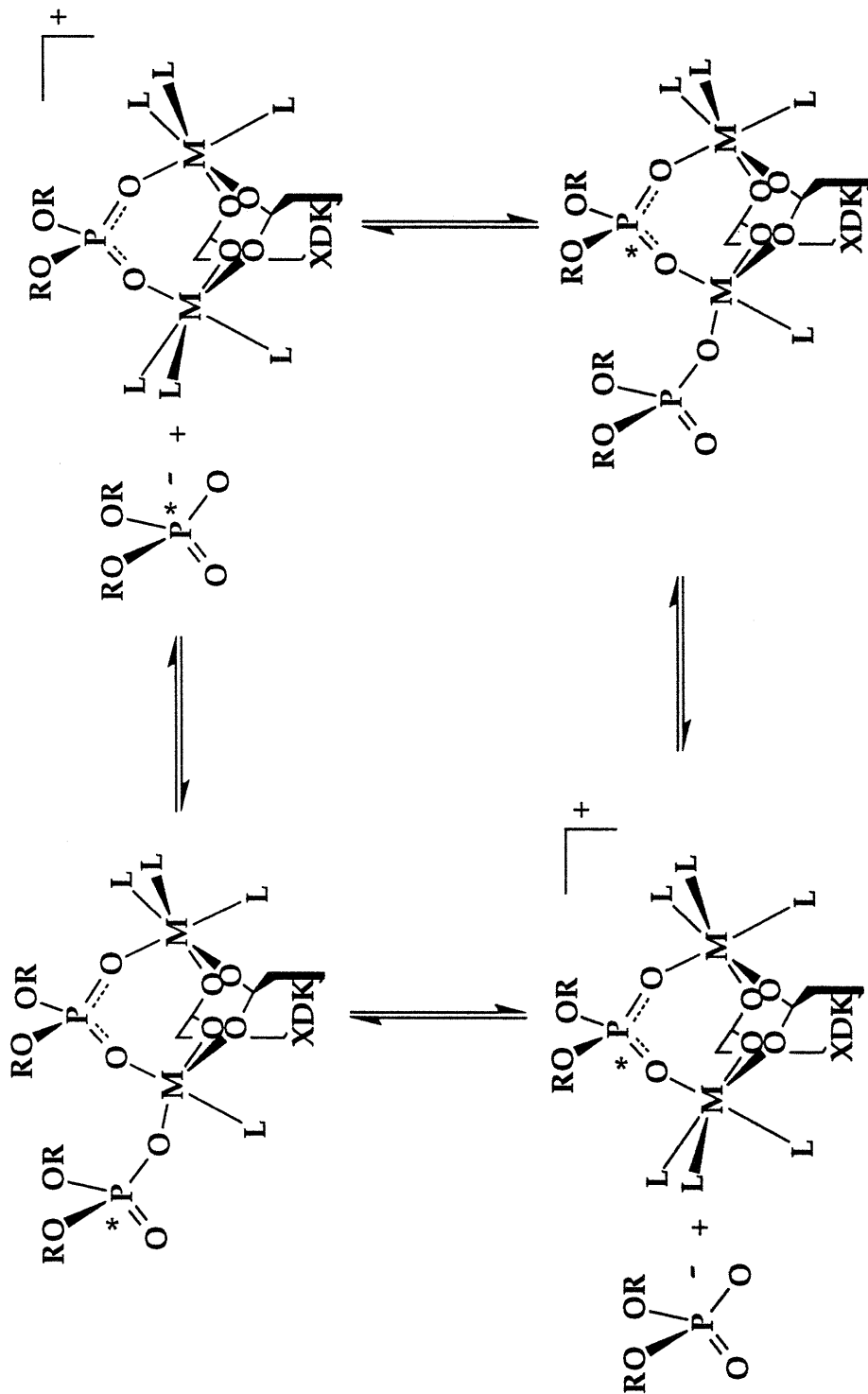
#### ACKNOWLEDGEMENT

Dr. Tomoaki Tanase is acknowledged for providing samples of the dizinc(II)-XDK complex, **2**, used in this study.

#### REFERENCES

- (1) Lippard, S. J.; Berg, J. M. *Principles of Bioinorganic Chemistry*; University Science Books: Mill Valley, CA, 1994.
- (2) Beese, L. S.; Steitz, T. A. *EMBO J.* **1991**, *10*, 25-33.
- (3) Cotton, F. A.; Hazen, E. E., Jr.; Legg, M. J. *Proc. Natl. Acad. Sci. USA* **1979**, *76*, 2551-2555.
- (4) Loll, P. J.; Quirk, S.; Lattman, E. E.; Garavito, R. M. *Biochemistry* **1995**, *34*, 4316-4324.
- (5) Kemp, D. S.; Petrakis, K. S. *J. Org. Chem.* **1981**, *46*, 5140-5143.
- (6) Rebek, J., Jr.; Marshall, L.; Wolak, R.; Parris, K.; Killoran, M.; Askew, B.; Nemeth, D.; Islam, N. *J. Am. Chem. Soc.* **1985**, *107*, 7476-7481.
- (7) Yun, J. W. Ph.D. Thesis, Massachusetts Institute of Technology, 1996, Chapter 2.
- (8) Tanase, T.; Yun, J. W.; Lippard, S. J. *Inorg. Chem.* **1996**, in press.
- (9) SMART *Siemens Industrial Automation, Inc.*; Analytical Instrumentation: Madison, WI, 1994.

- (10) Feig, A. L.; Bautista, M. T.; Lippard, S. J. **1996**, submitted for publication.
- (11) SAINT *Siemens Industrial Automation, Inc.*; Analytical Instrumentation: Madison, WI, 1995.
- (12) Sheldrick, G. M. *Siemens Industrial Automation, Inc.*; Analytical Instrumentation: Madison, WI, 1994.
- (13) Sandstrom, J. *Dynamic NMR Spectroscopy*; Academic Press Inc.: London, 1982.
- (14) Carrell, C. J.; Carrell, H. L.; Erlebacher, J.; Glusker, J. P. *J. Am. Chem. Soc.* **1988**, *110*, 8651-8656.
- (15) Shannon, R. B. *Acta Crystallogr.* **1976**, *32A*, 751-767.
- (16) Cohn, M.; Hughes, T. R., Jr. *J. Biol. Chem.* **1962**, *237*, 176-181.
- (17) Kost, D.; Carlson, E. H.; Raban, M. *Chem. Commun.* **1971**, 656-657.
- (18) Lehman, I. R.; Richardson, C. C. *J. Biol. Chem.* **1964**, *239*, 233-241.
- (19) Cuatrecasas, P.; Fuchs, S.; Anfinsen, C. B. *J. Biol. Chem.* **1967**, *242*, 3063-3067.
- (20) Eigen, M. *Pure Appl. Chem.* **1963**, *6*, 97-115.
- (21) Radzicka, A.; Wolfenden, R. *Science* **1995**, *267*, 90-93.
- (22) Serpersu, E. H.; Shortle, D.; Mildvan, A. S. *Biochemistry* **1987**, *26*, 1289-1300.
- (23) Cunningham, L.; Catlin, B. W.; Privat de Garilhe, M. *J. Am. Chem. Soc.* **1956**, *78*, 4642-4645.
- (24) Cuatrecasas, P.; Fuchs, S.; Anfinsen, C. B. *J. Biol. Chem.* **1961**, *242*, 1541-1547.
- (25) Hale, S. P.; Poole, L. B.; Gerlt, J. A. *Biochemistry* **1993**, *32*, 7479-7487.



**Scheme 1.** Proposed mechanism for phosphate ester exchange.

M = Mg(II), Zn(II), or Ca(II); L = CD<sub>3</sub>OD or H<sub>2</sub>O

**Table 1.** Comparison of Magnesium(II), Calcium(II), and Zinc(II) Properties

	<b>Mg<sup>2+</sup></b>	<b>Ca<sup>2+</sup></b>	<b>Zn<sup>2+</sup></b>
Effective Ionic Radii (Å) <sup>a</sup>	0.66 (CN = 5) <b>0.72</b> (CN = 6)	1.00 (CN = 6) 1.06 (CN = 7) <b>1.18</b> (CN = 8)	<b>0.60</b> (CN = 4) 0.67 (CN = 5) 0.74 (CN = 6)
Water Exchange Rate (s <sup>-1</sup> ) <sup>b</sup>	10 <sup>5</sup>	~ 10 <sup>8</sup>	3 x 10 <sup>7</sup>

<sup>a</sup>Reference 15. Values for preferred coordination numbers are in bold face.

<sup>b</sup>Reference 20.



**Table 2.** Crystallographic and Experimental Data for 3·CH<sub>3</sub>OH

compound	3·CH <sub>3</sub> OH
formula	C <sub>60</sub> H <sub>76</sub> N <sub>2</sub> O <sub>21</sub> Ca <sub>2</sub> P <sub>2</sub>
fw	1303.33
crystal size	0.3 x 0.3 x 0.5 mm
crystal system	monoclinic
space group	<i>P</i> 2 <sub>1</sub> / <i>n</i>
<i>a</i> , Å	16.5471 (3)
<i>b</i> , Å	24.3415 (6)
<i>c</i> , Å	16.5865 (3)
$\beta$ , deg	104.2530 (10)
<i>V</i> , Å <sup>3</sup>	6475.1 (2)
<i>Z</i>	4
<i>T</i> , °C	-80
<i>D</i> <sub>calcd</sub> , g cm <sup>-3</sup>	1.34
abs coeff, cm <sup>-1</sup>	3.00
2 $\theta$ range, deg	3 < 2 $\theta$ < 46.53
no. of unique data	9251
no. of obsd data	7858
( <i>I</i> > 2 $\sigma$ ( <i>I</i> ))	
<i>R</i> <sub>merge</sub> (%)	0.044
no. of variables	764
<i>R</i> <sup>a</sup>	0.053
<i>wR</i> <sup>2a</sup>	0.142

<sup>a</sup>*R* =  $\Sigma ||F_o| - |F_c|| / \Sigma |F_o|$ ; *wR*<sup>2</sup> =  $\{\Sigma [w(F_o^2 - F_c^2)^2] / \Sigma [w(F_o^2)^2]\}^{1/2}$ , where *w* = 1/ $\sigma^2$ (*F*<sub>o</sub>).

More details about the weighting scheme and other experimental protocols may be found in reference 10.

Table 3. Selected Bond Distances (Å) and Angles (deg) for 3·CH<sub>3</sub>OH.<sup>a</sup>

## Bond Distances

Ca(1)	O(12)	2.295(3)	Ca(2)	O(202)	2.240(2)
Ca(1)	O(21)	2.306(2)	Ca(2)	O(11)	2.282(2)
Ca(1)	O(201)	2.318(2)	Ca(2)	O(22)A	2.289(2)
Ca(1)	O(101)	2.351(2)	Ca(2)	O(102)	2.298(2)
Ca(1)	O(51)	2.388(2)	Ca(2)	O(62)	2.394(2)
Ca(1)	O(52)	2.430(2)	Ca(2)	O(61)	2.457(2)
P(1)	O(12)	1.472(3)	P(2)	O(22)	1.475(2)
P(1)	O(11)	1.482(3)	P(2)	O(21)	1.477(2)
P(1)	O(13)	1.602(2)	P(2)	O(24)	1.594(2)
P(1)	O(14)	1.603(3)	P(2)	O(23)	1.600(3)

## Angles

O(12)	Ca(1)	O(21)	104.31(9)	O(202)	Ca(2)	O(11)	91.41(9)
O(12)	Ca(1)	O(201)	91.31(10)	O(202)	Ca(2)	O(22)A	94.05(9)
O(21)	Ca(1)	O(201)	86.66(9)	O(11)	Ca(2)	O(22)A	96.31(9)
O(12)	Ca(1)	O(101)	101.57(9)	O(202)	Ca(2)	O(102)	94.76(9)
O(21)	Ca(1)	O(101)	146.45(9)	O(11)	Ca(2)	O(102)	100.55(9)
O(201)	Ca(1)	O(101)	113.83(9)	O(22)A	Ca(2)	O(102)	160.75(9)
O(12)	P(1)	O(11)	118.5(2)	O(22)	P(2)	O(21)	119.67(14)
O(12)	P(1)	O(13)	110.8(2)	O(22)	P(2)	O(24)	110.11(14)
O(11)	P(1)	O(13)	109.69(14)	O(21)	P(2)	O(24)	106.92(13)
O(12)	P(1)	O(14)	106.69(14)	O(22)	P(2)	O(23)	104.71(13)
O(11)	P(1)	O(14)	111.55(14)	O(21)	P(2)	O(23)	110.81(14)
O(13)	P(1)	O(14)	97.52(13)	O(24)	P(2)	O(23)	103.50(14)
P(1)	O(11)	Ca(2)	139.1(2)	P(2)	O(21)	Ca(1)	151.3(2)
P(1)	O(12)	Ca(1)	151.1(2)	P(2)	O(22)	Ca(2)A	139.27(14)

<sup>a</sup>Estimated standard deviations are given in parentheses. See Figure 2 for atom labels.

**Table 4.** Structural Parameters of Compounds 1·CH<sub>3</sub>OH, 2, and 3·CH<sub>3</sub>OH.

	1	2	3
M1...M2, Å	4.108(3)	3.869(2)	4.4628(9)
M1-O(XDK) <sub>av</sub> , Å <sup>a</sup>	1.983(6)	1.938(6)	2.335(3)
M2-O(XDK) <sub>av</sub> , Å <sup>a</sup>	2.059(6)	2.084(7)	2.269(3)
O101-M1-O201, deg	122.2(2)	127.6(2)	113.83(9)
O102-M2-O202, deg	100.3(2)	96.6(2)	94.76(9)
O11-P1-O12, deg	118.9(3)	118.8(3)	118.5(2)
P1-O-M1, deg	141.9(3)	137.6(3)	151.1(2)
P1-O-M2, deg	138.4(3)	135.8(3)	139.1(2)
$\phi$ , deg <sup>b</sup>	19.4	21.7	23.7
$d$ (M1), Å <sup>c</sup>	0.50	0.70	0.87
$d$ (M2), Å <sup>c</sup>	0.71	0.61	0.71
[O(101)O(102)C(101)C(107)] vs [O(201)O(202)C(201)C(207)], deg <sup>d</sup>	8.3	11	6.1

<sup>a</sup> Average value. Estimated deviations in parentheses are derived from  $(\sigma_A^2 + \sigma_B^2)^{1/2}$ . <sup>b</sup> Dihedral angle between the [M1M2(OCCO<sub>2</sub>)<sub>2</sub>] and the dicarboxylate planes (average value). <sup>c</sup> Distance from the metal atom to the dicarboxylate plane. <sup>d</sup> Dihedral angle.

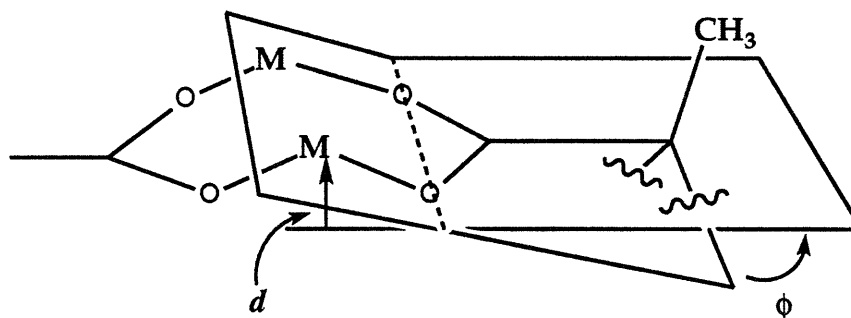


Table 5. Summary of Variable Temperature  $^{31}\text{P}\{^1\text{H}\}$  NMR Data

compound	$\Delta G^\ddagger$ (kJ mol $^{-1}$ )	$k_{\text{calc}}$ (s $^{-1}$ , 25 °C)	Coalescence T (°C)
1·CH $_3$ OH	60	$1.9 \times 10^2$	54
2	45	$7.5 \times 10^4$	-30
3·CH $_3$ OH	39	$9.1 \times 10^5$	-58

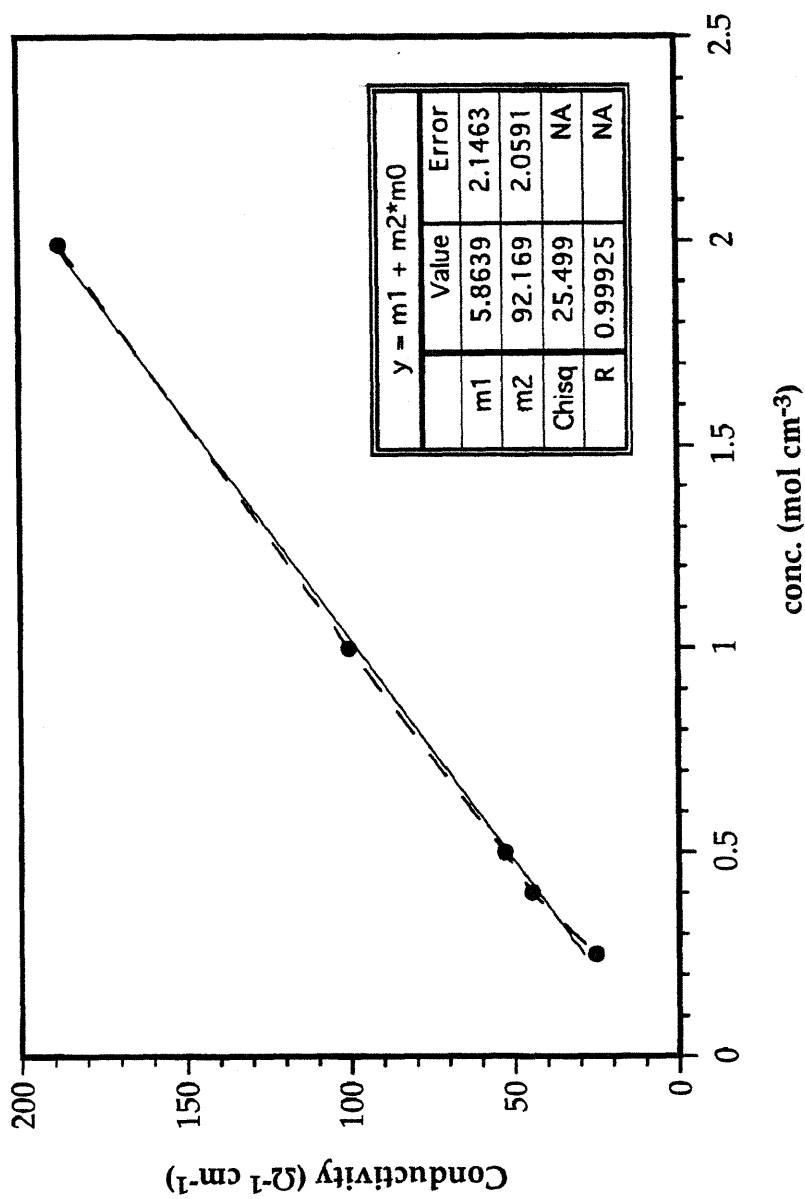
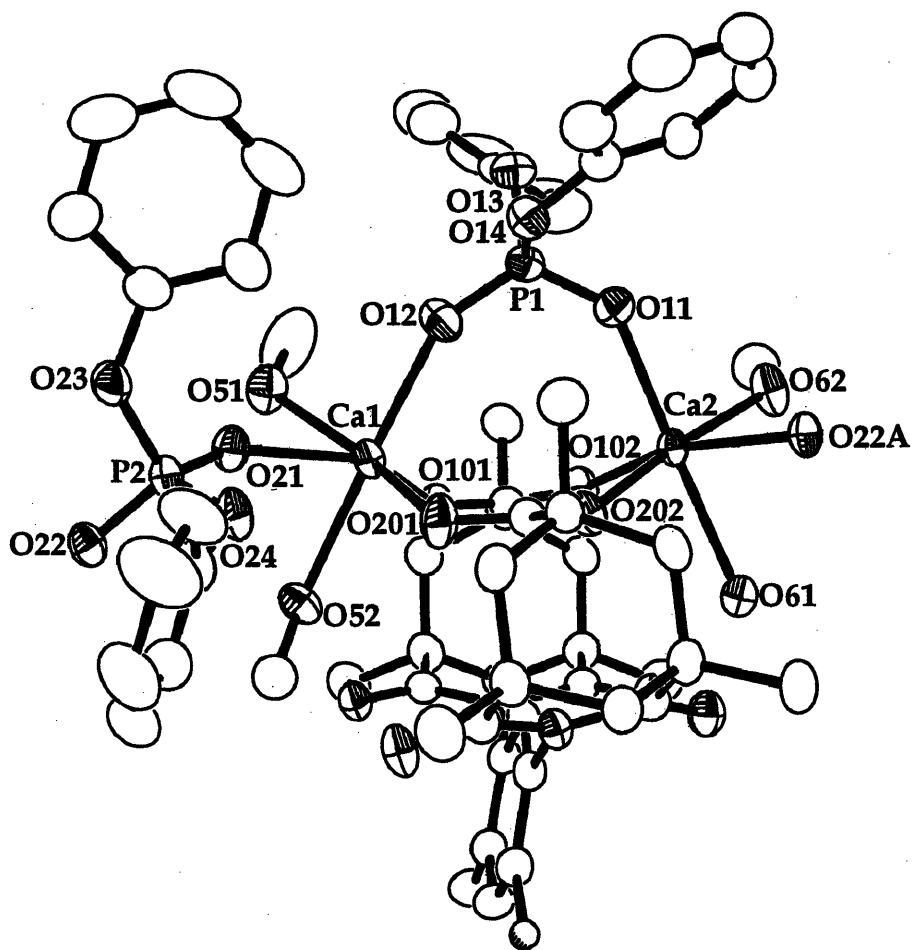


Figure 1. A plot of conductivity vs. concentration for  $3\cdot\text{CH}_3\text{OH}$ . The molar conductivity of  $92\ \Omega^{-1}\text{cm}^2\text{mol}^{-1}$  corresponded to 1:1 electrolyte behavior by comparison to  $[\text{Bu}_4\text{N}][\text{PF}_6]$  ( $95\ \Omega^{-1}\text{cm}^2\text{mol}^{-1}$ ).



**Figure 2.** An ORTEP diagram of [Ca<sub>2</sub>(XDK)(DPP)<sub>2</sub>(CH<sub>3</sub>OH)<sub>3</sub>(H<sub>2</sub>O)] (3). Thermal ellipsoids are drawn at the 50% probability level. Hydrogen atoms are omitted for clarity.



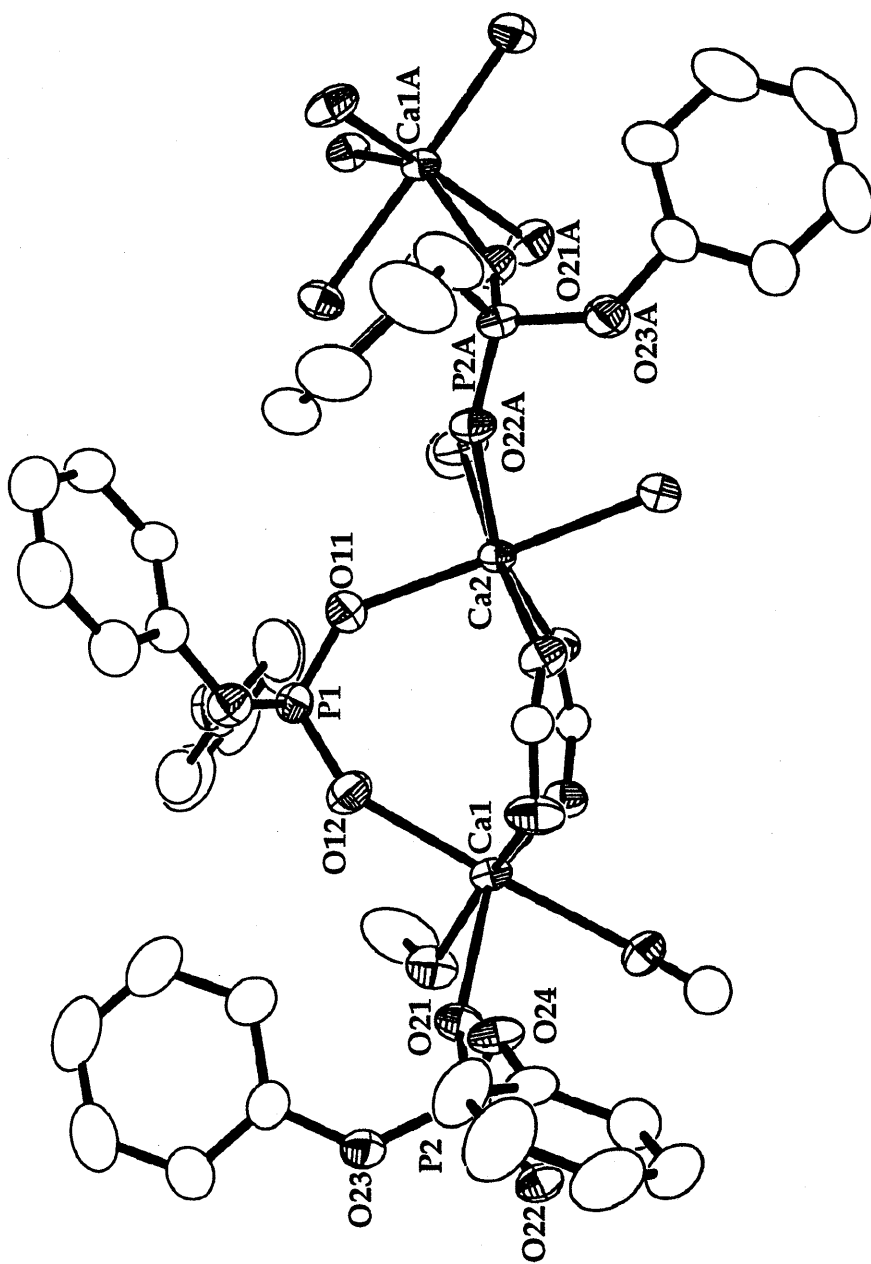


Figure 4. ORTEP view of the polymeric calcium center in 3.



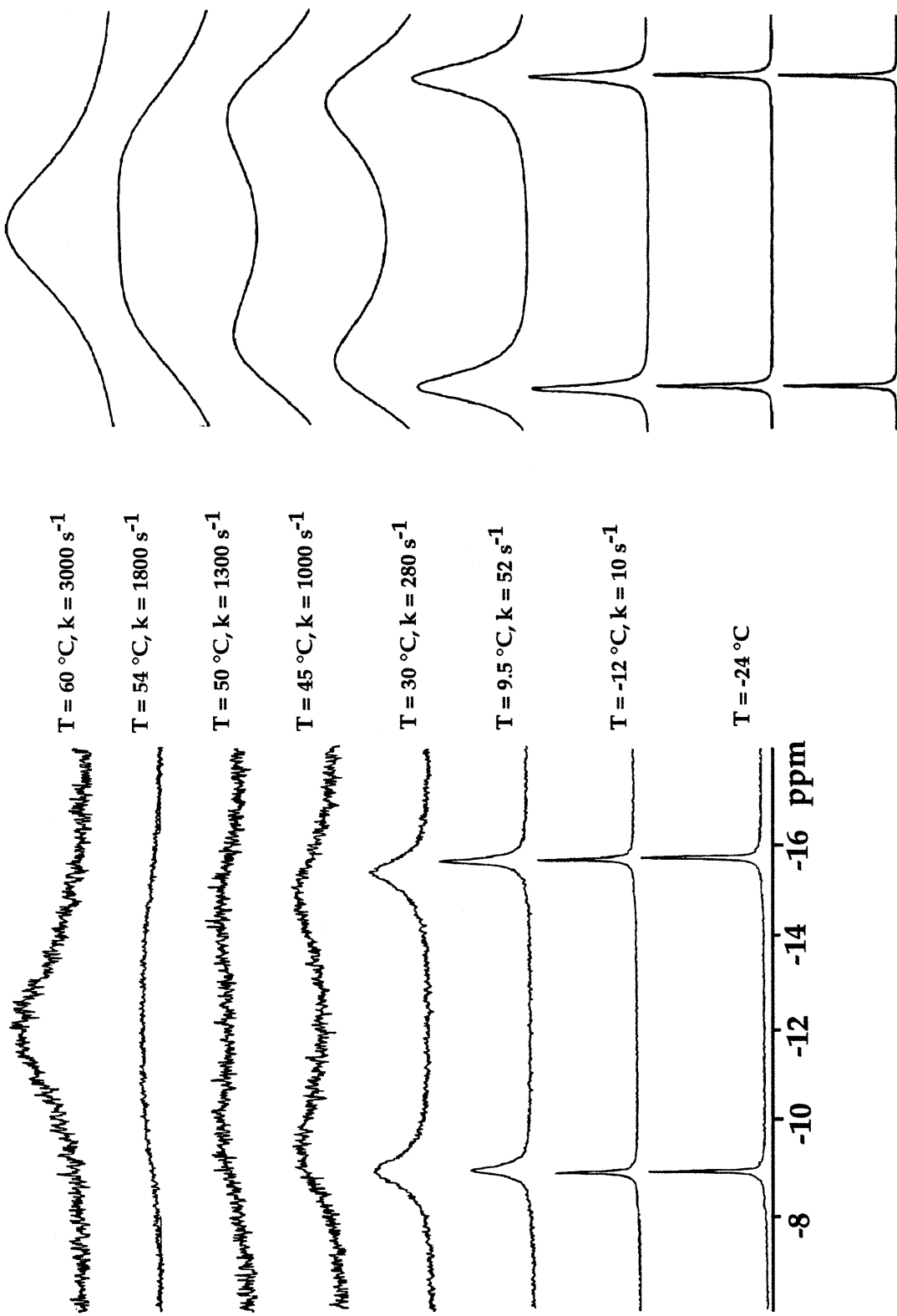


Figure 5. VT- ${}^{31}\text{P}\{^1\text{H}\}$  NMR Spectra for 1- $\text{CH}_3\text{OH}$  and DNMR Calculated Fits

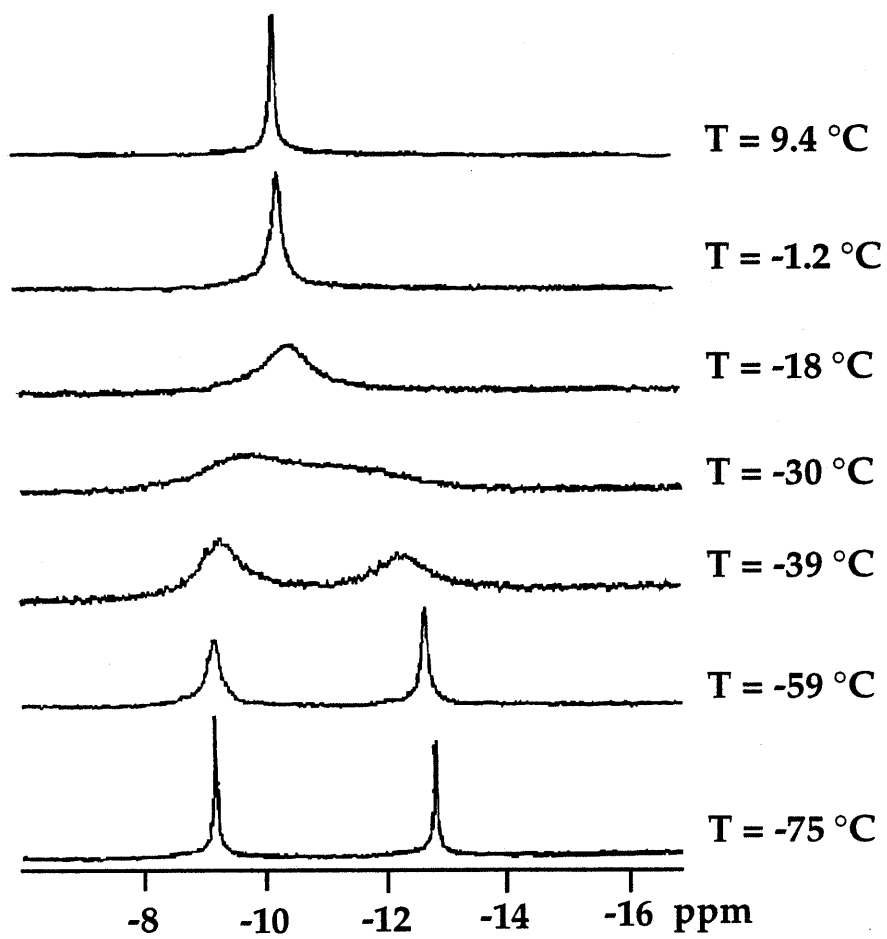


Figure 6. VT- $^{31}\text{P}\{^1\text{H}\}$  NMR Spectra for 2.

**Chapter 4****Studies of Water-Soluble Carboxylate-Bridged Dimagnesium(II) Complexes**

## INTRODUCTION

The formation and hydrolysis of phosphate ester bonds play important regulatory roles in biology. Nature employs kinases and phosphatases to catalyze these reactions under physiological conditions, and many of these enzymes require metal ions, such as magnesium, as cofactors. Enzymes such as the Klenow fragment of DNA polymerase I from *Escherichia coli*<sup>1</sup> have been structurally characterized to reveal a carboxylate-bridged dimetallic site responsible for the hydrolysis of phosphate esters. Several mechanisms have been proposed for phosphate ester hydrolysis in these enzymes. In the Klenow fragment, a two-metal-ion phosphoryl transfer mechanism has been postulated where the metal ions bind the substrate, then one metal ion generates the attacking nucleophile and the other stabilizes the transition state.<sup>1</sup> As shown in Scheme 1, the two carboxylate-bridged metal ions are proposed to be further bridged by a single oxygen atom of the scissile phosphate group and form two fused four-membered bidentate chelate rings with the phosphate. Scheme 2 illustrates the details of an alternative mechanism which has been recently been proposed to account for the results of phosphate ester hydrolysis in a dicobalt(III) model compound for phosphatases.<sup>2</sup> In this mechanism, a dimetallic center is bridged by a both bidentate phosphodiester ligand and hydroxide and oxide ions. The oxide ion has been shown to act as an internal nucleophile in the hydrolysis of the bridging phosphate ester.

We have developed a program to investigate the chemistry associated with the carboxylate-bridged dimagnesium(II) unit and to evaluate its potential as a phosphatase model. We began our studies by utilizing the dinucleating ligand XDK, where  $H_2XDK = m$ -xylylenediamine bis(Kemp's triacid imide).<sup>3,4</sup> From initial modelling studies in this laboratory with diiron(III) centers, the carboxylate groups of XDK were found to be highly effective in stabilizing dimetallic units of labile metal ions.<sup>5</sup> As we reported in chapter 2 of this thesis, a dimagnesium(II)-XDK

complex coordinated by labile solvent ligands was prepared and used as a platform to study phosphate ester chemistry. The stepwise addition of diphenyl phosphate to this complex afforded the first dimagnesium complexes coordinated by bridging and terminal phosphate ligands. The phosphate esters in the bis(phosphate)-dimagnesium compound exchanged with one another at elevated temperatures in methanol, and a similar phenomenon was examined for the dicalcium(II) and dizinc(II) analogs, as described in chapter 3.

In order to extend our modelling studies to aqueous media, we recently synthesized a water-soluble version of the XDK ligand, WXDK, where  $H_2WXDK = m$ -xylylenediamine bis(trihydroxymethyl-Kemp's triacid imide) (Figure 1). This new ligand has allowed us to prepare carboxylate-bridged dinuclear magnesium complexes which, in addition to their value as structural models for the enzyme active sites, can be studied in water. The synthesis of WXDK and its dimagnesium(II) complexes and phosphate ester-bridged derivatives are described in this chapter, together with the ability of carboxylate-bridged dimagnesium compounds to hydrolyze phosphate esters.

## EXPERIMENTAL METHODS

### General

Air- and water-sensitive reactions were performed in oven- and flame-dried glassware under argon. Solvents were distilled over the appropriate drying agents under nitrogen. Tetramethylammonium bis(4-nitrophenyl)phosphate was crystallized from a methanolic solution containing bis(4-nitrophenyl)hydrogen phosphate (HBNPP) and  $(Me_4N)OH$  in a 1:1 ratio. All other reagents were commercially available and used without further purification.  $^1H$  and  $^{31}P\{^1H\}$  NMR spectra were taken on Varian XL-300 and Varian UNITY300 spectrometers.  $^{31}P\{^1H\}$  NMR spectra were measured at 121.4 MHz with 85%  $H_3PO_4$  as an external reference.

$^{19}\text{F}$  NMR spectra were recorded on at 282.2 MHz with fluorotrichloromethane in  $\text{C}_6\text{D}_6$  as an external reference. Infrared spectra were taken on a Bio-Rad FTS7 Fourier transform instrument. Conductivity measurements were made at 23 °C in deionized water with a Fisher Scientific conductivity bridge model 9-326 and a platinum-black electrode. All pH measurements were taken with an Orion 960 pH meter. Electronic spectra were recorded on a Cary Model 1E spectrophotometer.

### **Synthesis of 1,3,5-Tribenzyloxy-1,3,5-Cyclohexane-Trimethyl Ester, 1**

This compound was prepared by a literature procedure<sup>6</sup> with the following modifications. The cyclohexane-1,3,5-trimethyl ester (33.4 g, 0.129 mol) was dissolved in ~300 mL of toluene and added to a solution of LDA (300 mL, 1.5 M in cyclohexane) in toluene (~500 mL) which had been cooled to 0 °C. Benzylchloromethyl ether (60.9 mL, 0.411 mol) was added to this solution which was further cooled to -40 °C in an acetonitrile/dry ice bath and allowed to warm gradually to room temperature over a period of 3-4 h and stirred overnight (12 h). The reaction mixture was then heated to approximately 60 °C and stirred for another hour. Recrystallization of the product following work-up was carried out in the following manner. Approximately 30 g of the brown, viscous oil was diluted with 300 mL of methanol, and the solution was heated to 65 °C. A white fluffy product precipitated. The solution was cooled gradually to room temperature and placed in a refrigerator (4 °C) overnight to afford more solid. Yield: 45% (36.2 g, 0.059 mol). The  $^1\text{H}$  NMR spectrum was consistent with that in the literature.<sup>6</sup>

### **Synthesis of 1,3,5-Tribenzyloxy-1,3,5-Cyclohexane-Tricarboxylic Acid, 2**

This compound was obtained as described in the literature.<sup>6</sup> Yield: 95% (32.1 g, 0.056 mol).

**Synthesis of 1,3,5-Tribenzyloxy-1,3,5-Cyclohexane Anhydride Acid Chloride, 3**

A solution of the tricarboxylic acid (2) (32.1 g, 0.056 mol) in thionyl chloride (200 mL) was heated to reflux for 4-5 h. Thionyl chloride (~ 150 mL) was distilled off and hexane was added to give a pale white precipitate. The product was filtered, washed with hexane, and dried under vacuum overnight. Yield: 85% (27.2 g, 0.047 mol).  $^1\text{H}$  NMR, 300 MHz (DMSO- $d_6$ ):  $\delta$  1.63 (m, 3 H), 2.28 (d, 2 H,  $J = 13.7$  Hz), 3.36-3.46 (m, 3 H), 3.79 (d, 4 H,  $J = 8.57$  Hz), 4.43 (s, 2 H), 4.51 (s, 4 H), 7.25-7.35 (m, 15 H).

**Synthesis of *m*-Xylylenediamine Bis(tribenzyloxy-Kemp's triacid imide), 4**

A 500 mL Schlenk flask containing the anhydride acid chloride 3 (27.2 g, 0.047 mol) was fitted with a reflux condenser and purged with argon. Pyridine (200 mL) was added, followed by *m*-xylylenediamine (3.20 g, 0.024 mol) and a catalytic amount of dimethylaminopyridine (DMAP). The solution was heated to reflux overnight under argon. Pyridine was distilled off and hexane was added to give a yellow-white precipitate. Hexane was removed in vacuo, and the precipitate was dissolved in methylene chloride (150 mL). This solution was washed with HCl (2 x 200 mL, 3M) and H<sub>2</sub>O (200 mL), then dried over Na<sub>2</sub>SO<sub>4</sub>. The solvent was removed in vacuo and dried under vacuum. The solid was recrystallized by vapor diffusion of ethyl ether into a chloroform solution to give block-shaped crystals of 4. Yield: 67% (19.7 g, 0.016 mol).  $^1\text{H}$  NMR, 300 MHz (CDCl<sub>3</sub>):  $\delta$  1.58-1.63 (m, 6 H), 1.88 (s, 6 H), 2.51 (d, 4 H,  $J = 13.8$  Hz), 2.68 (d, 2 H,  $J = 13.4$  Hz), 3.32-3.43 (m, 8 H), 3.83 (m, 4 H), 4.39-4.52 (m, 12 H), 6.58 (s, 1 H), 7.07 (s, 1 H), 7.14-7.26 (m, 15 H).

**Synthesis of *m*-Xylenediamine Bis(trihydroxymethyl-Kemp's triacid imide) (H<sub>2</sub>WXDK), 5**

A suspension of 4 (1.0 g, 0.821 mmol) in 8 mL of formic acid was stirred at 0 °C. Anhydrous HBr(g) generated from NaBr(s) and H<sub>2</sub>SO<sub>4</sub>(l) was transferred via a

teflon cannula into the formic acid mixture and passed through the suspension for approximately 8 min, resulting in a clear solution. Argon was then bubbled through the solution for at least 15 min, and the solution was concentrated in vacuo and dried under vacuum. The dried residue was triturated with  $\text{CHCl}_3$  and recrystallized from a methanol/ethyl ether solvent system to afford crystalline product. X-ray crystallography indicated the composition to be  $\text{H}_2\text{WXDK}\cdot\text{H}_2\text{O}\cdot\text{MeOH}$ . Yield: 81% (448 mg, 0.662 mmol).  $^1\text{H}$  NMR, 300 MHz ( $\text{D}_2\text{O}$ ):  $\delta$  1.52 (d, 4 H,  $J = 14.2$  Hz), 1.61 (d, 2 H,  $J = 13.1$  Hz), 2.02 (s, 6 H), 2.51 (d, 4 H,  $J = 14.3$  Hz), 2.80 (d, 2 H,  $J = 12.5$  Hz), 3.51 - 3.60 (m, 8 H), 4.11 (d, 4 H,  $J = 11.7$  Hz), 4.7 ( $\text{D}_2\text{O}$ ), 6.95 (s, 1 H), 7.39 (s, 1 H). IR (nujol): 3530 (m), 3471 (m), 3378 (br), 1727 (m), 1698 (s), 1682 (m), 1323 (m), 1247 (m), 1191 (m), 1048 (m), 956, 875, 790, 726  $\text{cm}^{-1}$ . Samples submitted for elemental analysis were heated to 100 °C under vacuum for 12 h to remove solvent in the lattice. Anal. Calcd. for  $\text{C}_{32}\text{H}_{40}\text{O}_{14}\text{N}_2$ : C, 56.80; H, 5.96; N, 4.14. Found: C, 56.37; H, 5.99; N, 4.05. HRMS (EI). Calcd. for  $\text{C}_{32}\text{H}_{40}\text{O}_{14}\text{N}_2$ : 676.2480. Found: 676.2472.

**Synthesis of  $[\text{Mg}_2(\text{WXDK})(\mu\text{-}\eta^2\text{OCH}_2\text{CH}_2\text{OCH}_3)(\text{CH}_3\text{OCH}_2\text{CH}_2\text{OH})_2(\text{H}_2\text{O})](\text{OTf})\cdot\text{CH}_3\text{OCH}_2\text{CH}_2\text{OH}$ ,  $6(\text{OTf})\cdot\text{CH}_3\text{OCH}_2\text{CH}_2\text{OH}$**

Method 1: A methanol solution (500  $\mu\text{L}$ ) of  $\text{Mg}(\text{CF}_3\text{SO}_3)_2$  (19 mg, 0.0591 mmol) was added to a solution of  $\text{H}_2\text{WXDK}$  (20 mg, 0.0296 mmol) and tetrabutylammonium hydroxide (65  $\mu\text{L}$ , 1.0 M in MeOH, 0.0650 mmol) in methanol (3 mL). The solution was stirred for at least 15 min, then the solvent was removed in vacuo to give a white product which was dried under vacuum. Recrystallization of the product by vapor diffusion of ethyl ether ( $\text{Et}_2\text{O}$ ) into a 2-methoxyethanol (HMOE) solution afforded long colorless block crystals which were collected and washed with  $\text{Et}_2\text{O}$ . Yield: 30% (11 mg, 0.0092 mmol). Method 2: A HMOE solution containing  $\text{H}_2\text{WXDK}$  (20 mg, 0.0296 mmol) and  $(\text{Bu}_4\text{N})\text{OH}\cdot 30\text{H}_2\text{O}$  (71 mg, 0.0888



mmol) was stirred for 10 min, then  $\text{Mg}(\text{CF}_3\text{SO}_3)_2$  (19 mg, 0.0591 mmol) was added. The solution was stirred for an additional 30 min, and the solvent was removed *in vacuo*. The dried residue was recrystallized from a HMOE/ethyl ether solvent system. Yield: 37% (13 mg, 0.0109 mmol).  $^1\text{H}$  NMR, 300 MHz ( $\text{D}_2\text{O}$ ):  $\delta$  1.29 (d, 4 H,  $J = 13.4$  Hz), 1.43 (d, 2 H,  $J = 13.1$  Hz), 1.90 (s, 6 H), 2.37 (d, 4 H,  $J = 13.7$  Hz), 2.68 (d, 2 H,  $J = 13.3$  Hz), 3.0 - 3.6 (m), 4.02 (d, 4 H,  $J = 11.5$  Hz), 4.7 ( $\text{D}_2\text{O}$ ), 7.14 (s, 1 H), 7.23 (s, 1 H). IR (Nujol): 3426 (br), 1724 (m), 1685 (s), 1616 (m), 1504 (s), 1258 (s), 1143 (s), 1036 (s), 947 (s)  $\text{cm}^{-1}$ . Samples prepared for elemental analysis were dried to remove HMOE. Anal. Calcd. for  $\text{Mg}_2\text{C}_{42}\text{H}_{67}\text{O}_{26}\text{N}_2\text{SF}_3 \cdot 6(\text{OTf}) \cdot 2\text{H}_2\text{O}$ : C, 43.73; H, 5.85; N, 2.43. Found: C, 43.44; H, 5.66; N, 2.40.

#### Synthesis of $[\text{Mg}_2(\text{WXDK})\{\mu\text{-}\eta^2\text{-(PhO)}_2\text{PO}_2\}(\text{CH}_3\text{OCH}_2\text{CH}_2\text{OH})_2(\text{H}_2\text{O})_2](\text{NO}_3)\cdot 2\text{CH}_3\text{OH}, 7(\text{NO}_3)\cdot 2\text{CH}_3\text{OH}$

A methanolic solution (1 mL) of  $\text{Mg}(\text{NO}_3)_2 \cdot 6\text{H}_2\text{O}$  (211 mg, 0.822 mmol) was added to a solution of  $\text{H}_2\text{WXDK}$  (278 mg, 0.411 mmol) and tetrabutylammonium hydroxide (822  $\mu\text{L}$ , 1.0 M in MeOH, 0.822 mmol) in methanol (3 mL). The solution was stirred for about 15 min, then a methanolic solution (1 mL) of  $(\text{Me}_4\text{N})\text{DPP}$  (tetramethylammonium diphenyl phosphate, 133 mg, 0.411 mmol) was added, and this solution was stirred for an additional 15 min. The solvent was removed *in vacuo*, and the product was dried under vacuum. The white, flaky solid was recrystallized by vapor diffusion of ethyl ether into a 2-methoxyethanol (HMOE) solution to give long needles. The dried crystalline product was treated with excess pyridine (5 mL) in chloroform (10 mL) and the insoluble salt contaminants were removed by filtration. The  $\text{CHCl}_3/\text{py}$  filtrate containing the complex was placed under vacuum to remove the solvents, and the residue was again dried under vacuum. The dried sample was then redissolved in HMOE, and vapor diffusion of ethyl ether into the resulting solution afforded colorless crystals of 7. Yield: 70% (358

mg, 0.285 mmol).  $^1\text{H}$  NMR, 300 MHz ( $\text{D}_2\text{O}$ ):  $\delta$  1.30 (d, 4 H,  $J = 13.8$  Hz), 1.45 (d, 2 H,  $J = 12.8$  Hz), 1.92 (s, 6 H), 2.39 (d, 4 H,  $J = 13.7$  Hz), 2.69 (d, 2 H,  $J = 13.0$  Hz), 3.09 - 3.64 (m), 4.02 (d, 4 H,  $J = 11.4$  Hz), 4.7 ( $\text{D}_2\text{O}$ ), 7.11 - 7.34 (m, 12 H).  $^{31}\text{P}\{^1\text{H}\}$  NMR, 121.4 MHz ( $\text{D}_2\text{O}$ ):  $\delta$  -8.1 (s).  $^{31}\text{P}\{^1\text{H}\}$  NMR, 121.4 MHz ( $\text{CD}_3\text{OD}$ ):  $\delta$  -15.1 (s, br). IR (Nujol): 3413 (br), 1723 (m), 1677 (s), 1621 (m), 1262 (s), 1193 (m), 1135 (m), 1038 (m), 933 (m), 799, 719  $\text{cm}^{-1}$ . Samples prepared for elemental analysis were dried to remove methanol. Anal. Calcd. for  $\text{Mg}_2\text{C}_{50}\text{H}_{71}\text{N}_3\text{O}_{28.5}\text{P}$  ( $7(\text{NO}_3) \cdot 1.5\text{H}_2\text{O}$ ): C, 48.06; H, 5.73; N, 3.36. Found: C, 47.83; H, 6.01; N, 3.85.

**Synthesis of  $[\text{Mg}_2(\text{WXDK})\{\mu\text{-}\eta^2\text{-(PhO)}_2\text{PO}_2\}\{\text{CH}_3\text{OCH}_2\text{CH}_2\text{OH}\}_2(\text{H}_2\text{O})_2](\text{OTf}) \cdot \text{CH}_3\text{OCH}_2\text{CH}_2\text{OH}$ ,  $8(\text{OTf}) \cdot \text{CH}_3\text{OCH}_2\text{CH}_2\text{OH}$**

A methanolic solution (1 mL) of  $\text{Mg}(\text{CF}_3\text{SO}_3)_2$  (133 mg, 0.414 mmol) was added to a solution of  $\text{H}_2\text{WXDK}$  (140 mg, 0.207 mmol) and tetramethylammonium hydroxide (174  $\mu\text{L}$ , 25 wt. % soln in MeOH, 0.414 mmol) in methanol (3 mL). The solution was stirred for about 15 min, following which a methanol solution (1 mL) of  $(\text{Me}_4\text{N})\text{DPP}$  (tetramethylammonium diphenyl phosphate, 67 mg, 0.207 mmol) was added, and this solution was stirred for another 15 min. The solvent was removed in vacuo, and the product was dried under vacuum. The dried residue was recrystallized by vapor diffusion of ethyl ether into a 2-methoxyethanol (HMOE) solution to give long needles and small amounts of  $\text{Me}_4\text{N}^+$  salt contaminants. The dried crystalline product was treated with excess pyridine in chloroform, and the insoluble salt contaminants were removed by filtration. The  $\text{CHCl}_3/\text{py}$  filtrate containing the complex was placed under vacuum to remove the solvents, and the residue was dried under vacuum. The dried sample was then redissolved in HMOE, and vapor diffusion of ethyl ether afforded colorless crystals. Yield: 33% (94 mg, 0.068 mmol).  $^1\text{H}$  NMR, 300 MHz ( $\text{D}_2\text{O}$ ):  $\delta$  1.29 (d, 4 H,  $J = 13.8$  Hz), 1.43 (d, 2 H,  $J = 13.4$  Hz), 1.91 (s, 6 H), 2.38 (d, 4 H,  $J = 13.2$  Hz), 2.68 (d, 2 H,  $J = 13.1$  Hz), 3.07 - 3.63

(m), 4.01 (d, 4 H,  $J = 11.7$  Hz), 4.7 (D<sub>2</sub>O), 7.10 - 7.33 (m, 12 H). <sup>31</sup>P{<sup>1</sup>H} NMR, 121.4 MHz (D<sub>2</sub>O):  $\delta$  -8.0 (s). <sup>31</sup>P{<sup>1</sup>H} NMR, 121.4 MHz (CD<sub>3</sub>OD):  $\delta$  -15.2 (s, br). IR (Nujol): 3476 (br), 1720 (s), 1683 (s), 1630 (s), 1590 (m), 1258 (m, br), 1196, 1170, 1121, 1029, 914, 827, 780 cm<sup>-1</sup>. Elemental analysis samples were dried to remove HMOE. Anal. Calcd. for Mg<sub>2</sub>C<sub>51</sub>H<sub>70</sub>N<sub>2</sub>O<sub>28</sub>PSF<sub>3</sub> (8(OTf)·H<sub>2</sub>O): C, 46.14; H, 5.31; N, 2.11. Found: C, 45.93; H, 5.63; N, 2.08.

**Synthesis of [Mg<sub>2</sub>(WXDK){ $\mu$ - $\eta^2$ -(*p*-NO<sub>2</sub>PhO)<sub>2</sub>PO<sub>2</sub>}(CH<sub>3</sub>OCH<sub>2</sub>CH<sub>2</sub>OH)<sub>3</sub>(H<sub>2</sub>O)<sub>2</sub>]-  
(OTf)<sub>0.5</sub>(BNPP)<sub>0.5</sub>·0.5CH<sub>3</sub>OCH<sub>2</sub>CH<sub>2</sub>OH, 9(OTf)<sub>0.5</sub>(BNPP)<sub>0.5</sub>·0.5CH<sub>3</sub>OCH<sub>2</sub>CH<sub>2</sub>OH**

A methanolic solution (1 mL) of Mg(CF<sub>3</sub>SO<sub>3</sub>)<sub>2</sub> (48 mg, 0.148 mmol) was added to a solution of H<sub>2</sub>WXDK (50 mg, 0.074 mmol) and tetramethylammonium hydroxide (25  $\mu$ L, 25 wt. % soln in MeOH, 0.148 mmol) in methanol (3 mL). The solution was stirred for at least 15 min, then a methanol solution of (Me<sub>4</sub>N)BNPP (tetramethylammonium bis(4-nitrophenyl)phosphate, 31 mg, 0.074 mmol) was added. This light-yellow solution was stirred for an additional 15 min. The solvent was removed in vacuo, and the light-yellow product was dried under vacuum. Recrystallization by vapor diffusion of ethyl ether into a 2-methoxyethanol (HMOE) solution gave colorless crystals. The crystalline material was treated with pyridine in excess chloroform and the salt contaminants were removed by filtration. The py/CHCl<sub>3</sub> filtrate was placed under vacuum to remove the solvents, and the dried residue was redissolved in HMOE. Vapor diffusion of ethyl ether into the HMOE solution gave 9 in 55% yield (64 mg, 0.041 mmol). <sup>1</sup>H NMR, 300 MHz (CD<sub>3</sub>OD):  $\delta$  1.43 (m, 6 H), 1.98 (s, 6 H), 2.56 (d, 4 H,  $J = 13.5$  Hz), 2.77 (d, 2 H,  $J = 12.3$  Hz), 3.3 - 3.7 (m), 4.07 (d, 4 H,  $J = 11.4$  Hz), 4.9 (s), 7.15 (s, 1 H), 7.30 (s, 1 H), 7.40 (d, 6 H,  $J = 9.3$  Hz), 8.20 (d, 6 H,  $J = 9.3$  Hz). <sup>31</sup>P{<sup>1</sup>H} NMR, 121.4 MHz (D<sub>2</sub>O):  $\delta$  -10.5 (s). <sup>31</sup>P{<sup>1</sup>H} NMR, 121.4 MHz (CD<sub>3</sub>OD):  $\delta$  -11.2 (br), 16.9 (s). <sup>19</sup>F NMR, 282.2 MHz, (D<sub>2</sub>O):  $\delta$  -78.8 (s). IR (Nujol): 3502 (br), 3444 (br), 1720 (m), 1676 (s), 1632 (s), 1518 (s), 1340 (s), 1260 (s), 1220,

1122, 1076, 1031, 908 (m), 762  $\text{cm}^{-1}$ . Samples prepared for elemental analysis were dried to remove HMOE. Anal. Calcd. for  $\text{Mg}_2\text{C}_{59.5}\text{H}_{80}\text{O}_{36.5}\text{N}_5\text{F}_{1.5}\text{P}_{1.5}\text{S}_{0.5}(\text{OTf})_{0.5}(\text{BNPP})_{0.5}\cdot\text{H}_2\text{O}$ : C, 44.98; H, 5.07; N, 4.41. Found: C, 44.83; H, 5.15; N, 4.28.

### X-ray Crystallography

Single-crystal X-ray diffraction studies were carried out on a Siemens CCD X-ray diffraction system controlled by a pentium-based PC running the SMART version 4.0 software package,<sup>7</sup> as previously described.<sup>8</sup> Crystals were mounted at room temperature on the ends of quartz fibers in Paratone and data collection was carried out at -80 or -85 °C. The crystals were judged to be of acceptable quality on the basis of initial unit cell matrices and reflection profiles. Crystallographic data for compounds 5, 6, 8, and 9 are given in Table 1. Crystallographic data for 7 are as follows: monoclinic,  $P2_1/c$ , cell constants (-80 °C):  $a = 16.8182(9)$  Å,  $b = 23.8189(9)$  Å,  $c = 14.8326(7)$  Å,  $\beta = 92.691(1)$  °;  $V = 5935.3(4)$  Å<sup>3</sup>;  $Z = 4$ ;  $R_{\text{merge}} = 0.21$ ;  $R1 = 0.188$  and  $wR2 = 0.453$  for 5321 independent reflections with  $I > 2\sigma(I)$  and 785 variable parameters. The data for the structures described in this chapter, including tables of atomic positional parameters and anisotropic temperature factors, are available on a 4mm DAT tape.

### Structure Solution and Refinement

All computations were carried out on Silicon Graphics Indy workstations. The raw data frames were processed by the SAINT version 4.0 software package.<sup>9</sup> All aspects of the structure solution and refinement were handled by the SHELXTL version 5.0 software package.<sup>10</sup> Space groups for all structures were determined by examining the systematic absences in the data. For 6 and 8, the polar space group assignment was made by inverting the structure and reviewing the least squares refinement output. Non-hydrogen atoms were located by direct methods and a

series of structure factor calculations, least squares refinements, and difference Fourier maps. Absorption corrections were not applied to the data sets since the absorption coefficients were quite small for 5, 6, 8, and 9 (Table 1). The structure of compound 7 was not refined owing to the poor quality of the data set.

### **pH Titrations**

A stock solution of  $(\text{Me}_4\text{N})\text{OH}$  was prepared in deionized water and standardized by  $\text{HNO}_3$ , which was purchased as a standardized 0.1 M solution. The  $\text{HNO}_3$  solution was titrated with  $(\text{Me}_4\text{N})\text{OH}$  by using phenolphthalein as an indicator. Approximately 40-60 points were taken for the titration curves and used to calculate the  $\text{pK}_a$  values with the computer program PKAS.<sup>11</sup>

### **Kinetic Measurements in Aqueous Solutions**

The rates of phosphate ester hydrolysis reactions of bis(4-nitrophenyl)phosphate ( $\text{BNPP}^-$ ) in aqueous solution were monitored by following the increase in absorbance at 400 nm for released 4-nitrophenolate at room temperature, according to previously described procedures.<sup>12,13</sup> Buffer solutions containing 50 mM buffer (CHES, 2-(cyclohexylamino)propane sulfonic acid, pH 9.0; CAPS, 3-(*N*-cyclohexylamino)propane sulfonic acid, pH 10.0, 10.7, 10.8, and 10.9) were used. Reactions were also investigated under unbuffered conditions. Typically, equimolar quantities (2 mM) of  $(\text{Me}_4\text{N})\text{BNPP}$  and 7 were mixed, and the UV absorption increase was followed for 4-nitrophenolate formation, where the  $\log \epsilon$  values for 4-nitrophenolate were taken from the literature.<sup>12</sup>

## RESULTS

### Characterization of a Water-Soluble XDK Analog (5, H<sub>2</sub>WXDK)

We have synthesized a water-soluble analog of XDK, WXDK, by procedures analogous to that used for the preparation of tribenzyloxy-Kemp's triacid<sup>6,14</sup> and H<sub>2</sub>XDK<sup>4</sup> (Scheme 3). Tribenzyloxy-Kemp's triacid (2) was prepared as previously described<sup>6</sup> and used as a precursor to form the anhydride acid chloride (3). Compound 3 was coupled to *m*-xylylenediamine to give a product mixture which contained the desired *m*-xylylenediamine bis(tribenzyloxy-Kemp's triacid imide) (4). Compound 4 was purified by recrystallization from a chloroform-ether solvent system. Crystals of 4 were obtained and used for X-ray crystallographic analysis. The crystals were of poor quality, but were sufficient to confirm that the structure of 4 was that shown in Scheme 3. Removal of the benzyl groups from 4 with HBr(g) generated the *m*-xylylenediamine bis(trihydroxymethyl-Kemp's triacid imide) (5, H<sub>2</sub>WXDK). An X-ray analysis of 5 confirmed its structure to be that shown in Figure 1. Compound 5 crystallizes with a water and a methanol in the lattice which are hydrogen-bonded to the H<sub>2</sub>WXDK ligand (Figures 2 and 3). The hydrogen atoms for the solvent molecules were located from difference Fourier maps and refined isotropically. All other carbon- and oxygen-bound hydrogen atoms were calculated at their ideal positions and were assigned a thermal parameter equivalent to 1.2 times the thermal parameter of the atom to which it is attached. The bond distances and angles are given in Tables 2 and 3. The oxygen-oxygen hydrogen-bonded carboxylate distances are O101...O201 = 2.619 Å and O102...O202 = 2.624 Å. The hydrogen-bonded distances of the water molecule (O31) to O15, O24, O103, and O203 are 2.906, 2.762, 2.766, and 2.777 Å, respectively. The lattice methanol (O41) is hydrogen-bonded to O15 and O26, with oxygen-oxygen distances of 2.797 and 2.627 Å, respectively.

**Structure of  $[\text{Mg}_2(\text{WXDK})(\mu\text{-}\eta^2\text{OCH}_2\text{CH}_2\text{OCH}_3)(\text{CH}_3\text{OCH}_2\text{CH}_2\text{OH})_2(\text{H}_2\text{O})](\text{OTf})\cdot\text{CH}_3\text{OCH}_2\text{CH}_2\text{OH}$ ,  $6(\text{OTf})\cdot\text{CH}_3\text{OCH}_2\text{CH}_2\text{OH}$**

The reaction of  $\text{Mg}(\text{OTf})_2$  (2 equiv) with  $\text{H}_2\text{WXDK}$  (1 equiv) and  $(\text{Bu}_4\text{N})\text{OH}$  (2.2 equiv) in methanol and subsequent workup afforded colorless crystals of  $[\text{Mg}_2(\text{WXDK})(\mu\text{-}\eta^2\text{OCH}_2\text{CH}_2\text{OCH}_3)(\text{HMOE})_2(\text{H}_2\text{O})](\text{OTf})\cdot\text{HMOE}$ ,  $6(\text{OTf})\cdot\text{HMOE}$ . The IR spectrum of **6** indicated the presence of WXDK ( $1616 - 1724 \text{ cm}^{-1}$ ), triflate ( $1258 \text{ cm}^{-1}$ ), and hydroxyl groups ( $\sim 3400 \text{ cm}^{-1}$ ). The  $^1\text{H}$  NMR spectrum of **6** in  $\text{D}_2\text{O}$  showed a  $\text{C}_{2v}$  symmetrical set of WXDK ligand resonances, as evidenced by doublets observed for the methylene groups of the ligand.

Crystals of  $6(\text{OTf})\cdot\text{HMOE}$  were grown from a 2-methoxyethanol/ethyl ether mixed solvent system, and an X-ray crystallographic analysis revealed its structure to be a carboxylate-bridged dimagnesium complex (Figure 4). Selected bond distances and angles are given in Table 4. There is a slightly disordered triflate anion and a 2-methoxyethanol in the crystal lattice. The triflate anion has one fluorine atom and two oxygen atoms which were each disordered over two positions. The two metal ions are bridged by the carboxylate oxygens of the WXDK ligand and the oxygen atom of  $^-\text{OCH}_2\text{CH}_2\text{OCH}_3$ , a deprotonated 2-methoxyethanol. The coordination sphere of Mg1 is octahedral comprising O51 and O52, another bidentate HMOE (O31 and O32), and the two carboxylate atoms of WXDK (O101 and O201). The Mg1-O bond to the charged oxygen atoms O51, O101, and O201 are distinctly shorter than those to the other oxygen atoms (O52, O31, and O32). Mg2 is octahedrally coordinated to the bridging oxygen atom (O51), a bidentate HMOE (O41 and O42), a water molecule (O43), and the carboxylates of WXDK (O102 and O202). The Mg2 bond distances to O51, O102, and O202 are also shorter than those to O41, O42, and O43. The metal-metal separation in **6** is  $3.402(3) \text{ \AA}$ , and the Mg1-O51-Mg2 bond angle is  $111.8(2)^\circ$ . Mg1 and Mg2 are displaced by 1.1 and 1.2  $\text{ \AA}$ , respectively, from the dicarboxylate plane (Table 7). The dihedral angles between the  $[\text{Mg1-O51-Mg2}]$  plane

and the [Mg1-O31-O32-C31-C32], [Mg2-O41-O42-C41-C42], and [Mg1-O51-O52-C51-C52] planes are 34, 36, and 112°, respectively. The [Mg1-O51-Mg2] plane is 84° to the plane of the xylyl spacer. The [Mg1-O51-O52-C51-C52] plane is 89° from the [Mg1-O31-O32-C31-C32] plane and 123° from the plane of the Mg2-HMOE five-membered chelate ring.

**Structure of [Mg<sub>2</sub>(WXDK){μ-η<sup>2</sup>-(PhO)<sub>2</sub>PO<sub>2</sub>}(CH<sub>3</sub>OCH<sub>2</sub>CH<sub>2</sub>OH)<sub>2</sub>(H<sub>2</sub>O)<sub>2</sub>](NO<sub>3</sub>)·2CH<sub>3</sub>OH, 7(NO<sub>3</sub>)·2CH<sub>3</sub>OH**

Compound 7 was prepared by the reaction of Mg(NO<sub>3</sub>)<sub>2</sub>·6H<sub>2</sub>O (2 equiv) with H<sub>2</sub>WXDK (1 equiv) and tetrabutylammonium hydroxide (2 equiv) in methanol, followed by the addition of (Me<sub>4</sub>N)DPP (1 equiv). Recrystallization of 7 from a 2-methoxyethanol/ethyl ether solvent system gave the desired compound, [Mg<sub>2</sub>(WXDK){μ-η<sup>2</sup>-(PhO)<sub>2</sub>PO<sub>2</sub>}(MOE)<sub>2</sub>(H<sub>2</sub>O)<sub>2</sub>](NO<sub>3</sub>). The IR spectrum indicated the presence of WXDK, diphenyl phosphate (1262 cm<sup>-1</sup>), and hydroxyl groups. The <sup>1</sup>H NMR spectrum of 7 in D<sub>2</sub>O indicated a symmetrical WXDK ligand environment and the presence of diphenyl phosphate in a 1:1 ratio with WXDK. The <sup>31</sup>P{<sup>1</sup>H} NMR spectrum in D<sub>2</sub>O showed one signal at δ -8.1, corresponding to free diphenyl phosphate. The <sup>31</sup>P{<sup>1</sup>H} NMR spectrum of 7 in CD<sub>3</sub>OD had one signal at δ -15.2, arising from bound phosphate ester, an assignment made by comparison with that of [Mg<sub>2</sub>(XDK){μ-η<sup>2</sup>-(PhO)<sub>2</sub>PO<sub>2</sub>}(CH<sub>3</sub>OH)<sub>3</sub>(H<sub>2</sub>O)(NO<sub>3</sub>)] (δ -15.5).<sup>15</sup>

Crystals of 7(NO<sub>3</sub>)·2CH<sub>3</sub>OH were grown by vapor diffusion of ethyl ether into a concentrated HMOE solution. These crystals were very fine needles that diffracted weakly, but were of sufficient quality to obtain an X-ray structure by Chemical Crystallographic Analysis (CCA). The structure of 7 consists of a dinuclear magnesium center, bridged by the carboxylates of WXDK and a bidentate diphenyl phosphate, along with a nitrate in the lattice. The octahedral coordination spheres of both magnesium ions are completed by a bidentate 2-methoxyethanol and a water



molecule on each metal. This structure was not fully refined owing to the poor quality of the data set. The triflate salt of this complex,  $[\text{Mg}_2(\text{WXDK})\{\mu\text{-}\eta^2\text{-(PhO)}_2\text{PO}_2\}(\text{MOE})_2(\text{H}_2\text{O})_2](\text{OTf})$  (**8**) was also prepared and its structure is discussed below.

**Structure of  $[\text{Mg}_2(\text{WXDK})\{\mu\text{-}\eta^2\text{-(PhO)}_2\text{PO}_2\}(\text{CH}_3\text{OCH}_2\text{CH}_2\text{OH})_2(\text{H}_2\text{O})_2](\text{OTf})\cdot\text{CH}_3\text{OCH}_2\text{CH}_2\text{OH}$ ,  $8(\text{OTf})\cdot\text{CH}_3\text{OCH}_2\text{CH}_2\text{OH}$**

The reaction of  $\text{Mg}(\text{CF}_3\text{SO}_3)_2$  (2 equiv) and  $(\text{Me}_4\text{N})\text{DPP}$  (1 equiv) with  $\text{H}_2\text{WXDK}$  (1 equiv) and  $(\text{Me}_4\text{N})\text{OH}$  (2 equiv) in methanol, followed by recrystallization from 2-methoxyethanol/ethyl ether afforded  $[\text{Mg}_2(\text{WXDK})\{\mu\text{-}\eta^2\text{-(PhO)}_2\text{PO}_2\}(\text{HMOE})_2(\text{H}_2\text{O})_2](\text{OTf})$  (**8**). The IR spectrum of **8** revealed the presence of WXDK, hydroxyl groups, and a feature at  $1258\text{ cm}^{-1}$  which could arise from both triflate and diphenyl phosphate. The  $^1\text{H}$  and  $^{31}\text{P}\{^1\text{H}\}$  NMR spectra of **8** in  $\text{D}_2\text{O}$  and  $\text{CD}_3\text{OD}$  were similar to those of **7**.

Long, crystalline needles of  $8(\text{OTf})\cdot\text{CH}_3\text{OCH}_2\text{CH}_2\text{OH}$  were grown from a HMOE/ethyl ether solvent system, and an X-ray crystallographic analysis revealed its structure to be analogous to that of **7** (Figure 4). Selected bond distances and angles are given in Table 5. There is a triflate anion and two half-occupied 2-methoxyethanol molecules in the crystal lattice. The two magnesium atoms are situated  $4.200(4)\text{ \AA}$  apart, bridged by the carboxylate oxygens of WXDK and a bidentate diphenyl phosphate.  $\text{Mg}1$  and  $\text{Mg}2$  are displaced by  $0.49$  and  $0.79\text{ \AA}$ , respectively, from the dicarboxylate plane (Table 7). Each metal ion is further coordinated in an octahedral manner by a bidentate 2-methoxyethanol and a water molecule. The bond length of  $\text{Mg}1$  to the bridging phosphate oxygen (O31) is  $2.020(7)\text{ \AA}$ , which is slightly longer than that of  $\text{Mg}2\text{-O}41$  ( $1.998(8)\text{ \AA}$ ). The  $\text{Mg}1\text{-O}101$  and  $\text{-O}201$  bonds are also slightly longer than those of  $\text{Mg}2$  to  $\text{O}102$  and  $\text{O}202$ . The  $\text{O}31\text{-P}1\text{-O}41$  bond angle is distorted from its tetrahedral value to  $119.3(4)^\circ$ . The

magnesium atoms are coordinated to the syn lone pairs of the diphenyl phosphate, similar to that observed previously for the XDK analog,  $[\text{Mg}_2(\text{XDK})\{\mu\text{-}\eta^2\text{-(PhO)}_2\text{PO}_2\}\text{-(CH}_3\text{OH)}_3(\text{H}_2\text{O})(\text{NO}_3)]$ .<sup>15</sup> The  $[\text{Mg1-Mg2-O31-O41}]$  plane is approximately perpendicular to the dicarboxylate plane ( $90^\circ$ ) and the plane of the xylyl spacer ( $88^\circ$ ). The  $[\text{Mg1-O31-O41-P1}]$  plane is roughly coplanar with the  $[\text{Mg2-O31-O41-P1}]$  plane, with a dihedral angle of  $7.4^\circ$ .

**Structure of  $[\text{Mg}_2(\text{WXDK})\{\mu\text{-}\eta^2\text{-(}p\text{-NO}_2\text{PhO)}_2\text{PO}_2\}(\text{CH}_3\text{OCH}_2\text{CH}_2\text{OH)}_3(\text{H}_2\text{O})_2\text{-(OTf)}_{0.5}(\text{BNPP})_{0.5}\cdot 0.5\text{CH}_3\text{OCH}_2\text{CH}_2\text{OH}$ , **9**(OTf)<sub>0.5</sub>(BNPP)<sub>0.5</sub>·0.5CH<sub>3</sub>OCH<sub>2</sub>CH<sub>2</sub>OH**

Compound **9** was prepared by the reaction of  $\text{Mg}(\text{CF}_3\text{SO}_3)_2$  (2 equiv) and  $(\text{Me}_4\text{N})\text{BNPP}$  (1 equiv) with  $\text{H}_2\text{WXDK}$  (1 equiv) and  $(\text{Me}_4\text{N})\text{OH}$  (2 equiv) in methanol, followed by recrystallization of the product from a 2-methoxyethanol/ethyl ether solvent system. The IR spectrum of **9** indicated the presence of WXDK, triflate anion, bis(4-nitrophenyl)phosphate, and hydroxyl groups. The  $^1\text{H}$  NMR spectrum of **9** in  $\text{CD}_3\text{OD}$  (Figure 7) revealed the WXDK ligand to be in a symmetrical environment and indicated the presence of bis(4-nitrophenyl)phosphate in a 1.5:1 ratio of  $\text{BNPP}^-$  to WXDK. The  $^{31}\text{P}\{^1\text{H}\}$  NMR spectrum of **9** in  $\text{D}_2\text{O}$  showed one signal at  $\delta$  -10.5, which is similar to that of free  $(\text{Me}_4\text{N})\text{BNPP}$  ( $\delta$  -10.8). The  $^{31}\text{P}\{^1\text{H}\}$  NMR spectrum of **9** in  $\text{CD}_3\text{OD}$  consisted of two signals, a broad signal at  $\delta$  -11.2 and a singlet at  $\delta$  -15.2. The former signal was assigned to free  $\text{BNPP}^-$ , and the latter was assigned to the bound species since our previous studies have shown that an upfield shift occurs upon coordination to the dimagnesium center.<sup>15</sup> The free-to-bound phosphodiester ratio integrated to be 1:2. The  $^{19}\text{F}$  NMR spectrum of **9** in  $\text{D}_2\text{O}$  showed a signal at  $\delta$  -78.8, corresponding to triflate anion.

Crystals of  $9(\text{OTf})_{0.5}(\text{BNPP})_{0.5}\cdot 0.5\text{CH}_3\text{OCH}_2\text{CH}_2\text{OH}$  were grown by vapor diffusion of ethyl ether into a concentrated 2-methoxyethanol solution. An X-ray analysis of **9** revealed its structure to comprise a dinuclear magnesium center,

bridged by the carboxylate oxygen atoms of WXDK and a bidentate bis(4-nitrophenyl)phosphate ligand (Figure 5). Selected bond distances and angles are given in Table 6. There is a disordered BNPP<sup>-</sup> at half occupancy in the lattice, along with a half occupied triflate anion in the crystal lattice. This structure is consistent with our NMR studies, which indicated the presence of triflate anion by <sup>19</sup>F NMR and a 1:2 free-to-bound BNPP<sup>-</sup> ratio in the <sup>31</sup>P{<sup>1</sup>H} NMR spectrum. Both magnesium atoms in **9** are octahedrally coordinated. Mg1 and Mg2 are displaced by 0.64 and 0.72 Å, respectively, from the dicarboxylate plane (Table 7). Mg1 is coordinated by O31 of the bridging phosphate, O101 and O201 of WXDK, two monodentate 2-methoxyethanol ligands (O32 and O34), and one water molecule (O36). Mg2 is coordinated by O41 of bis(4-nitrophenyl)phosphate, O102 and O202 of WXDK, a bidentate HMOE (O42 and O43), and a water molecule (O44). The magnesium atoms are situated 4.340(3) Å apart. The O31-P1-O41 bond angle is 120.6(3)°, whereas the other angles around P1 are roughly tetrahedral. The [Mg1-O31-O41-Mg2] plane is 84° and 93° from the dicarboxylate and xylyl spacer planes, respectively. The dihedral angle between the [Mg1-O31-O41-P1] and [Mg2-O31-O41-P1] planes is 14°.

### Solution Properties of Dimagnesium-WXDK Complexes

A pH titration of the H<sub>2</sub>WXDK ligand revealed the second pK<sub>a</sub> of the carboxylate groups to be unusually high (pK<sub>a2</sub> ~ 11), although similar to that previously reported for the H<sub>2</sub>XDK ligand (pK<sub>a2</sub> = 11.1).<sup>16</sup> Since metal ions lower the pK<sub>a</sub> values of their ligands, we expected to find that the pK<sub>a2</sub> of the dimagnesium WXDK complexes would be lowered by about 3-4 pK<sub>a</sub> units. For example, in the presence of Mg<sup>2+</sup>, the pK<sub>a</sub> value of DL-3-hydroxybutanoic acid (CH<sub>3</sub>-CH(OH)-CH<sub>2</sub>-CO<sub>2</sub>H) is lowered from 4.28 to 0.60.<sup>17</sup> A pH titration of **7** with (Me<sub>4</sub>N)OH and HNO<sub>3</sub> revealed a titratable group at pH ~ 9 (Figure 8), which we

attribute to the  $pK_a$  value of the metal-bound WXDK ligand. Tetramethylammonium hydroxide was used for the titrations to avoid competition of  $Na^+$  with  $Mg^{2+}$  for coordination to the ligand carboxylates.

Protonation of the carboxylate oxygen atoms in WXDK ligand could lead to displacement of magnesium ion from 7. Conductivity measurements of 7 in deionized water revealed it to be a 2:1 electrolyte. This finding was initially attributed to dissociation of the bridging diphenyl phosphate ligand. The results of the pH titration, however, suggest that the 2:1 electrolyte behavior could also be attributed to  $Mg^{2+}$ ,  $NO_3^-$ ,  $DPP^-$ , and  $[Mg(HWXDK)_2L_n]^0$ . The structure of  $[Mg(HWXDK)_2L_n]$  is suggested by that of the known  $[Mg(HXDK)_2(H_2O)_2]$  complex, which was isolated from the reaction of a dinuclear magnesium XDK complex under acidic conditions.<sup>15</sup> In order to avoid formation of such a complex, the phosphate ester hydrolysis studies were carried out at pH values above 10.

The ability of complex 7 to hydrolyze bis(4-nitrophenyl)phosphate was investigated. Phosphate ester hydrolysis was not observed below pH 10.5, which is not surprising since the  $pK_a$  of water bound to magnesium is 11.4.<sup>18</sup> and the rate of hydrolysis appeared to be maximized at pH 10.9. Moreover, the rate of phosphate ester hydrolysis in 7 was comparable to that observed for free  $Mg(NO_3)_2 \cdot 6H_2O$  under the same conditions. From preliminary kinetic experiments, initial second order rate constants for  $BNPP^-$  hydrolysis were determined to be  $6 \times 10^{-8} M^{-1} s^{-1}$  and  $4 \times 10^{-8} M^{-1} s^{-1}$  for 7 and  $Mg(NO_3)_2 \cdot 6H_2O$ , respectively, at pH 10.9 (Figure 9). Since the  $[Mg^{2+}]$  concentration in 7 is two times that of  $Mg(NO_3)_2 \cdot 6H_2O$ , these rates of hydrolysis are currently considered to be comparable in our studies. Similar results were obtained for the hydrolysis of  $BNPP^-$  by the  $[Mg_2(XDK)(CH_3OH)_4(H_2O)_2(NO_3)](NO_3)$  complex and free magnesium nitrate in methanol, as reported in chapter 2.

## DISCUSSION

The H<sub>2</sub>WXDK ligand (5) was synthesized to afford water-soluble models of magnesium-dependent phosphate ester hydrolyzing enzymes. The synthesis of the new ligand was relatively straightforward and the precursor, *m*-xylylenediamine bis(tribenzyloxy-Kemp's triacid imide) (4), could be obtained in large quantities (~ 20 g). Removal of the benzyl groups in 4 to yield H<sub>2</sub>WXDK was carried out on smaller scales (~ 1 g).

Initial attempts to synthesize and crystallize dimagnesium(II) WXDK complexes were carried out by procedures analogous to those employed for the [Mg<sub>2</sub>(XDK)L<sub>n</sub>] analogs.<sup>15</sup> These methods were ineffective for crystallizing [Mg<sub>2</sub>(WXDK)L<sub>n</sub>] complexes, however. Since the WXDK ligand has six hydroxymethyl groups, we decided to try to crystallize the [Mg<sub>2</sub>(WXDK)L<sub>n</sub>] complexes by vapor diffusion of ethyl ether into 2-methoxyethanol (HMOE) solutions. 2-Methoxyethanol is recognized as a useful solvent for crystallizing sugars, of which WXDK may be considered an analogue.<sup>19</sup> With this solvent, we could obtain crystals of several dimagnesium(II) WXDK complexes which were suitable for X-ray analyses.

The X-ray structure of 6 reveals some new features for carboxylate-bridged dimagnesium centers (Figure 4). It demonstrates the ability of a carboxylate-bridged dinuclear magnesium unit to form a single atom bridge, a feature not previously encountered in our structural studies of dimagnesium XDK complexes.<sup>15</sup> The Mg1...Mg2 distance in 6 is 3.402(3) Å, which is about 0.5 Å shorter than the 3.9 Å metal-metal separation reported for a carboxylate-bridged dimetallic active site in the 2.6 Å resolution crystal structure of the Klenow fragment complexed with a deoxynucleoside monophosphate product.<sup>1</sup> In this protein crystal structure, there is one aspartate amino acid residue bridging the two metal ions, along with a monodentate oxygen atom of phosphate. One metal ion in the Klenow fragment

structure is further coordinated by a monodentate aspartate and a monodentate glutamate. The structure of 6 has two bidentate carboxylates bridging the two metal ions and differs from that seen in the protein crystal structure. It may be possible, however, that one of the monodentate carboxylate ligands undergoes a monodentate to bidentate "carboxylate shift"<sup>20</sup> during the phosphate ester hydrolysis reaction, which may help to facilitate product release by redistributing the charges around the metal center. If so, the resulting structure would resemble that of 6. The structural studies of the Klenow fragment have formed the basis for the proposed two-metal-ion mechanism of phosphoryl transfer (Scheme 1).<sup>1</sup> The shorter Mg...Mg separation in 6, which has a unidentate bridge, suggests the possibility that the bidentate carboxylate-bridged dimetallic active site in the Klenow fragment is not bridged by a single oxygen atom of the phosphate ester. The metal-metal distance of 3.9 Å observed is more consistent with a bidentate bridging phosphate (see below). Thus, the geometry at the dimagnesium center in 6 may be useful in reassessing the electron density in the protein active site and perhaps reevaluating the proposed two-metal-ion mechanism.

Compounds 7 and 8 are structurally quite similar to one another, with each containing a dinuclear magnesium center bridged by the carboxylate oxygen atoms of WXDK and a bidentate diphenyl phosphate. The crystals of 7 used for an X-ray analysis were of poor quality, so the triflate salt of this compound (8) was prepared in an effort to obtain a better structure (Figure 4). The metal-metal separation of 4.200(4) Å in 8 is similar to that observed in the XDK analog [Mg<sub>2</sub>(XDK){μ-η<sup>2</sup>-(PhO)<sub>2</sub>PO<sub>2</sub>}(CH<sub>3</sub>OH)<sub>3</sub>(H<sub>2</sub>O)(NO<sub>3</sub>)] of 4.240(5) Å.<sup>15</sup> These metal-metal distances are comparable, within the error limits of protein structural determination, to the 3.9 Å distance observed in the Klenow fragment.<sup>1</sup> Interestingly, the WXDK analog of [Mg<sub>2</sub>(XDK){μ-η<sup>2</sup>-(PhO)<sub>2</sub>PO<sub>2</sub>}{η<sup>1</sup>-(PhO)<sub>2</sub>PO<sub>2</sub>}(CH<sub>3</sub>OH)<sub>3</sub>(H<sub>2</sub>O)] did not form in the presence of two equivalents of diphenyl phosphate. The structures of both 7 and 8

suggest that coordination of 2-methoxyethanol is useful for crystallizing the diphenyl phosphate derivative. Our ability to synthesize and crystallize compound 9, a dimagnesium(II) WXDK complex bridged by a bidentate bis(4-nitrophenyl)phosphate, an activated phosphate ester, is interesting, since this phosphate ester binding mode has been proposed to activate the substrate for hydrolysis in monodentate carboxylate-bridged dimetallic enzymes<sup>21-24</sup> and in dicobalt(III) model compounds for phosphatases.<sup>2</sup> The  $^{31}\text{P}\{^1\text{H}\}$  NMR spectra of 7 - 9 in  $\text{D}_2\text{O}$  and  $\text{CD}_3\text{OD}$  are consistent with the observation that less polar solvents stabilize metal-chelate complexes.<sup>25</sup> In  $\text{D}_2\text{O}$ , diphenyl phosphate appears to be dissociated in solution, whereas in  $\text{CD}_3\text{OD}$ , the  $^{31}\text{P}\{^1\text{H}\}$  NMR spectra indicate the presence of a bridging phosphate ester, similar to our earlier results with the dimagnesium(II)-XDK analogs.<sup>15</sup>

Our present studies with carboxylate- and phosphate ester-bridged dimagnesium complexes as phosphatase models have led us to evaluate critically the current proposed mechanisms for phosphate ester hydrolysis. Our model compounds suggest several inconsistencies in the two-metal-ion mechanism proposed for the Klenow fragment. The metal-metal separation revealed by the protein crystal structure is too large for a single phosphate oxygen atom and a bidentate carboxylate bridge. Furthermore, the proposed mechanism required the metal ions to form two fused four-membered chelate rings to the phosphodiester substrate (Scheme 1), a geometry which has not been observed in metal-phosphodiester complexes and one which would be of very high energy even as a transition state.<sup>25-27</sup>

The results of our modelling studies better support a mechanism proposed for dicobalt(III) phosphatase model compounds.<sup>2</sup> As depicted in Scheme 2, this mechanism involves bidentate coordination of a phosphodiester, followed by intramolecular attack of a bridging hydroxide or oxide ion on the phosphorus

center. Such a bidentate coordination mode to the dimetallic center has been proposed to be more effective for activation of the phosphate group.<sup>28-31</sup> We, and others, have observed that bidentate coordination of a phosphodiester to a dimetallic center results in a  $\sim 120^\circ$  O-P-O bond angle at phosphorus,<sup>15</sup> which would lower the energy of a pentavalent transition state for phosphate ester hydrolysis by preassembling one of the required trigonal bipyramidal bond angles. Furthermore, the bridged bidentate coordination mode favors an  $S_N2$ -like in-line attack of a bridging  $\text{OH}^-$  which results in inversion of configuration at the terminal phosphorus. Such an inversion has been observed in enzymatic studies with the Klenow fragment.<sup>32</sup>

The phosphate ester hydrolysis experiments carried out here support the mechanism illustrated in Scheme 2. Our model compounds have two magnesium ions bridged by two bidentate carboxylate groups, as well as a bidentate phosphodiester. We attribute the failure of these complexes to accelerate the rate of phosphate ester hydrolysis by comparison to the hydrolysis rate of free magnesium ions in water or in methanol to the inability to form the additional bridging hydroxide ion required in this mechanism. We are currently investigating alternative ligand systems that contain only one carboxylate group which can be used for assembling dimagnesium phosphatase model complexes.

## CONCLUSIONS

We have synthesized and structurally characterized a water-soluble dicarboxylate ligand, WXDK, which has been used to prepare carboxylate-bridged dinuclear magnesium complexes as models for phosphate ester processing metalloenzymes. The dinuclear magnesium model compounds provide insights into the possible geometries around similar metal centers in phosphatase enzymes. These model compounds should therefore be useful to X-ray crystallographers for



fitting the electron density of carboxylate-bridged dimetallic units in protein active sites. The dimagnesium-WXDK complexes have also allowed us to investigate the properties of such carboxylate-bridged centers in aqueous media. Our phosphate ester hydrolytic studies with dimagnesium-WXDK complexes, and previous work with analogous XDK complexes, have revealed no enhancement in the rates of hydrolysis by comparison to free magnesium ions. The results of our modelling studies support a mechanism for phosphate ester hydrolysis where a phosphate ester coordinated in a bidentate manner to a carboxylate-bridged dimagnesium center is attacked by a bridging hydroxide ion. These observations may suggest alternative mechanisms for phosphate ester processing enzymes which employ a carboxylate-bridged dimetallic active site, and this information may be useful to biochemists studying the mechanisms of phosphate ester hydrolysis.

#### ACKNOWLEDGEMENTS

I would like to thank Rene Lachicotte, Mike Scott, Dan LeCloux, and Susanna Herold for helping make our transition to the new Siemens CCD X-ray diffraction system easier. Chuan He is also acknowledged for his assistance with the pH titrations and kinetic experiments carried out in this study.

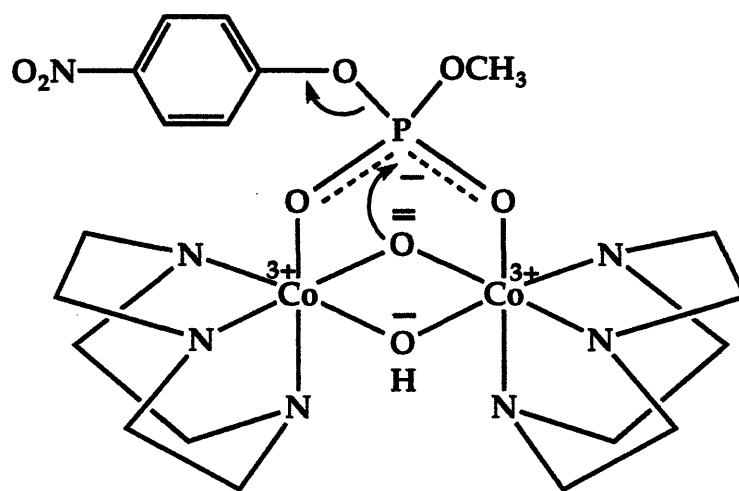
#### REFERENCES

- (1) Beese, L. S.; Steitz, T. A. *EMBO J.* **1991**, *10*, 25-33.
- (2) Wahnon, D.; Lebusis, A.-M.; Chin, J. *Angew. Chem. Int. Ed. Engl.* **1995**, *34*, 2412-2414.
- (3) Kemp, D. S.; Petrakis, K. S. *J. Org. Chem.* **1981**, *46*, 5140-5143.
- (4) Rebek, J., Jr.; Marshall, L.; Wolak, R.; Parris, K.; Killoran, M.; Askew, B.; Nemeth, D.; Islam, N. *J. Am. Chem. Soc.* **1985**, *107*, 7476-7481.

- (5) Watton, S. P.; Masschelein, A.; Rebek, J., Jr.; Lippard, S. J. *J. Am. Chem. Soc.* **1994**, *116*, 5196-5205.
- (6) Kato, Y.; Conn, M. M.; Rebek, J., Jr. *J. Am. Chem. Soc.* **1994**, *116*, 3279-3284.
- (7) SMART *Siemens Industrial Automation, Inc.*; Analytical Instrumentation: Madison, WI, 1994.
- (8) Feig, A. L.; Bautista, M. T.; Lippard, S. J. **1996**, submitted for publication.
- (9) SAINT *Siemens Industrial Automation, Inc.*; Analytical Instrumentation: Madison, WI, 1995.
- (10) Sheldrick, G. M. *Siemens Industrial Automation, Inc.*; Analytical Instrumentation: Madison, WI, 1994.
- (11) Motekaitis, R. J. *PKAS program*; VCH Publishers: New York, 1988.
- (12) Kimura, E.; Kodama, Y.; Koike, T.; Shiro, M. *J. Am. Chem. Soc.* **1995**, *117*, 8304-8311.
- (13) Koike, T.; Inoue, M.; Kimura, E.; Shiro, M. *J. Am. Chem. Soc.* **1996**, *118*, 3091-3099.
- (14) Rotello, V. M.; Viani, E. A.; Deslongchamps, G.; Murray, B. A.; Rebek, J., Jr. *J. Am. Chem. Soc.* **1993**, *115*, 797-798.
- (15) Yun, J. W. Ph.D. Thesis, Massachusetts Institute of Technology, 1996, Chapter 2.
- (16) Rebek, J., Jr.; Duff, R. J.; Gordon, W. E.; Parris, K. J. *J. Am. Chem. Soc.* **1986**, *108*, 6068-6069.
- (17) Martell, A. E.; Smith, R. M. *Critical Stability Constants*; Plenum Press: New York, 1977.
- (18) Martin, R. B. In *Metal Ions in Biological Systems*; Sigel, H., Eds.; Marcel Dekker, Inc.: New York, 1992; Vol. 26.
- (19) Gordon, A. J.; Ford, R. A. *The Chemist's Companion*; John Wiley & Sons: New York, 1973.

- (20) Rardin, R. L.; Tolman, W. B.; Lippard, S. J. *New J. Chem.* **1991**, *15*, 417-430.
- (21) Egloff, M.-P.; Cohen, P. T. W.; Reinemer, P.; Barford, D. *J. Mol. Biol.* **1995**, *254*, 942-959.
- (22) Strater, N.; Klabunde, T.; Tucker, P.; Witzel, H.; Krebs, B. *Science* **1995**, *268*, 1489-1492.
- (23) Taylor, W. P.; Widlanski, T. S. *Chemistry & Biology* **1995**, *2*, 713-718.
- (24) Griffith, J. P.; Kim, J. L.; Kim, E. E.; Sintchak, M. D.; Thomson, J. A.; Fitzgibbon, M. J.; Fleming, M. A.; Caron, P. R.; Hsiao, K.; Navia, M. A. *Cell* **1995**, *82*, 507-522.
- (25) Connolly, J. A.; Kim, J. H.; Banaszczyk, M.; Drouin, M.; Chin, J. *Inorg. Chem.* **1995**, *34*, 1094-1099.
- (26) Hendry, P.; Sargeson, A. M. *J. Am. Chem. Soc.* **1989**, *111*, 2521-2527.
- (27) Alexander, R. S.; Kanyo, Z. F.; Chirlian, L. E.; Christianson, D. W. *J. Am. Chem. Soc.* **1990**, *112*, 933-937.
- (28) Handry, P.; Sargeson, A. M. In *Prog. Inorg. Chem.*; Lippard, S. J., Eds.; John Wiley & Sons, Inc.: 1990; Vol. 38; pp 201-258.
- (29) Wall, M.; Hynes, R. C.; Chin, J. *Angew. Chem. Int. Ed. Engl.* **1993**, *32*, 1633-1635.
- (30) Young, M. J.; Chin, J. *J. Am. Chem. Soc.* **1995**, *117*, 10577-10578.
- (31) Williams, N. H.; Chin, J. *Chem. Commun.* **1996**, 131-132.
- (32) Gupta, A. P.; Benkovic, S. J. *Biochemistry* **1984**, *23*, 5874-5881.





**Scheme 2.** Proposed mechanism for phosphate ester hydrolysis by a dicobalt(III) phosphatase model compound. Adapted from reference 2.



**Table 1.** Crystallographic and Experimental Data for 5·H<sub>2</sub>O·CH<sub>3</sub>OH, 6(OTf)·HMOE, 8(OTf)·HMOE, and 9(OTf)<sub>0.5</sub>(BNPP)<sub>0.5</sub>·0.5HMOE<sup>a</sup>

compound	5·H <sub>2</sub> O·CH <sub>3</sub> OH	6(OTf)·HMOE	8(OTf)·HMOE	9(OTf) <sub>0.5</sub> (BNPP) <sub>0.5</sub> ·0.5HMOE
formula	C <sub>33</sub> H <sub>46</sub> N <sub>2</sub> O <sub>16</sub>	C <sub>45</sub> H <sub>71</sub> N <sub>2</sub> O <sub>26</sub> Mg <sub>2</sub> -F <sub>3</sub> S <sub>1</sub>	C <sub>54</sub> H <sub>68</sub> N <sub>2</sub> O <sub>29</sub> Mg <sub>2</sub> -P <sub>1</sub> F <sub>3</sub> S <sub>1</sub>	C <sub>61</sub> H <sub>82</sub> N <sub>5</sub> O <sub>36.5</sub> Mg <sub>2</sub> -P <sub>1.5</sub> F <sub>1.5</sub> S <sub>0.5</sub>
fw	726.72	1159.49	1365.15	1608.93
crystal size (mm)	0.4 x 0.5 x 0.5	0.2 x 0.2 x 0.6	0.2 x 0.4 x 0.6	0.2 x 0.3 x 0.6
crystal system	monoclinic	orthorhombic	orthorhombic	triclinic
space group	P2 <sub>1</sub> /c	P2 <sub>1</sub> 2 <sub>1</sub> 2 <sub>1</sub>	Iba2	P-1
a, Å	11.7721 (6)	12.6078 (2)	28.6509 (10)	14.56520 (10)
b, Å	12.0160 (6)	18.9330 (3)	32.4566 (11)	16.9746 (2)
c, Å	24.5551 (13)	23.0694 (2)	14.7440 (5)	17.3764 (2)
α, deg				80.6690 (10)
β, deg	92.3470 (10)			80.1490 (10)
γ, deg				69.8220 (20)
V, Å <sup>3</sup>	3470.5 (3)	5506.75 (13)	13710.6 (8)	3948.21 (7)
Z	4	4	8	2
T, °C	-80	-80	-85	-85
D <sub>calcd</sub> , g cm <sup>-3</sup>	1.39	1.40	1.32	1.28
abs coeff, cm <sup>-1</sup>	1.12	1.77	1.79	1.69
2θ range, deg	3 < 2θ < 46.53	3 < 2θ < 45	3 < 2θ < 45	3 < 2θ < 45
no. of unique data	4948	7180	8136	9912
no. of obsd data	4257	6154	7376	8196
(I > 2σ(I))				
R <sub>merge</sub> (%)	0.032	0.0652	0.048	0.057
no. of variables	493	679	755	908
R <sup>b</sup>	0.056	0.078	0.094	0.104
wR2 <sup>b</sup>	0.141	0.190	0.252	0.306

<sup>a</sup>HMOE is 2-methoxyethanol.  $bR = \sum ||F_o| - |F_c|| / \sum |F_o|$ ;  $wR2 = \{\sum [w(F_o^2 - F_c^2)]^2 / \sum [w(F_o^2)]^2\}^{1/2}$ , where  $w = 1/\sigma^2(F_o)$ . More details about the weighting scheme and other experimental protocols may be found in reference 8.

Table 2. Intramolecular Distances Involving the Nonhydrogen Atoms for 5.<sup>a</sup>

atom	atom	distance	atom	atom	distance
O(14)	C(104)	1.389(4)	C(107)	C(112)	1.535(4)
O(15)	C(105)	1.419(4)	C(108)	C(109)	1.549(4)
O(16)	C(106)	1.424(4)	C(109)	C(110)	1.524(4)
O(24)	C(204)	1.406(4)	C(110)	C(111)	1.518(4)
O(25)	C(205)	1.421(4)	C(111)	C(112)	1.523(4)
O(26)	C(206)	1.415(4)	C(201)	C(207)	1.517(4)
O(101)	C(101)	1.274(4)	C(202)	C(209)	1.524(4)
O(102)	C(101)	1.248(4)	C(203)	C(211)	1.516(4)
O(103)	C(102)	1.217(3)	C(204)	C(207)	1.560(4)
O(104)	C(103)	1.209(3)	C(205)	C(209)	1.532(4)
O(201)	C(201)	1.255(4)	C(206)	C(211)	1.529(4)
O(202)	C(201)	1.270(4)	C(207)	C(208)	1.531(4)
O(203)	C(203)	1.216(3)	C(207)	C(212)	1.542(4)
O(204)	C(202)	1.208(3)	C(208)	C(209)	1.538(4)
N(101)	C(102)	1.400(4)	C(209)	C(210)	1.517(4)
N(101)	C(103)	1.408(4)	C(210)	C(211)	1.523(4)
N(101)	C(302)	1.456(3)	C(211)	C(212)	1.541(4)
N(201)	C(202)	1.399(4)	C(301)	C(302)	1.381(4)
N(201)	C(203)	1.400(4)	C(301)	C(306)	1.383(4)
N(201)	C(306)	1.457(4)	C(302)	C(303)	1.389(4)
C(101)	C(107)	1.523(4)	C(303)	C(304)	1.395(4)
C(102)	C(109)	1.526(4)	C(303)	C(307)	1.508(4)
C(103)	C(111)	1.518(4)	C(304)	C(305)	1.386(4)
C(104)	C(107)	1.553(4)	C(305)	C(306)	1.387(4)
C(105)	C(109)	1.515(4)	C(305)	C(308)	1.510(4)
C(106)	C(111)	1.528(4)	O(41)	C(41)	1.387(7)
C(107)	C(108)	1.532(4)			

<sup>a</sup>Estimated standard deviations are given in parentheses. See Figure 1 for atom labels.



**Table 3.** Intramolecular Bond Angles Involving the Nonhydrogen Atoms for 5.<sup>a</sup>

atom	atom	atom	angle	atom	atom	atom	angle
C(102)	N(101)	C(103)	125.2(2)	C(103)	C(111)	C(106)	108.4(2)
C(102)	N(101)	C(302)	118.2(2)	C(112)	C(111)	C(106)	107.5(2)
C(103)	N(101)	C(302)	116.5(2)	C(111)	C(112)	C(107)	115.9(2)
C(202)	N(201)	C(203)	124.4(2)	O(201)	C(201)	O(202)	123.0(3)
C(202)	N(201)	C(306)	118.4(2)	O(201)	C(201)	C(207)	120.1(3)
C(203)	N(201)	C(306)	117.1(2)	O(202)	C(201)	C(207)	116.8(3)
O(102)	C(101)	O(101)	123.2(3)	O(204)	C(202)	N(201)	119.2(3)
O(102)	C(101)	C(107)	119.3(3)	O(204)	C(202)	C(209)	122.6(3)
O(101)	C(101)	C(107)	117.5(3)	N(201)	C(202)	C(209)	118.1(2)
O(103)	C(102)	N(101)	120.0(3)	O(203)	C(203)	N(201)	119.9(3)
O(103)	C(102)	C(109)	122.6(3)	O(203)	C(203)	C(211)	122.8(3)
N(101)	C(102)	C(109)	117.4(2)	N(201)	C(203)	C(211)	117.3(3)
O(104)	C(103)	N(101)	118.9(3)	O(24)	C(204)	C(207)	112.4(2)
O(104)	C(103)	C(111)	123.9(3)	O(25)	C(205)	C(209)	111.5(3)
N(101)	C(103)	C(111)	117.2(2)	O(26)	C(206)	C(211)	111.7(2)
O(14)	C(104)	C(107)	115.4(3)	C(201)	C(207)	C(208)	111.5(2)
O(15)	C(105)	C(109)	110.2(3)	C(201)	C(207)	C(212)	112.8(2)
O(16)	C(106)	C(111)	109.9(3)	C(208)	C(207)	C(212)	111.2(2)
C(101)	C(107)	C(108)	112.5(2)	C(201)	C(207)	C(204)	102.4(2)
C(101)	C(107)	C(112)	112.9(2)	C(208)	C(207)	C(204)	109.2(2)
C(108)	C(107)	C(112)	110.7(2)	C(212)	C(207)	C(204)	109.4(2)
C(101)	C(107)	C(104)	103.7(2)	C(207)	C(208)	C(209)	115.2(2)
C(108)	C(107)	C(104)	111.8(2)	C(210)	C(209)	C(202)	109.4(2)
C(112)	C(107)	C(104)	104.8(2)	C(210)	C(209)	C(205)	111.5(2)
C(107)	C(108)	C(109)	115.9(2)	C(202)	C(209)	C(205)	107.6(2)
C(105)	C(109)	C(110)	111.9(3)	C(210)	C(209)	C(208)	109.3(2)
C(105)	C(109)	C(102)	109.7(2)	C(202)	C(209)	C(208)	110.1(2)
C(110)	C(109)	C(102)	108.3(2)	C(205)	C(209)	C(208)	108.8(2)
C(105)	C(109)	C(108)	106.7(2)	C(209)	C(210)	C(211)	109.5(2)
C(110)	C(109)	C(108)	109.2(2)	C(203)	C(211)	C(210)	109.4(2)
C(102)	C(109)	C(108)	111.0(2)	C(203)	C(211)	C(206)	107.9(2)
C(111)	C(110)	C(109)	110.0(2)	C(210)	C(211)	C(206)	110.9(2)
C(110)	C(111)	C(103)	109.1(2)	C(203)	C(211)	C(212)	109.8(2)
C(110)	C(111)	C(112)	111.0(2)	C(210)	C(211)	C(212)	110.7(2)
C(103)	C(111)	C(112)	109.5(2)	C(206)	C(211)	C(212)	108.1(2)
C(110)	C(111)	C(106)	111.3(2)	C(211)	C(212)	C(207)	115.5(2)

<sup>a</sup>Estimated standard deviations are given in parentheses. See Figure 1 for atom labels.

**Table 3 (continued).** Intramolecular Bond Angles Involving the Nonhydrogen Atoms for 5.<sup>a</sup>

atom	atom	atom	angle
C(302)	C(301)	C(306)	119.6(3)
C(301)	C(302)	C(303)	121.2(3)
C(301)	C(302)	N(101)	118.5(2)
C(303)	C(302)	N(101)	120.2(2)
C(302)	C(303)	C(304)	117.1(3)
C(302)	C(303)	C(307)	121.7(3)
C(304)	C(303)	C(307)	121.2(3)
C(305)	C(304)	C(303)	123.4(3)
C(304)	C(305)	C(306)	117.0(3)
C(304)	C(305)	C(308)	121.2(3)
C(306)	C(305)	C(308)	121.8(3)
C(301)	C(306)	C(305)	121.6(3)
C(301)	C(306)	N(201)	118.7(2)
C(305)	C(306)	N(201)	119.7(2)

<sup>a</sup>Estimated standard deviations are given in parentheses. See Figure 1 for atom labels.

**Table 4.** Selected Bond Distances (Å) and Angles (deg) for 6.<sup>a</sup>

<b>Bond Distances</b>							
Mg(1)	O(201)	2.021(5)		Mg(2)	O(102)	2.035(5)	
Mg(1)	O(101)	2.054(5)		Mg(2)	O(202)	2.038(5)	
Mg(1)	O(51)	2.057(5)		Mg(2)	O(51)	2.052(5)	
Mg(1)	O(32)	2.112(6)		Mg(2)	O(43)	2.084(5)	
Mg(1)	O(31)	2.119(6)		Mg(2)	O(42)	2.168(5)	
Mg(1)	O(52)	2.149(6)		Mg(2)	O(41)	2.181(5)	
<b>Angles</b>							
O(201)	Mg(1)	O(101)	103.8(2)	O(102)	Mg(2)	O(43)	85.0(2)
O(201)	Mg(1)	O(51)	88.7(2)	O(202)	Mg(2)	O(43)	174.4(2)
O(101)	Mg(1)	O(51)	98.5(2)	O(51)	Mg(2)	O(43)	94.7(2)
O(201)	Mg(1)	O(32)	95.4(2)	O(102)	Mg(2)	O(42)	89.6(2)
O(101)	Mg(1)	O(32)	89.0(2)	O(202)	Mg(2)	O(42)	83.3(2)
O(51)	Mg(1)	O(32)	170.4(3)	O(51)	Mg(2)	O(42)	167.9(2)
O(201)	Mg(1)	O(31)	88.6(2)	O(43)	Mg(2)	O(42)	93.1(2)
O(101)	Mg(1)	O(31)	159.5(2)	O(102)	Mg(2)	O(41)	163.5(2)
O(51)	Mg(1)	O(31)	98.1(2)	O(202)	Mg(2)	O(41)	86.7(2)
O(32)	Mg(1)	O(31)	73.3(2)	O(51)	Mg(2)	O(41)	95.3(2)
O(201)	Mg(1)	O(52)	166.1(2)	O(43)	Mg(2)	O(41)	88.3(2)
O(101)	Mg(1)	O(52)	86.3(2)	O(42)	Mg(2)	O(41)	75.6(2)
O(51)	Mg(1)	O(52)	80.2(2)				
O(32)	Mg(1)	O(52)	94.4(2)				
O(31)	Mg(1)	O(52)	84.8(2)				

<sup>a</sup>Estimated standard deviations are given in parentheses. See Figures 1 and 4 for atom labels.

Table 5. Selected Bond Distances (Å) and Angles (deg) for 8.<sup>a</sup>

Bond Distances							
Mg(1)	O(201)	2.014(6)		Mg(2)	O(102)	1.973(7)	
Mg(1)	O(101)	2.021(6)		Mg(2)	O(41)	1.998(8)	
Mg(1)	O(31)	2.020(7)		Mg(2)	O(202)	1.998(7)	
Mg(1)	O(34)	2.133(6)		Mg(2)	O(42)	2.052(13)	
Mg(1)	O(32)	2.152(6)		Mg(2)	O(43)	2.131(12)	
Mg(1)	O(33)	2.158(6)		Mg(2)	O(44)	2.212(11)	
P(1)	O(41)	1.472(7)		P(1)	O(51)	1.587(8)	
P(1)	O(31)	1.480(7)		P(1)	O(61)	1.612(7)	
Angles							
O(201)	Mg(1)	O(101)	109.7(3)	O(102)	Mg(2)	O(41)	97.2(3)
O(201)	Mg(1)	O(31)	94.2(3)	O(102)	Mg(2)	O(202)	104.0(3)
O(101)	Mg(1)	O(31)	93.4(3)	O(41)	Mg(2)	O(202)	95.5(3)
O(201)	Mg(1)	O(34)	85.0(3)	O(102)	Mg(2)	O(42)	96.3(4)
O(101)	Mg(1)	O(34)	87.6(2)	O(41)	Mg(2)	O(42)	96.6(5)
O(31)	Mg(1)	O(34)	178.9(3)	O(202)	Mg(2)	O(42)	154.8(4)
O(201)	Mg(1)	O(32)	90.3(2)	O(102)	Mg(2)	O(43)	169.3(4)
O(101)	Mg(1)	O(32)	159.3(3)	O(41)	Mg(2)	O(43)	90.4(4)
O(31)	Mg(1)	O(32)	90.3(3)	O(202)	Mg(2)	O(43)	82.7(4)
O(34)	Mg(1)	O(32)	88.9(3)	O(42)	Mg(2)	O(43)	75.3(5)
O(201)	Mg(1)	O(33)	163.6(2)	O(102)	Mg(2)	O(44)	85.5(4)
O(101)	Mg(1)	O(33)	85.2(2)	O(41)	Mg(2)	O(44)	177.3(4)
O(31)	Mg(1)	O(33)	91.6(3)	O(202)	Mg(2)	O(44)	83.4(3)
O(34)	Mg(1)	O(33)	89.0(2)	O(42)	Mg(2)	O(44)	83.5(5)
O(32)	Mg(1)	O(33)	74.3(2)	O(43)	Mg(2)	O(44)	87.0(5)
O(41)	P(1)	O(31)	119.3(4)	P(1)	O(31)	Mg(1)	140.5(4)
O(41)	P(1)	O(51)	105.1(4)	P(1)	O(41)	Mg(2)	144.8(5)
O(31)	P(1)	O(51)	111.5(4)				
O(41)	P(1)	O(61)	110.5(4)				
O(31)	P(1)	O(61)	109.0(4)				
O(51)	P(1)	O(61)	99.6(4)				

<sup>a</sup>Estimated standard deviations are given in parentheses. See Figures 1 and 5 for atom labels.

Table 6. Selected Bond Distances (Å) and Angles (deg) for 9.<sup>a</sup>

Bond Distances							
Mg(1)	O(101)	2.015(5)		Mg(2)	O(202)	1.986(5)	
Mg(1)	O(31)	2.022(5)		Mg(2)	O(102)	2.013(5)	
Mg(1)	O(201)	2.052(5)		Mg(2)	O(41)	2.061(6)	
Mg(1)	O(36)	2.063(5)		Mg(2)	O(44)	2.067(5)	
Mg(1)	O(32)	2.090(5)		Mg(2)	O(42)	2.129(5)	
Mg(1)	O(34)	2.196(5)		Mg(2)	O(43)	2.143(5)	
P(1)	O(31)	1.461(5)		P(1)	O(61)	1.588(6)	
P(1)	O(41)	1.485(5)		P(1)	O(51)	1.600(6)	

Angles							
O(101)	Mg(1)	O(31)	92.5(2)	O(202)	Mg(2)	O(102)	105.1(2)
O(101)	Mg(1)	O(201)	98.8(2)	O(202)	Mg(2)	O(41)	99.0(2)
O(31)	Mg(1)	O(201)	96.9(2)	O(102)	Mg(2)	O(41)	86.4(2)
O(101)	Mg(1)	O(36)	88.4(2)	O(202)	Mg(2)	O(44)	88.1(2)
O(31)	Mg(1)	O(36)	171.2(2)	O(102)	Mg(2)	O(44)	91.9(2)
O(201)	Mg(1)	O(36)	91.7(2)	O(41)	Mg(2)	O(44)	172.9(2)
O(101)	Mg(1)	O(32)	173.5(2)	O(202)	Mg(2)	O(42)	90.1(2)
O(31)	Mg(1)	O(32)	88.2(2)	O(102)	Mg(2)	O(42)	164.5(2)
O(201)	Mg(1)	O(32)	87.5(2)	O(41)	Mg(2)	O(42)	87.9(2)
O(36)	Mg(1)	O(32)	89.9(2)	O(44)	Mg(2)	O(42)	91.9(2)
O(101)	Mg(1)	O(34)	90.9(2)	O(202)	Mg(2)	O(43)	164.4(2)
O(31)	Mg(1)	O(34)	86.3(2)	O(102)	Mg(2)	O(43)	89.8(2)
O(201)	Mg(1)	O(34)	169.7(2)	O(41)	Mg(2)	O(43)	86.4(2)
O(36)	Mg(1)	O(34)	85.0(2)	O(44)	Mg(2)	O(43)	86.7(2)
O(32)	Mg(1)	O(34)	82.7(2)	O(42)	Mg(2)	O(43)	75.4(2)
O(31)	P(1)	O(41)	120.6(3)	P(1)	O(31)	Mg(1)	137.9(3)
O(31)	P(1)	O(61)	110.8(3)	P(1)	O(41)	Mg(2)	139.8(3)
O(41)	P(1)	O(61)	105.6(3)				
O(31)	P(1)	O(51)	105.4(3)				
O(41)	P(1)	O(51)	109.4(3)				
O(61)	P(1)	O(51)	103.8(3)				

<sup>a</sup>Estimated standard deviations are given in parentheses. See Figures 1 and 6 for atom labels.

Table 7. Structural Parameters of Compounds 6, 8, and 9

	(6)	(8)	(9)
Mg1...Mg2, Å	3.402(3)	4.200(4)	4.340(3)
Mg1-O(XDK) <sub>av</sub> , Å <sup>a</sup>	2.038(7)	2.018(8)	2.034(7)
Mg2-O(XDK) <sub>av</sub> , Å <sup>a</sup>	2.037(7)	1.986(9)	2.000(7)
O101-Mg1-O201, °	103.8(2)	109.7(3)	98.8(2)
O102-Mg2-O202, °	99.2(2)	104.0(3)	105.1(2)
O31-P1-O41, °		119.3(4)	120.6(3)
P1-O31-Mg1, °		140.5(4)	137.9(3)
P1-O41-Mg2, °		144.8(5)	139.8(3)
$\phi$ , ° <sup>b</sup>	36.1	22.1	23.6
$d(\text{Mg1})$ , Å <sup>c</sup>	1.1	0.49	0.64
$d(\text{Mg2})$ , Å <sup>c</sup>	1.2	0.79	0.72
[O(101)O(102)C(101)C(107)] vs [O(201)O(202)C(201)C(207)], ° <sup>d</sup>	7.0	10.4	2.5

<sup>a</sup> Average value. Estimated deviations in parentheses are derived from  $(\sigma_A^2 + \sigma_B^2)^{1/2}$ . <sup>b</sup> Dihedral angle between the [Mg1Mg2(O<sub>2</sub>C<sub>2</sub>)<sub>2</sub>] and the dicarboxylate planes (average value). <sup>c</sup> Distance from the metal atom to the dicarboxylate plane. <sup>d</sup> Dihedral angle.



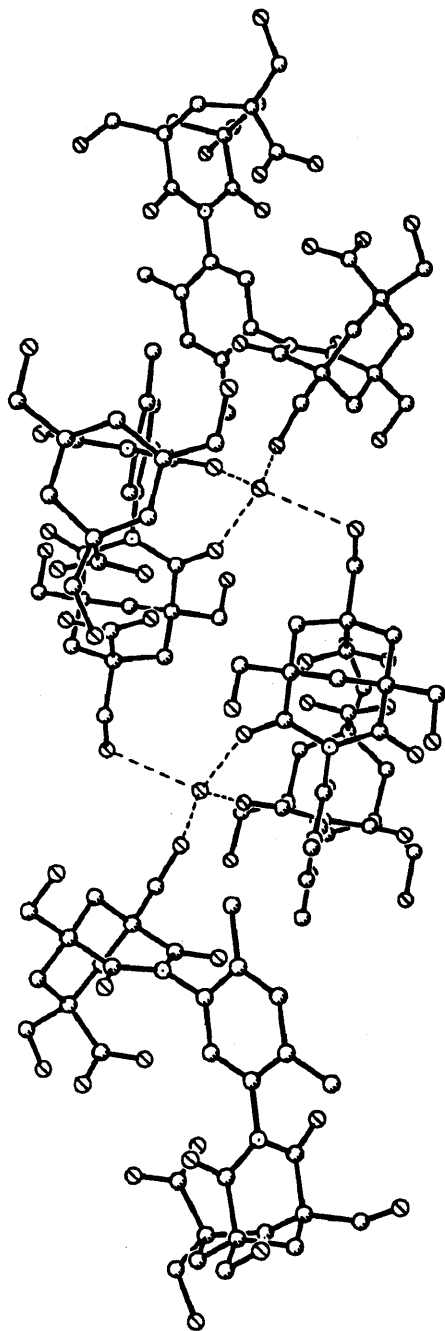


Figure 2. A packing diagram of  $5 \cdot \text{H}_2\text{O}$  illustrating the hydrogen-bonding interactions of the lattice water molecule.



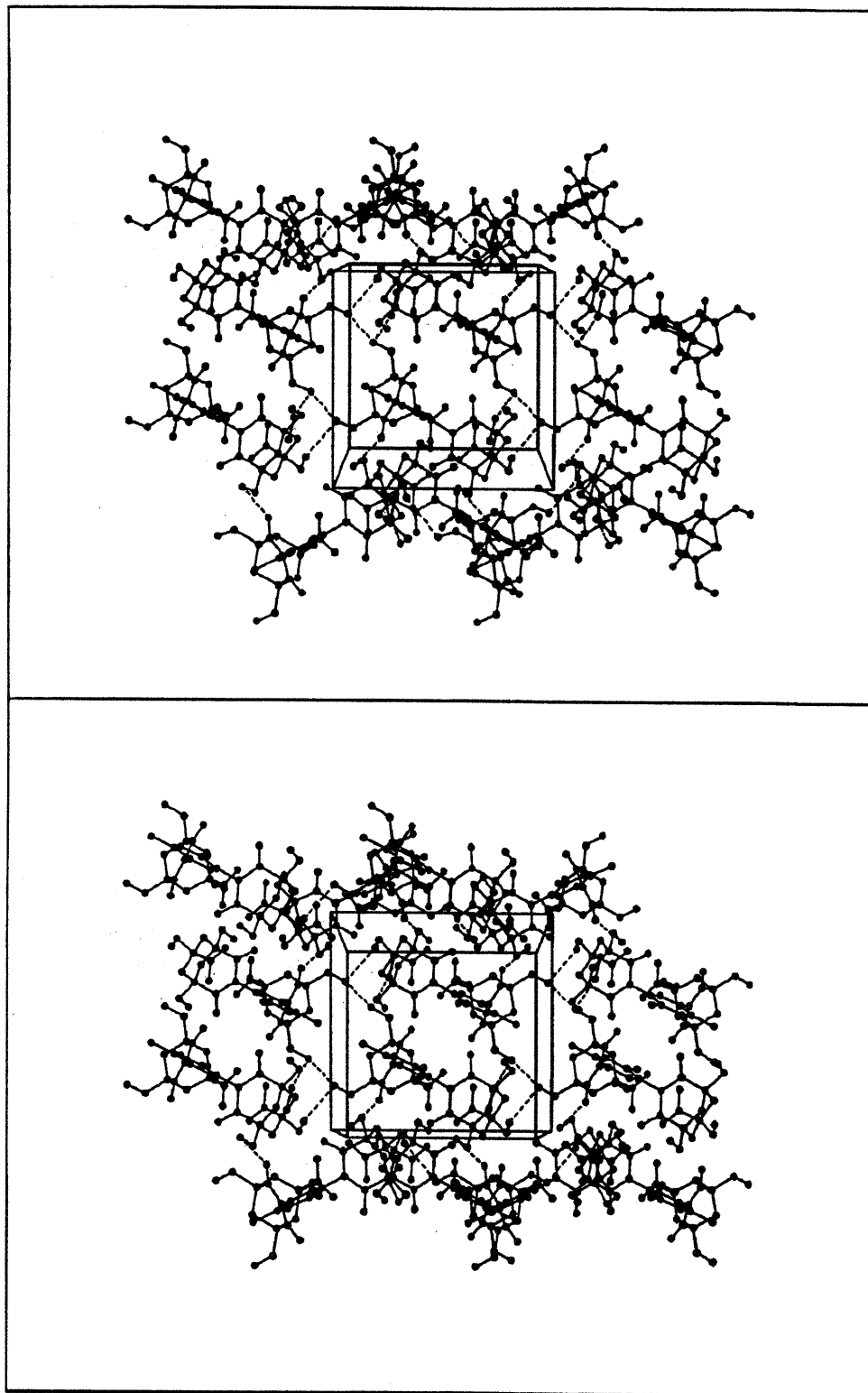
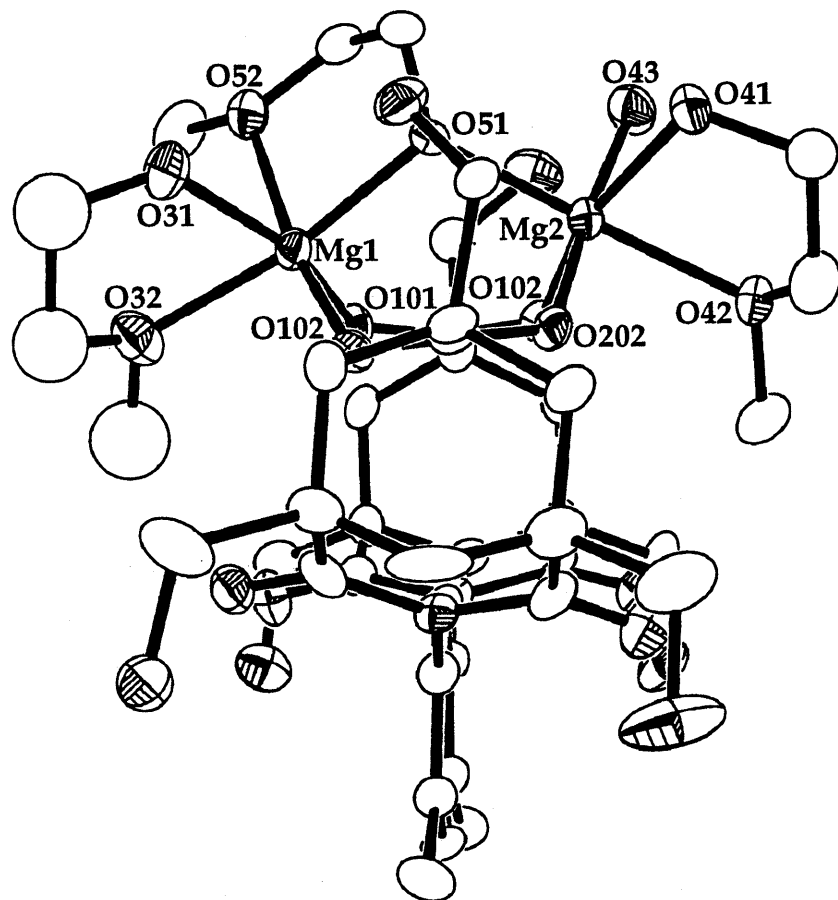
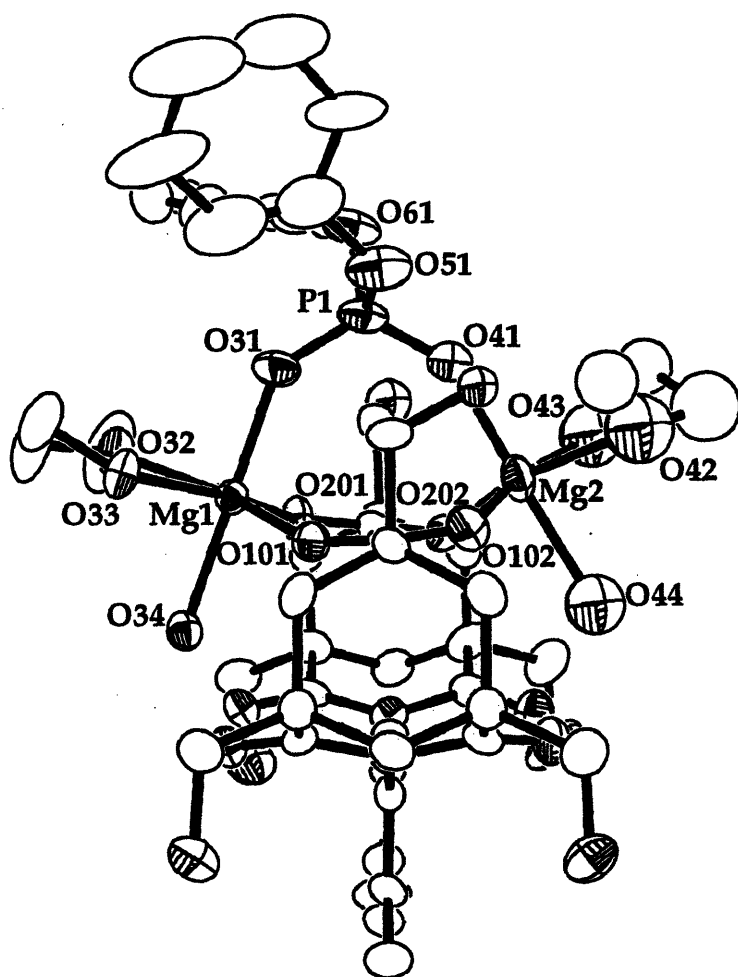


Figure 3. A stereoview of the packing diagram of  $5 \cdot \text{H}_2\text{O} \cdot \text{CH}_3\text{OH}$ , as viewed along the c-axis.



**Figure 4.** An ORTEP view of **6**. Hydrogen atoms are omitted for clarity. Thermal ellipsoids are drawn at the 40% probability level. Atomic labelling scheme for the WXDK ligand is given in Figure 1.



**Figure 5.** An ORTEP view of **8**. Hydrogen atoms are omitted for clarity. Thermal ellipsoids are drawn at the 40% probability level. The atomic numbering scheme for the WXDK ligand is given in Figure 1.



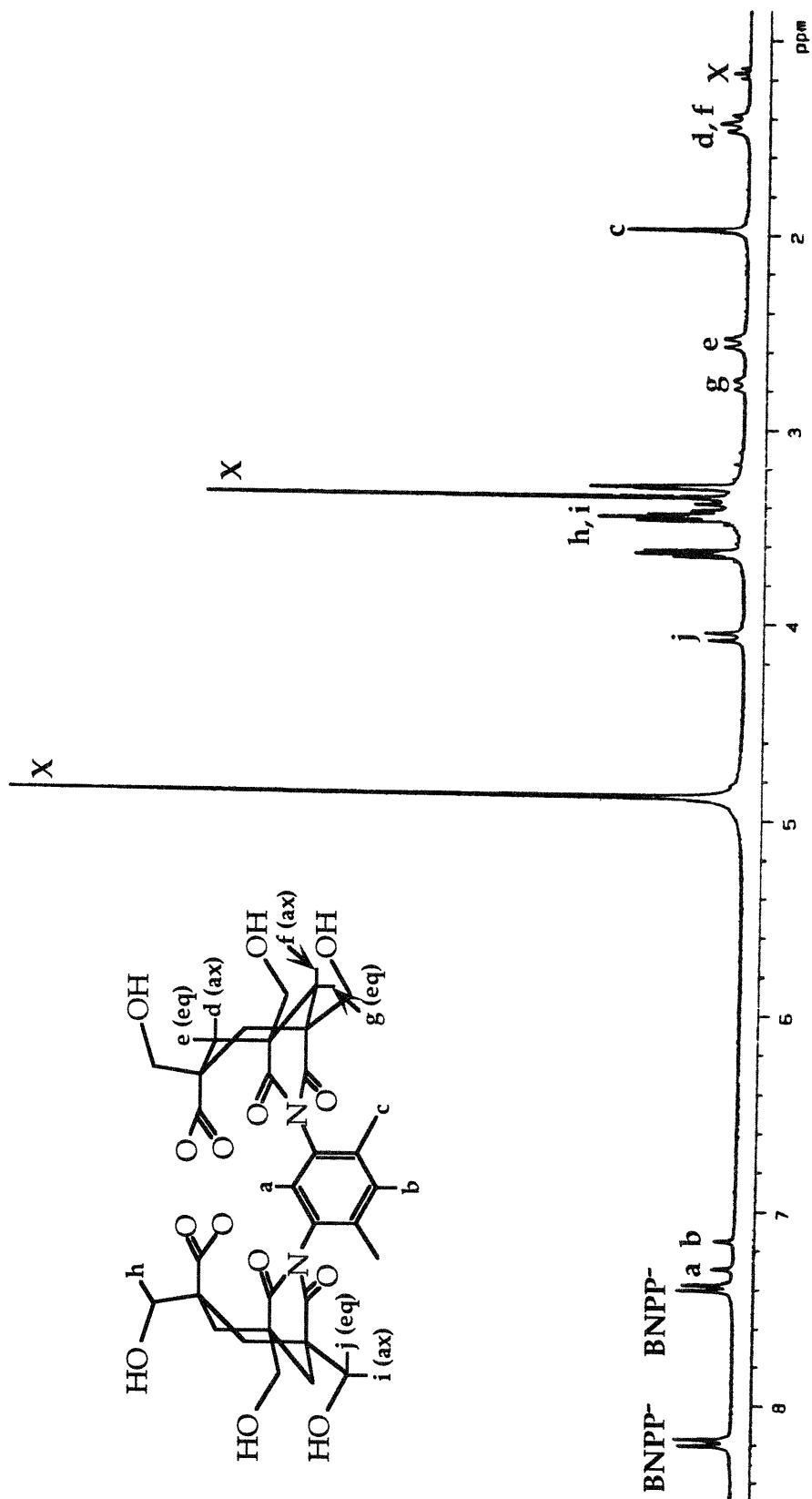


Figure 7.  $^1\text{H}$  NMR spectrum of  $9(\text{OTf})_{0.5}(\text{BNPP})_{0.5}$  in  $\text{CD}_3\text{OD}$ . The WXDK ligand assignments are given.

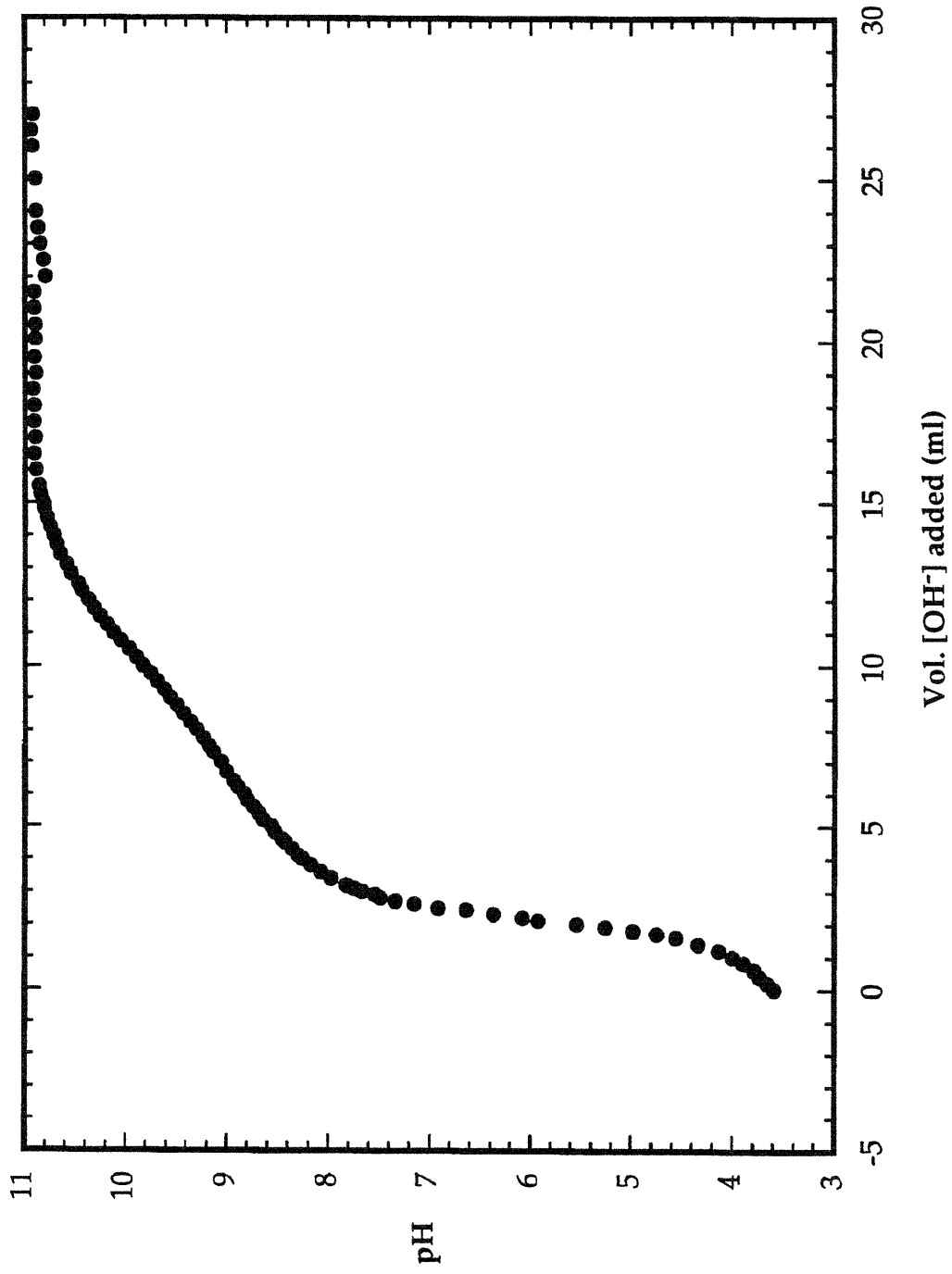


Figure 8. The pH titration curve of 7(NO<sub>3</sub>).

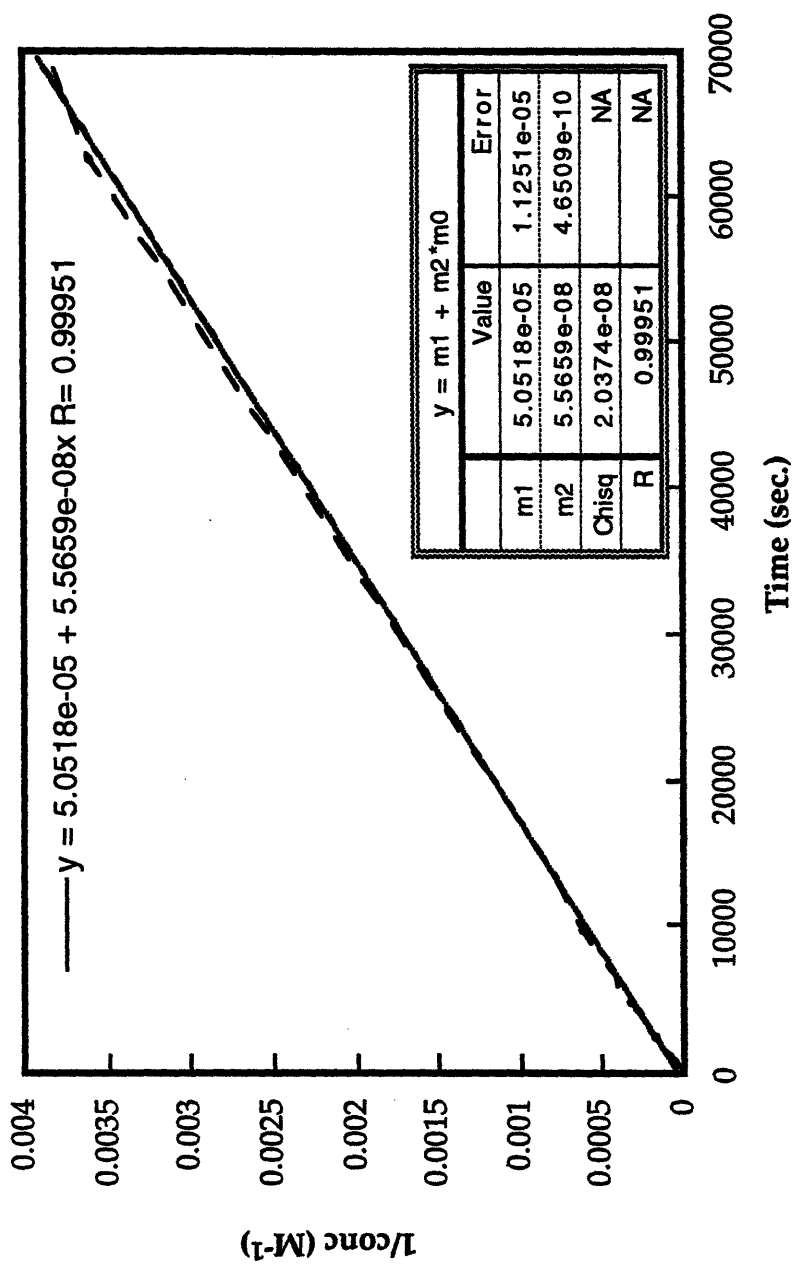


Figure 9. Fitted data of initial second order rate constant determination for 7(NO<sub>3</sub>).

### Biographical Note

Joanne W. Yun was born on September 25, 1970 in Hong Kong, B. C. C. to Edmond and Denise Yun. She has an older brother, Johnny, and a younger sister, Janet. At the age of three, Joanne and her family moved to Portland, Oregon where her grandparents were settled. She attended Reynolds High School in Troutdale, Oregon where chemistry teacher Larry Callister inspired her interest in the subject. Joanne was Vice-President and Valedictorian of her senior class and graduated in June 1988. At Amherst College, she graduated *summa cum laude* with B.A. degrees in French and chemistry in May 1992 and received the Everett H. Pryde Research Prize for excellence in teaching and research. She studied bio-inorganic chemistry in the laboratory of Professor David M. Dooley for her senior thesis project. She acquired additional research experience as a Summer Undergraduate Research Fellow at the California Institute of Technology and as a summer intern with Eli Lilly and Company at the Lilly Research Laboratories. Joanne continued her chemistry education by pursuing graduate studies with Professor Stephen J. Lippard at the Massachusetts Institute of Technology. Upon completion of her Ph.D. studies, she will move to The Scripps Research Institute where she will conduct postdoctoral research with Professor Chi-Huey Wong. She has written and co-published five scientific articles to date.